DEPARTMENT OF CHEMISTRY, UNIVERSITY OF JYVÄSKYLÄ
RESEARCH REPORT No. 141

GELATION AND GEL PROPERTIES OF TWO- AND THREE-COMPONENT PYRENE BASED LOW MOLECULAR WEIGHT ORGANOGELATORS

BY

KIMMO LEIVO

Academic Dissertation
for the degree of
Doctor of Philosophy

To be presented, by permission of the Faculty of Mathematics and Science of the University of Jyväskylä, for public examination in Auditorium FYS1, on March 25th 2011, at 12 noon

UNIVERSITY OF JYVÄSKYLÄ

Jyväskylä, Finland
ISBN 978-951-39-4231-1
ISSN 0357-346X
ISBN 978-951-39-4232-8(PDF)
URN:ISBN:978-951-39-4232-8

ABSTRACT

Leivo, Kimmo
Gelation and gel properties of two- and three-component pyrene based low molecular weight organogelators
Jyväskylä: University of Jyväskylä, 2011, 142 p.
Department of Chemistry, University of Jyväskylä Research Report
ISSN 0357-346X
ISBN 978-951-39-4231-1(nid.), 978-951-39-4232-8 (PDF)
Diss.

The research described in this thesis covers the synthesis, characterization and the study of the gelation ability of fifteen pyrene based low molecular weight organogelators (LMOGs). The gelation and gel properties were investigated by rheometry, scanning electron microscopy, differential scanning calorimetry, UV-Vis and fluorescence spectroscopy.

The pyrene based LMOGs form complexes with 2,4,7-trinitrofluorenone (TNF) and self-assemble non-covalently through π-π stacking, donor-acceptor and van der Waals interactions to form thermoreversible gels, which remain stable at least for two years. The strongest gels were obtained in primary alcohols whereas the poor solubility of TNF restricted gelation in nonpolar hydrocarbons. It was observed that the gelation behavior of the two-component gelator system can be estimated in both nonpolar and polar solvents by using the Hansen solubility parameters and distance. The unknown solubility parameters of the gelators were estimated by a group contribution method. The gelation ability of the two-component system was found to correlate with the hydrogen bonding solubility parameter of the solvent.

Electron microscopy showed that the gelation occurs due to self-assembly of the gelators into long gel fibers that form an entangled gel network. The solvent and the structure of the pyrene based LMOG have a large effect on the gel structure and; consequently, the properties. The gels with less fiber bundles and denser gel network were more elastic and had higher stability and viscosity. The organogels are viscoelastic soft materials showing shear thinning behavior and a yield point. The effect of the solvent, additives like pyrene, crosslinker molecule and aluminum nanoparticles, functionality and alkyl side chain length of the pyrene based gelator on the gel properties were studied by rheometry. The results of this work indicate that two- and three-component gelator systems open wide possibilities to control the gel properties in various solvents.

Keywords: gel, gelator, organogelator, low molecular weight organogelator, self-assembly, solubility parameters, rheology, scanning electron microscopy

Author's address Kimmo Leivo
Department of Chemistry
Nanoscience Center
P.O. Box 35
40014 University of Jyväskylä
Finland
kimmo.leivo@jyu.fi

Supervisors Dr Arno Hahma
Diehl BGT Defence GmbH & Co. KG
Röthenbach a.d. Pegnitz
Germany

Professor Henrik Kunttu
Department of Chemistry
University of Jyväskylä
Finland

Academy professor Kari Rissanen
Department of Chemistry
University of Jyväskylä
Finland

Reviewers Professor Mladen Žinić
Rudjer Bošković Institute
Zagreb, Croatia

Docent Sami Hietala
Department of Chemistry
University of Helsinki
Finland

Opponent Professor Jan H. van Esch
Department of Chemical Engineering
Delft University of Technology
the Netherlands

PREFACE

The present work was carried out during the years 2005 - 2011 at the Department of Chemistry, University of Jyväskylä and at the German Aerospace Center (DLR), Lampoldshausen in Germany.

First I would like to thank my supervisors Dr. Arno Hahma and Academy Professor Kari Rissanen for introducing me to the exciting field of gels. Especially, I am grateful to Dr. Hahma for his guidance and encouragement through these years, and for molecular modeling calculations and writing several Matlab programs enabling the analysis of the measurement data. I also owe big thanks to Professor Henrik Kunttu for his support and advice in the final stages of the thesis. Dr. Shreedhar Bhat and M.Sc. Jenni Ranta are greatly acknowledged for their substantial help in the synthesis work. I also want to thank Professor Seppo Syrjälä and M.Sc. student Juha-Pekka Pöyry for the rheological measurements carried out at Tampere University of Technology.

I want to express my warmest thanks to Dr Roland Pein for giving me the opportunity to work at DLR and for providing facilities for rheometry. My sincere thanks go to Rosa Brändle for her help and friendly discussions we had during the year in Germany. I want to thank Docent Manu Lahtinen for DSC and laboratory technicians Mirja Lahtiperä for MS, Reijo Kauppinen for NMR, Elina Hautakangas for elemental analysis, Paavo Niutanen for his help in SEM sample preparation, and Pia Petriläinen and Leena Koskela for their help when I needed something in the lab. I want to acknowledge all the colleagues in the Nanoscience Center for creating such a pleasant and relaxed working atmosphere. Professor Mladen Žinić and Docent Sami Hietala are acknowledged for the revisions and valuable comments concerning this thesis.

Finally, I am grateful to my family for their endless support throughout my studies. I wish to express my deepest gratitude to my wife Päivi, to our son Ikla, and Elli for their unfailing love and support, and for bringing the joy in my life.

Financial support from the Academy of Finland (grants 106998 and 107014) and the University of Jyväskylä are gratefully acknowledged.

Jyväskylä, February 2011

Kimmo Leivo

ABBREVIATIONS

ButOH	1-butanol
C_6H_6	benzene
CCl_4	carbon tetrachloride
CD	circular dichroism
cgc	critical gelation concentration
$CHCl_3$	chloroform
CT	charge transfer
DCE	1,2-dichloroethane
Decalin	decahydronaphthalene
DecOH	1-decanol
Digol	1,2-dichloroethane
DMF	*N*,*N*-dimethylformamide
DMSO	dimethyl sulfoxide
DodecOH	1-dodecanol
DSC	differential scanning calorimetry
EtOAc	ethyl acetate
EtOH	ethanol
HSP	Hansen solubility parameter
FTIR	Fourier transform infrared spectroscopy
IR	infrared spectroscopy
LMOG	low molecular weight organogelator
LVE	linear viscoelastic
MeOH	methanol
2-MeOEtOH	2-methoxyethanol
MIAK	5-methyl-2-hexanone (methyl isoamyl ketone)
mgc	minimum gelation concentration
MS	mass spectroscopy
NMR	nuclear magnetic resonance
OctOH	1-octanol
PentOH	1-pentanol
PhMe	toluene
PrOH	1-propanol
SEM	scanning electron microscopy
TeNF	2,4,5,7-tetranitrofluorenone
THF	tetrahydrofuran
TNF	2,4,7-trinitrofluorenone
UV-Vis	ultraviolet - visible

Contents

1 Introduction

The discovery and design of low molecular weight organogelators (LMOGs) has been an expanding research area in the last few decades due to their promising physical and morphological properties as well as their potential industrial applications[1–3]. The LMOGs are small organic molecules which have the ability to self-assemble into a complex three-dimensional network, and already at low concentrations turn a wide variety of organic solvents into gels. Most gels are thermoreversible as LMOGs aggregate through a combination of non-covalent interactions such as hydrogen bonding, π-π stacking, donor-acceptor, van der Waals and solvophobic interactions[2,4].

There exists an enormous structural diversity among these gelators; however, in most reported cases immobilization of the solvent is based on a single gelator component. In recent years, there has been a growing interest in two- or multicomponent gelator systems, since the "bottom-up" fabrication of LMOGs the two-component systems increase the possibility to control the self-assembly process and gel properties[5].

The aims of this thesis were the synthesis of self-assembling materials capable of acting as efficient gelators for hydrocarbons and alcohols, and investigation of the gel properties and the factors effecting gelation. One objective was to prepare LMOGs with ability to bind metal nanoparticles or other molecules into the gel structure. The gelation is based on non-covalent interactions to obtain thermoreversible organogels. In order to use the gelator to bind other materials than the solvent it is essential to design a system that forms a gel by such interactions that do not bind readily to the adsorbent surfaces, such surfaces are typically very polar compared to the organic solvent to be gelled. If gelation is based on polar interactions the gelators contain typically functional groups which form a gel by intermolecular (hydrogen) bonding and hence functional groups are not available to bind other materials into the gel.

Pyrene based LMOGs were discovered about five years before this study was initiated[6]. In light of the objectives of this study, two-component pyrene based low molecular weight organogelators were selected as the base system

due to the promising properties of the gels based on them. Pyrene based LMOGs have shown the ability to gelate various solvents below 1 wt-% concentration through donor-acceptor and π-π stacking interactions. The melting points of the thermoreversible gels, typically 60 - 90 °C, are suitable for applications. A two-component gelator system enables better control on the gelation ability and the properties of the gel.

One goal for the work was to elucidate the relationship between molecular structure of the gelators and gel formation. It was tried to understand the gelation ability of the two-component system in different solvents by correlating the gelation results with solubility parameters that are widely used to predict solubility of polymers[7]. In this study, experimental results from various methods were used to gain information on the properties of the gels of 15 different pyrene based LMOGs. The experimental research is mainly focused on the rheological properties of the nanostructural and multidimensional gels. The effect of the solvent, gelator equivalency, pyrene, crosslinker molecule, functional groups and alkyl side chain length of the pyrene based gelator on the gel properties have been studied.

This thesis presents the efforts made for understanding the complex self-assembly process of pyrene based LMOGs and the factors effecting the properties of the gels of alcohols. The self-assembly of low molecular weight organogelators is not thoroughly understood in general, the results obtained in this work constitute a step forward in estimation and control of gelation ability and gel properties of the two-component gelator system. The methods utilized in this study include rheometry, UV-Vis spectroscopy, scanning electron microscopy, differential scanning calorimetry and computer modeling.

2 Review of the literature

2.1 Definition of gel

Gels are common in everyday life and their applications can be found in many fields such as food processing, medicine, cosmetics, materials science, hydrometallurgy, lubrication, pharmacology and electronics[1,2,8]. Lipowitz was one of the first to report on gelation of aqueous solutions by lithium urate in 1841[9]. Although gels are nowadays abundant and widely studied the definition of a gel is still somehow illegible from the scientific point of view. In 1861 Thomas Graham[10] gave the following description:

> *While the rigidity of the crystalline structure shuts out external expressions, the softness of the gelatinous colloid partakes of fluidity, and enables the colloid to become a medium for liquid diffusion, like water itself.*

In 1926 Dorothy Jordon Lloyd[11] stated that the colloid condition, the gel, is one which is easier to recognize than to define and made the following statement:

> *Only one rule seems to hold for all gels, and that is that they must be built up from two components, one of which is a liquid at the temperature under consideration, and the other which, the gelling substance proper, often spoken of as the gelator, is a solid. The gel itself has the mechanical properties of a solid, i.e. it can maintain its form under the stress of its own weight, and under any mechanical stress it shows the phenomenon of strain.*

Due to several subclasses of gels attempts to link the microscopic and macroscopic properties of a gel have resulted many different definitions[12,13]. Recently Weiss and Terech gave general criteria to classify a substance as a gel: (1) it has a continuos microscopic structure with macroscopic dimensions that is permanent on the time scale of an analytical experiment and

(2) it is solid-like in its rheological behaviour despite being mostly liquid[8]. This classification contains no clear statement about the minimum number of components in the system, but generally a gel consists of two or more components, one of which is a liquid, present in a substantial quantity[14]. The gels themselves have mechanical properties of solids and under any mechanical stress the gels show strain. Macroscopically, for the screening purposes the definition of Lloyd is still practical: if it looks like a "Jello", it must be a gel[11].

2.2 Gelation and classification of gels

Gels are comprised of a solvent and an elastic cross-linked network, which prevents the solvent form flowing at the microscopic level as the solvent is trapped mainly by surface tension[1]. Gels can be classified based on their origin, constitution, the type of cross-linking that creates the network and the medium they hold (Figure 2.1). Organogels are gels where the medium is an organic solvent like hexane or octanol. If the medium is water or mixture of water with minor component of an organic solvent the gel is called a hydrogel. If there is no medium at all, the gel is called a xerogel.

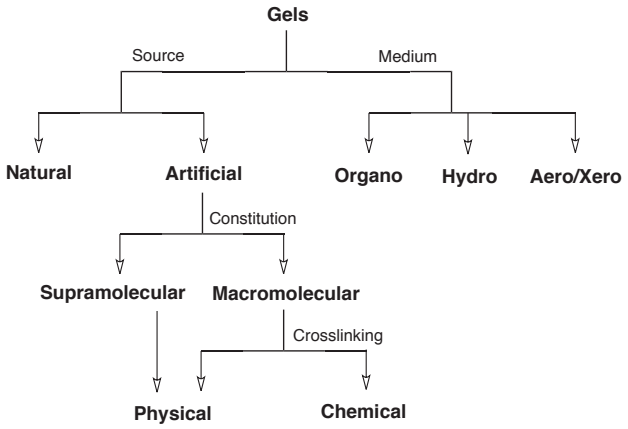

Figure 2.1: Classification of the gels[2].

Most of the naturally occurring gelators like gelatin and starch are macromolecular species and they form gels by physical cross-linking, mainly hydrogen bonding. Synthetic gelator molecules can be divided on the basis of their constitution into macromolecular and molecular. The gel network from macromolecules can form through chemical cross-linking or physical interactions (Figure 2.2). Chemical gels are crosslinked covalently and the gelation

is irreversible. Compounds able to form chemical gels include cross-linked polymers[2] and inorganic oxides[15]. Physical gels are formed by weak non-covalent interactions such as van der Waals interactions, hydrogen bonding, $\pi - \pi$ stacking, donor-acceptor interactions, metal coordination, solvophobic forces and even by London dispersion forces alone[4,16,17]. Usually the self-assembly of the gelator molecules is not the result of only one type of interaction but rather a combination of different interactions. Due to non-covalent interactions physical gels are thermally reversible and easily liquefied by heating. Examples of these systems include mineral clays, polymers, proteins, colloids and small organic compounds called low molecular weight gelators (LMWGs). In polymer gels molecular sub-units are relatively large (Figure 2.2) compared to LMWGs which form a network by self-assembly of small gelator molecules (usually $\lesssim$ 2000 Da) through a combination of non-covalent interactions[8]. These compounds are the topic of this thesis and from now on only organogels based on these compounds will be discussed, and these will be referred to as low molecular weight organogelators (LMOGs).

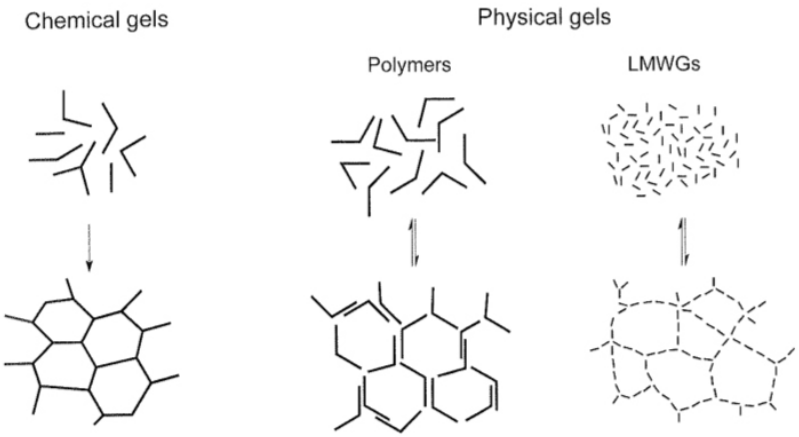

Figure 2.2: Schematic representation of chemical and physical gels[18].

Gelation is not thoroughly understood phenomenon and the design of new LMOGs is a challenging task where one should consider the events and intermolecular interactions, which occur during the gelation. There are interactions between the gelator molecules themselves and between the gelator and the solvent molecules. Gelator molecules aggregate and form long fibrous structures. There must be an interaction between the individual fibers in order to form a 3D-network. However, this interaction should not be too strong to avoid precipitation or even crystallization. The solvent also has a crucial role in the gelation process. Gelation of LMOGs is taken to be a

hierarchical assembly process including the following steps:[19]

1. Dimerization of two individual molecules.
2. Oligomer formation by interaction of dimers with further molecules.
3. Formation of polymer fibrils of approximately the same width as the molecular building blocks (ca. 1-2 nm) by extension of the oligomers.
4. Fiber formation by bundling of fibrils (ca. 20 - 50 nm width).
5. Interactions of fibers to give an effectively infinite, interconnected network spanning the entire sample (the least well understood aspect of the gelation process).
6. Immobilization of the solvent by the fiber network, generally by surface tension effects.

Gelation can be considered to be a competition between solubilization and phase separation. The growth of gel fibers is usually directional and in competition with other forms of aggregation such as micelles, lamellae and crystals[20].

2.3 Structural diversity of low molecular weight organogelators

A wide diversity of low molecular weight compounds have been discovered that are able to gelate organic solvents. Traditionally, gelators have been found serendipitously eg. from failed crystallization attempts. In the recent years the interest in LMOGs has grown rapidly due to the striking and versatile properties of these systems and many potential applications of such gels. As the state of knowledge on self-assembly of gelator molecules has broadened factors effecting on gelation, it has increased interest in controlling gelation and designing of the new LMOGs.

Any given molecule may have gelation ability if the following general criteria apply[19,21]: 1) the molecule must be partially soluble in the solvent of choice but not too soluble, otherwise it will simply dissolve, 2) the molecule must be partially insoluble in the solvent of choice but not too insoluble otherwise it will simply precipitate, 3) the molecule must have the potential to form multiple non-covalent interactions with itself, 4) van der Waals forces are usually present to support the gelation process, 5) these non-covalent

interactions should occur in a directional manner and 6) there is a factor to induce fiber cross-linking for network formation.

It was recently estimated that over 1000 low molecular weight gelators have been reported[22]. Even though there is a large structural diversity within LMOGs, they have a common feature that they gelate many organic solvents through intermolecular self-assembly due to a combination of non-covalent interactions. LMOGs have been derived from various systems including hydrocarbons, fatty acids, saccharides, steroids, amides, amino acids, ureas, aromatic molecules, metal complexes and dendrimers. Only a brief overview will be given here to describe various types of LMOGs and the interactions leading to self-assembly. Several reviews have been published for more extensive overview of LMOGs[1–4,13,20,23–26].

2.3.1 LMOGs based on hydro- and fluorocarbons, fatty acids and esters

A series of elongated hydrocarbons (C_{24} **1**, C_{28} and C_{36}) gelate short alkanes, alcohols, halogenated liquids and silicone oil (Figure 2.3)[16,27]. Gelation occurs through van der Waals forces and the diversity of the gelated liquids and the gel stability increase with increasing length of the alkane chain. Long *n*-alkanes are structurally the simplest possible LMOGs and their gels with *n*-alkanes are the simplest class of organogels that can be formed.

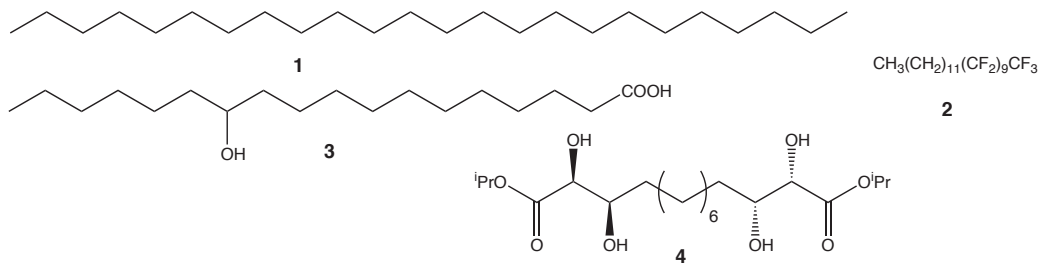

Figure 2.3: LMOGs based on simple structures include alkanes, fluorocarbons, fatty acids and esters.

Semifluorinated n-alkanes, like **2** (Figure 2.3), are capable to gelate aliphatic and aromatic solvents[28,29]. The self-assembly occurs due to the immiscibility of the fluorocarbon part of the molecule with the hydrocarbon solvent indicating that solvophopic effects play an important role in gelation. Significantly higher gelator concentrations are needed for gelation compared to *n*-alkanes.

The fatty acid compound 12-hydroxystearic acid **3** (Figure 2.3) is an example of functionalised fatty acids that are known to gelate chloroform, aliphatic and aromatic hydrocarbons[30–32]. In addition to van der Waals forces gelation process is driven by hydrogen bonding. From a series of tetrahydroxy diesters, the compound **4** with eight methylene connections resulted the lowest minimum gelation concentration and was able to gelate through hydrogen bonding both polar and nonpolar solvents including toluene, cyclohexane and water and even lager and wine[33].

2.3.2 LMOGs based on saccharides

Saccharide based LMOGs gelate solvents through formation of intermolecular hydrogen-bond based gel network. The monosaccharide derivatives (Figure 2.4) can be divided into three groups based on their structure: open-chain[34] (**5**, **6**), cyclic[35] (**7**) and acetal-protected cyclic monosaccharides[36–38] (**8** - **10**). Disaccharide derivatives[39] and acetylated cyclodextrins[40] have also been reported to function as organogelators. Many of the saccharide derivatives are able to form a gel in both organic solvents and aqueous mixtures.

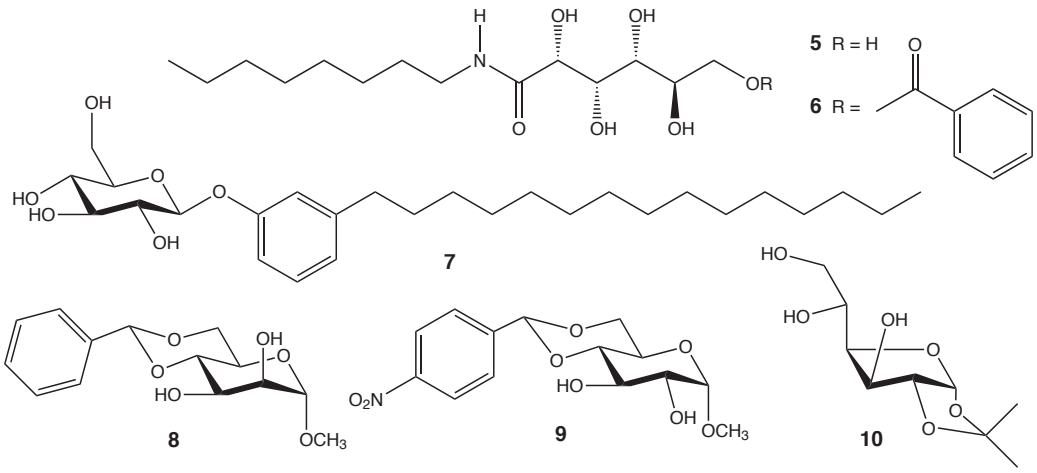

Figure 2.4: LMOGs based on saccharides.

Glucose derivative of open-chain monosaccharide **5** (Figure 2.4) is able to gelate 1,2-xylene; however, addition of a benzoyl group yields **6** which forms a thermoreversible gel in various solvents such as alcohols, acetonitrile, acetone, chloroform and aromatic solvents[34]. The gels in aromatic solvents were clearly the most thermally stable. Cyclic saccharide compound **7** gelates through hydrogen bonding and solvophobic interaction cyclohexane and several aromatic solvents. It can not form a gel in acetone, DMF,

DMSO, alcohols or water but all these solvents were gelated as a 1:1 mixtures with water[35]. The gelation ability was strongly decreased by unsaturation of the aliphatic alkyl chain.

Acetal-protected cyclic monosaccharide examples include methyl 4,6-benzylidene derivatives **8** and **9** (Figure 2.4). The α-manno derivative **8** forms colorless gels in alkanes, aromatic solvents, carbon disulfide, diphenyl ether and water[36]. FTIR, NMR and X-ray diffraction analyses indicated that gelation occurs through hydrogen bonding, π-π and van der Waals interactions. The α-glucopyranoside derivate **9** gelates alcohols and the similar range of solvents as the derivative **8** with the exception of alkanes[37]. Acetal-protected **10** has also three unprotected hydroxyl groups in the five-membered glucofuranose ring and is able to gelate CCl_4, chloroform, cyclohexane and various aromatic solvents[38,41]. The 1,3:2,4-dibenzylidene sorbitol (DBS) is another well known acetal-protected organogelator[42].

2.3.3 LMOGs based on steroids

Steroids are a class of naturally occurring lipids. The first steroid based LMOGs for hydrocarbon solvents were *D*-3β-hydroxy-17,17,dipropyl-17a-aza-homoandrostanyl-17a-oxy **11** and its amino analogue (Figure 2.5)[43] The gelation ability of steroids vary with the position of the unsaturated functionalities.

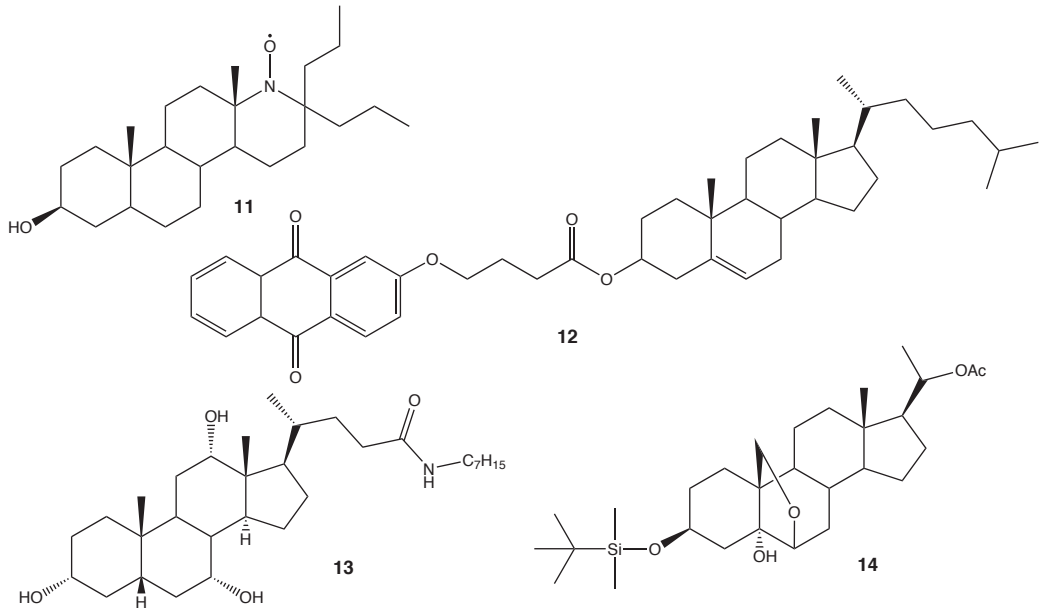

Figure 2.5: LMOGs based on steroids.

The ALS gelators consist of an aromatic group (A) which is connected by a linker (L) to a steroid (S) based molecule[1]. Mukkamala and Weiss[44] prepared a series of anthraquinone-steroid based LMOGs and found that the functionality and the length of the linker group between anthraquinone and steroid have a strong effect on the gelation ability. Compound **12** is one example of ALS molecules that is able to gelate various hydrocarbons, alcohols, acrylates and silicone oil (Figure 2.5). Various ALS-type organogelators have been reported including anthracene[45,46], azobenzene[47], porphyrine[48] and stilbene[49] as the aromatic group.

Bile acids derivatives are another type of steroid based LMOGs[50]. An alkyl derivative of cholic acid **13** (Figure 2.5) forms a transparent and thermoreversible gel in cyclohexene and several aromatic solvents[51]. A silylated non-cholesteryl steroid LMOG **14** has an unique asymmetric structure due to the presence of an oxygen bridge which acts as a hydrogen bond acceptor and is able to gelate hydrocarbons and tetraethyl orthosilicate[52].

2.3.4 LMOGs based on amides, amino acids and ureas

Intermolecular hydrogen bonding between N-H and C=O plays an important role in gelation with LMOGs based on amides, amino acids, ureas and urethanes[24]. Compound **15** (Figure 2.6) is an example of *N*-alkyl perfluoroalkanamides which forms gels in several organic solvents including aliphatic hydrocarbons, alcohols, toluene, CCl_4 and silicone oil[53]. Gelation occurs due to the incompatibility of perfluoroalkyl and alkyl chains leading to formation of lamellar aggregates that are stabilized by intermolecular hydrogen bonding between the amide groups.

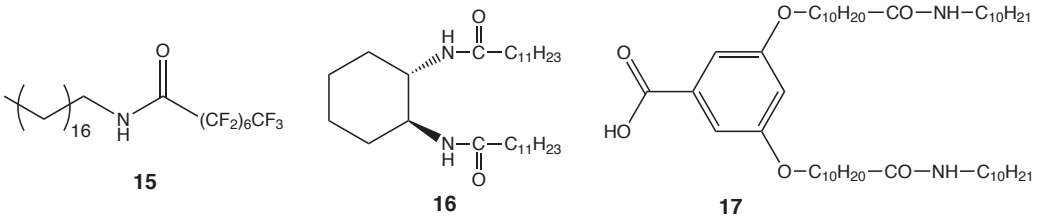

Figure 2.6: LMOGs based on amides.

The hydrogen bonding between the amide groups of adjacent molecules and van der Waals interaction of the long alkyl chains enable enantio-pure *trans*-isomers (1R, 2R and 1S, 2S) of bis-amide derivate **16** (Figure 2.6) to gelate various solvents like hydrocarbons, alcohols, ketones, esters and mineral oil[54,55]. The corresponding *cis*-isomers did not gelate any of the solvents

gelated by the *trans*-isomers and the racemic mixture of *trans*-**16** resulted weaker gels than the pure enantiomers did. Aromatic bisamide derivative **17** is able to gelate benzene, toluene and *p*-xylene, but not hexane due to insolubility[56]. The analogue of **17** without the amide groups was not a LMOG for aromatic solvents showing that hydrogen bonding between the amide groups is required for gelation.

Different functional groups in the amino acid based LMOGs allow formation of gel fibers through hydrogen bonding, dipole-dipole and other van der Waals interactions. The gelation ability depends on the structure of the amino acid residue and typically the gelation efficiency increases when a molecule includes more than one peptide unit[4]. The solvent also has significant effect on the gel fiber network structure as well as on the properties of the gel[57]. Compound **18** (Figure 2.7) is a fatty acid amide of *L*-alanine which is able to gelate various aliphatic and aromatic hydrocarbons[58]. FTIR studies showed that the gelation by **18** occurs via hydrogen bonding that is significantly affected by the polarity and protic nature of the solvent. Elongation of the fatty acid chain increases van der Waals interaction as well as mechanical strength and thermal stability of the gel.

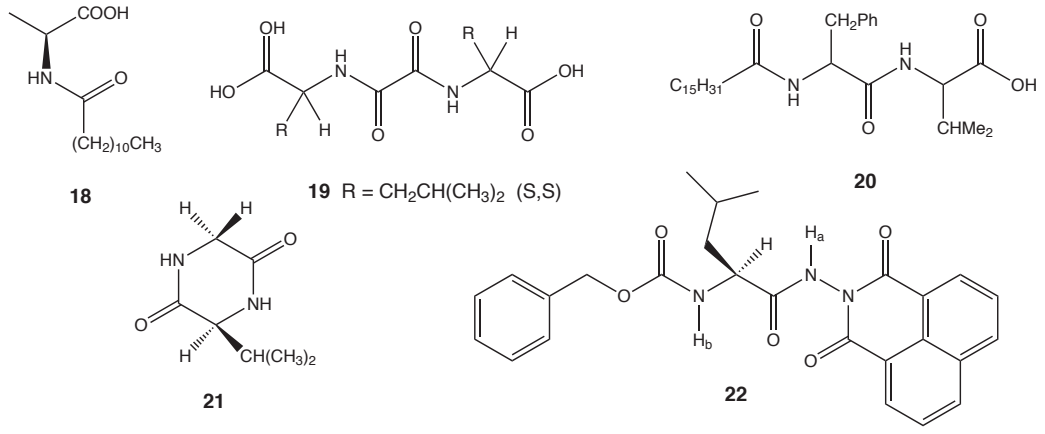

Figure 2.7: LMOGs based on amino acids.

Bis-leucine oxalyl amide **19** is an efficient LMOG for various organic solvents such as alcohols, dioxane, acetone, THF and water (Figure 2.7)[59]. However, its racemate and meso-diastereoisomer is not a gelator. Stabilization of the gels is mainly due to intermolecular hydrogen bonding involving the oxalyl amide fragments and carboxylic groups. Another dipeptide example **20** includes a free carboxylic group but also a long alkyl chain and a phenyl group, and it forms stable gels in various aromatic solvents and carbon tetrachloride[60]. Corresponding sodium salt of **20** showed enhanced gelating

efficiency in aromatic solvents but could not gelate CCl_4. Other examples of linear amino acid organogelators include N-alkanoyl-alanine derivatives[61] and terminally protected tripeptides[62,63].

Cyclic amino acid compounds such as valine containing cyclophanes[64] and cyclo(dipeptide)s[65] have shown gelation ability. Compound **21** (Figure 2.7) represents an example of cyclic dipeptide of glycine and valine, which is able to immobilize organic solvents like ethanol, methoxybenzene, soybean and silicone oil. FTIR and X-ray studies indicated that solvents are gelated by **21** through hydrogen bonding between the amide bonds. Gelation in toluene with leucine based gelator **22** containing a naphthalimide group occurs in two phases. Firstly, the molecules are stacked up head-to-tail by hydrogen bonding and subsequently the columns are assembled into aggregates through intercolumnar π-π stacking interactions leading to a gel fiber network[66].

The lowest molecular mass LMOG currently known is N,N'-dimethylurea (M_W 88) which is able to form a gel in silicone oil and carbon tetrachloride[67]. Another monourea LMOG derivative **23** (Figure 2.8) gelates water and various solvents including cyclohexane, benzene, toluene and CCl_4. The compound **24**, containing a longer alkyloxy chain, gelates the above mentioned solvents, and in addition polar solvents such as methanol, acetone and dioxane[68]. Temperature variable ^{1}H NMR studies showed that both hydrogen bonding between the amide groups, and π-stacking interaction exist in gels.

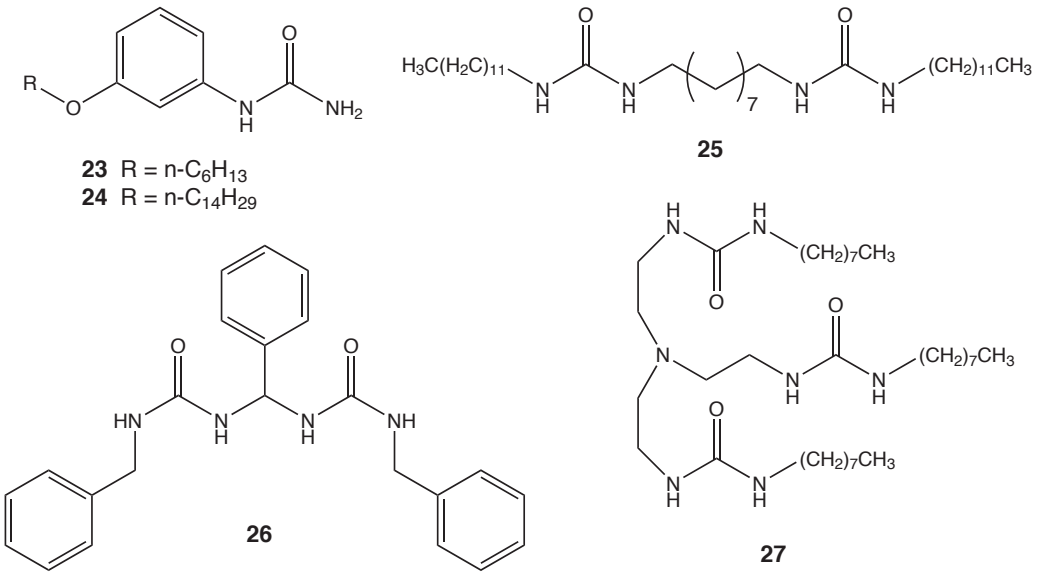

Figure 2.8: LMOGs based on ureas.

Bis-urea derivatives are well known for their gelation ability in organic solvent. Compound **25** (Figure 2.8) forms a three-dimensional gel network through hydrogen bonds between the urea moieties in hexadecane, *p*-xylene, tetralin, cyclohexanone and *n*-butyl acetate[69]. Also geminal bis-urea derivatives[70], like compound **26**, and tris-urea derivatives[71–73], like compound **27**, are efficient LMOGs for a wide variety of organic solvents.

2.3.5 LMOGs based on aromatic molecules

Many LMOGs contain aromatic groups such as benzene, pyridine, anthracene and porphyrin. The π-π stacking among aromatic moieties contribute to gelation and often aromatic groups can be considered as the major structural elements. One of the simplest LMOG based on aromatic molecules are the di-*n*-alkoxy-benzene derivatives, like **28** (Figure 2.9) which is able to gelate acetonitrile, propylene carbonate, DMF and dimethylacrylamide through π-π stacking, dipole-dipole and van der Waals interactions[74]. Substitution of the benzene moiety with an anthracene moiety[75–77] or an anthraquinone moiety[78] yields an efficient organogelator for hydrocarbons and alcohols.

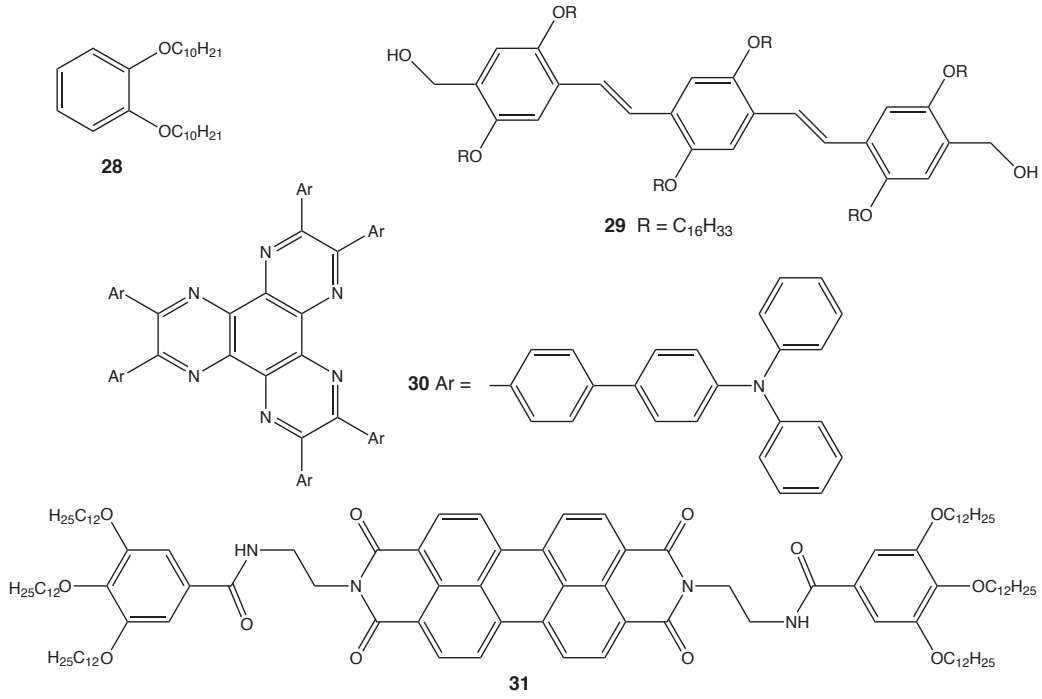

Figure 2.9: LMOGs based on aromatic molecules.

Compound **29** (Figure 2.9) is an example of oligo(*p*-phenylenevinylene)

(OPV) based organogelators[79,80]. The compound gelates via hydrogen bond assisted π-π interaction aliphatic and cyclic hydrocarbons, aromatic solvents and chloroform. Ajayaghosh *et al.*[17,81] observed that selective fluorescent resonance energy transfer occurs exclusively from the OPV gel nanostructures to entrapped Rhodamine B. The emission of the dye could be switched off in a thermoreversible fashion which revealed the importance of the self-assembly in energy transfer and light harvesting.

Compound **30** is composed of a rigid hexaazatriphenylene core and six flexible aromatic side chains, and gelates nitrobenzene, aniline and (R)-1-phenylethyl alcohol (Figure 2.9)[82]. In the self-assembly the central aromatic core is stabilized first by π-stacking and the flexible aromatic chains stabilize the aggregate to create phase separation and thus prevent crystallization. Perylene bisimide **31** is a semiconductor which is able to gelate various organic solvents including aliphatic and aromatic solvents, ethers and triethylamine at low concentrations[83,84]. The three dimensional fibrous network is generated from the self-assembly of **31** through hydrogen bonding between the benzamide groups and strong π-π stacking interaction. Other examples of efficient LMOGs containing large aromatic groups include pyrene[85] (see Chapter 2.4), porphyrin[86,87] and phthalocyanine[88–90] derivatives.

2.3.6 Metal complex based LMOGs

LMOGs containing a bound metal atom include systems in which the metal acts as a linker between the ligands. In another class of systems the metal coordination is not directly involved in linking LMOG molecules together and gelation is due to other non-covalent interactions. Binding of a metal ion to a gelator can affect self-assembly modes and allows the gelation ability to be tuned[91]. One of the earlier gelling complexes copper(II) β-diketonate **32** containing eight paraffinic chains formed green gels in cyclohexane (Figure 2.10)[92]. The role of the copper in the gelation and kinetics of aggregation were studied by electron paramagnetic resonance (EPR) which has been rarely used to study gels.

Trisubstituted zinc(II) porphyrin gelator **33** including three long ester linked alkyl chains and one carboxylic acid gelates cyclohexane at low concentration (Figure 2.10)[93]. The presence of both the free carboxylic acid and the metal center is essential for gelation because the corresponding tetraester is not a gelator[94]. Non-aromatic organogelators **34** and **35** represent iron(III) and aluminum(III) complexes of dodecylmethylphosphinic acid that are able to form a gel in dodecane[95]. Aggregates are formed by bridging where one ligand bridges two metal atoms.

A 8-quinolinol platinum(II) chelate derivative **36** gelates various sol-

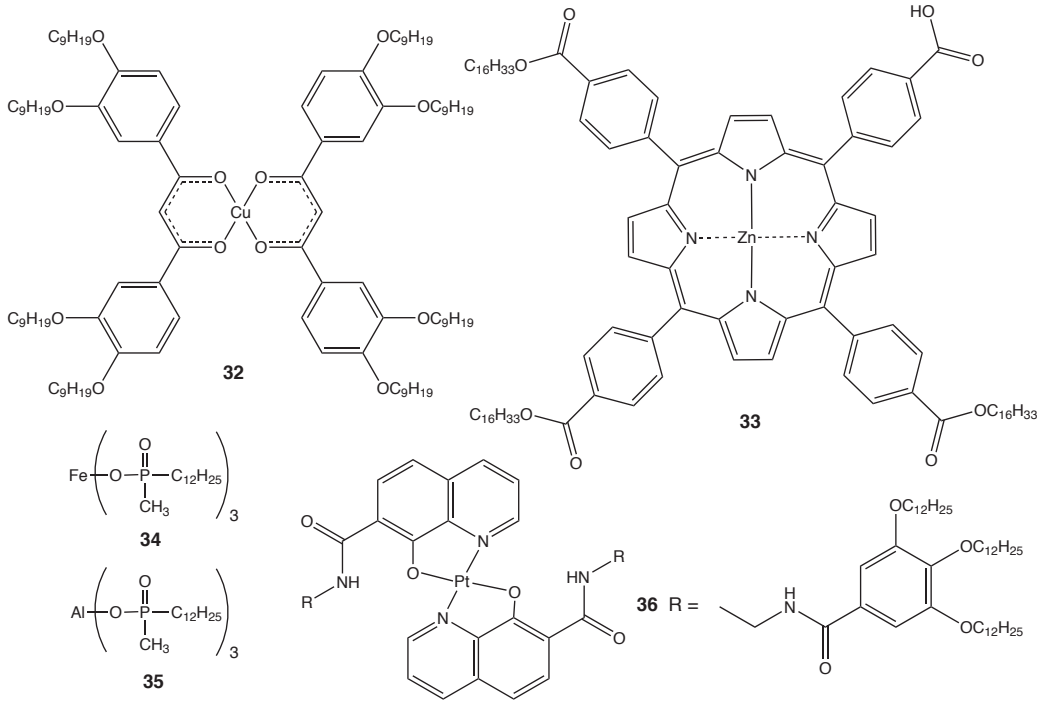

Figure 2.10: Metal-complex based LMOGs.

vents including hydrocarbons, alcohols, aromatic solvents, dichloromethane, acetone, THF, dioxane and DMF (Figure 2.10)[96]. Strong π-π interaction of the chelate moieties leads to gelation and sol-gel phase transition results in thermo- and solvatochromic behavior of visible colour and a colour change in the phosphorescence emission.

2.3.7 Two-component LMOGs

A true two-component LMOG system consists of two molecules in a way that neither component do not act as a gelator alone[5]. Such systems can be formed either from dissimilar but complementary molecules or from similar molecules that differ only in their structural motifs. A system is also referred to as a two-component system if the behavior of a one-component LMOG system can be altered significantly by adding a second component. Addition of the second component can increase the gelator efficiency[97] and the thermal stability of the gel[98]. Sometimes a two-component system is able to gelate solvents that are not gelated by one-component system[51,99]. The ratio of the components has typically significant effect on the gel structure and properties. In two-component gels, initially two distinct components form com-

plexes that subsequently self-assemble through various non-covalent interactions to form a gel fiber network. A wide variety of systems including saccharides[37], steroids[51,100], amines[101], amides[102], amino acids[103,104], ureas[105], aromatic molecules[106], metal complexes[107], and in many cases a combination of these systems[108–110] have been reported as two-component LMOGs. A few examples of two-component LMOGs are presented in Figure 2.11.

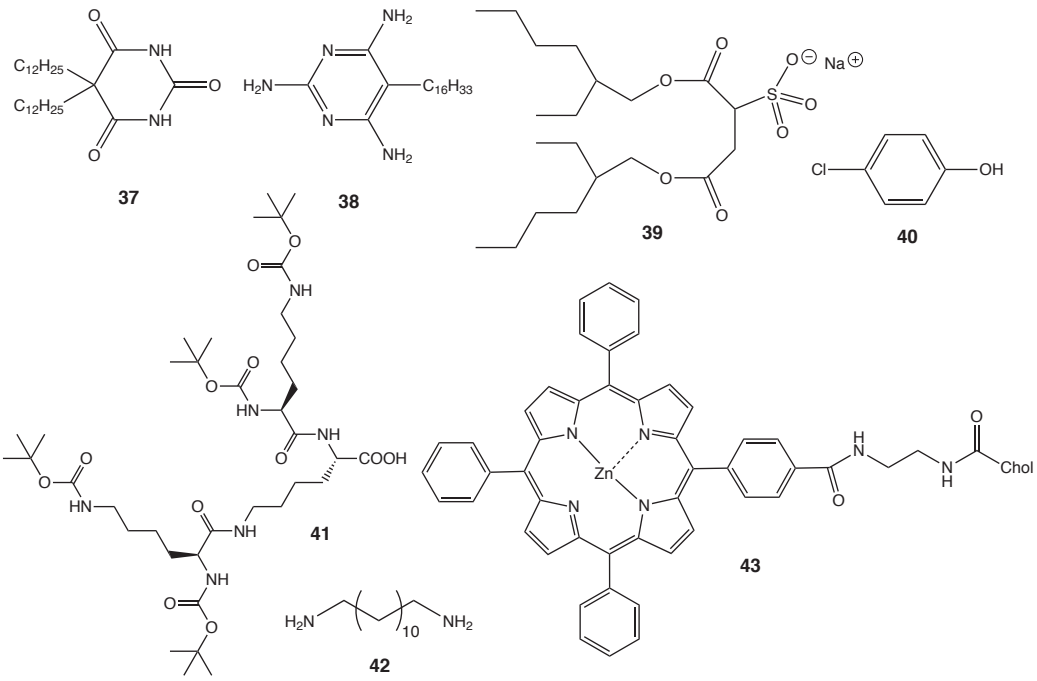

Figure 2.11: Two-component LMOGs.

Hanabusa *et al.*[111] were the first to report a two-component organogelator system in 1993. An equimolar mixture of barbituric acid **37** and triaminopyrimidine **38** derivatives (Figure 2.11) was able to gelate organic solvents including cyclohexane, chloroform, DMF and carbon tetrachloride via hydrogen bonding.

A well-known twin-tailed anionic surfactant sodium bis(2-ethylhexyl) sulfosuccinate **39** (AOT) forms spherical reverse micelles in nonpolar solvents but an addition of a phenol derivative, like *p*-chlorophenol **40**, results in gelation in isooctane, toluene and hexadecane (Figure 2.11)[112–115]. However, *ortho*-substituted phenols did not form gels, apparently due to the steric hindrance of the hydroxylic group[116]. Furthermore, a micellar solution of AOT in *n*-decane can be transformed into a transparent gel by adding a trace amount of a bile salt, sodium deoxycholate[117].

A dendritic two-component organogelator consisting of *L*-lysine based dendrimer **41** and diaminododecane **42** (Figure 2.11) forms a gel in toluene, dichloromethane and acetonitrile[118–120]. The individual components form a complex via acid-amine interaction and ^{1}H NMR spectroscopy indicated that the complexes are self-assembled into gel fibers through intermolecular dendron-dendron hydrogen bonding. The acid-amine interaction is a common interaction in various two-component systems[101,104,121,122].

A zinc(II) porphyrin and cholesterol (Chol) derivative **43** gelates aromatic solvents such as benzene, toluene and *p*-xylene (Figure 2.11)[98,123]. The gelation ability of **43** can be improved by adding [60]fullerene. The gel-sol transition temperature increases significantly with increasing equivalent of added [60]fullerene. UV-Vis and CD spectroscopy studies showed that the optimum ratio was 2:1 **43**/[60]fullerene when two porphyrin moieties form a sandwich complex with a fullerene. Despite the size of the fullerene unit also one component [60]fullerene based amphiphile derivative has been reported to form gel fibers in methanol[124]

Maitra *et al.*[6] were the first to report donor-acceptor (charge transfer) promoted gelation in organogels based on a two-component organogelator composed of a pyrene derivative and 2,4,7-trinitrofluorenone (see Chapter 2.4). Later donor-acceptor interaction has been reported in several other two-component systems including saccharides[37,125], anthrylidene derivative of arjunolic acid[99] and dinitrobenzoate derivatives[126].

2.4 Pyrene containing low molecular weight gelators

Pyrene is commercially widely used to make dyes and dye precursors. Pyrene is also one of the most popular molecular probes in fluorescence spectroscopy[127] because of many beneficial properties such as efficient excimer formation[128,129], long singlet life time[130], ready functionalization[131] and the appearance of delayed fluorescence[132]. Pyrene and its derivatives have been applied in liquid crystals[133–135], photonic devices[136,137] and in non-covalent modification of carbon nanotubes[138]. In the field of gels pyrene has been used as a fluorescent tag in low molecular weight gelators to evaluate their minimum gelation concentration, self-assembly, gel structure and morphology through UV-Vis, circular dichroism and fluorescence spectroscopy[139–143].

There exists a wide structural diversity in pyrene containing low molecular weight gelators. Pyrene derivatives act as one- or two-component hydro- or organogelators and the gelation ability depends on the linker and the side

chain attached to the pyrene moiety (Figure 2.12). There can be several side chains attached to pyrene moiety by linkers. In most cases the self-assembly of the gelators is driven by the π-π interaction between pyrenes and hydrogen bonding between the side chains.

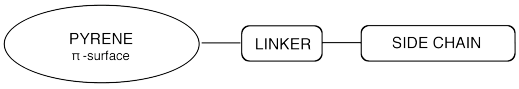

Figure 2.12: Schematic presentation of a pyrene based gelator which can include several side chains with linkers.

2.4.1 Pyrene containing low molecular weight organogelators

The Maitra group has carried out pioneering work on pyrene based low molecular weight organogelators (Figure 2.13) which they serendipitously discovered while studying pyrene substituted bile acid-based molecular tweezers[6,85,144–146]. The minimum gelation concentrations of these materials are typically below 1 wt-% range and the gel melting points are typically between 60 - 80 °C. The gels are thermally reversible and they remain stable for several months at room temperature.

Compounds with reverse amide (**44**, **45**), urethane (**47**, **48**) and urea linkers (**50**) are one-component organogelators which are able to gelate various organic solvents, primarily hydroxylic and hydrocarbon solvents[85]. In a reverse amide linker (NHCO) the bonding orientation is reversed compared to an amide group (CONH). Gelation ability depends on the alkyl side chain length as compounds **46** and **49** are not able to gel any of the solvents gelled by their long-chain analogues. The gelation ability depends also on the π-surface area because a naphthalene group instead of pyrene in **44** does not yield gelation.

Cooperation of π-π stacking and hydrogen bonding interactions are necessary for gel fiber formation for many pyrene based organogelators. The stacking and destacking of the pyrene units during gelation and melting were observed by temperature-variable UV-Vis and fluorescence spectroscopy. IR spectroscopy provided evidence for the presence of the hydrogen bonds in the gel[85]. Compounds **51** and **52** with an urethane linker and a chiral and branched side chain gelate only hydrocarbons. Formation of chiral aggregates was observed with optical rotation and circular dichroism (CD). Different enantiomers showed bands with opposite signs while the sol did not

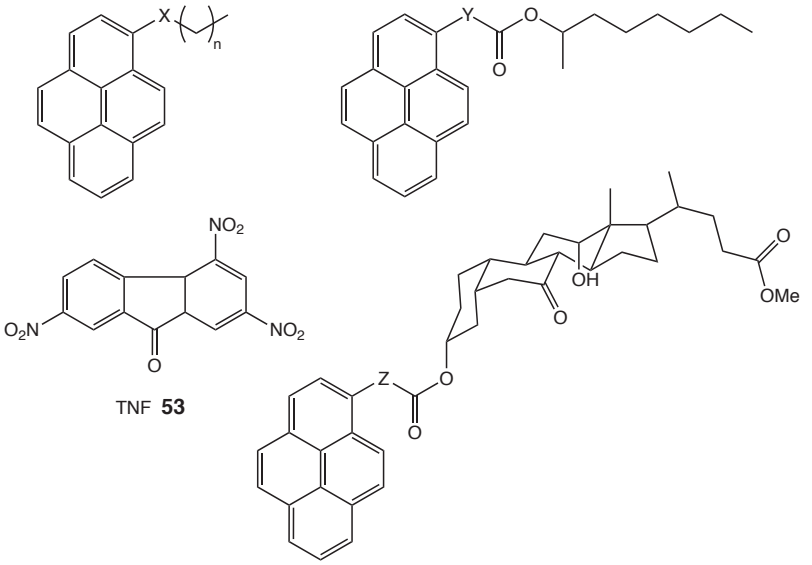

X	n	
NHCO	16	**44**
NHCO	10	**45**
NHCO	6	**46**
NHCOO	15	**47**
NHCOO	11	**48**
NHCOO	9	**49**
NHCONH	15	**50**

Y = NH	(R)-**51**
Y = NH	(S)-**52**

X	n	
COO	15	**54**
COO	7	**55**
CH_2	14	**56**
CH_2	10	**57**
CH_2	0	**58**
O	13	**59**
CONH	15	**60**
OCO	14	**61**

Y = --	(R)-**62**
Y = --	(S)-**63**

Z = --	**64**
Z = NH	**65**

Figure 2.13: Pyrene based one- and two-component organogelators by Maitra's group[6,85,145] and TNF (**53**).

show any CD band[85,145]. The X-ray crystal structure of a chiral gelator also indicated the presence of the π-π stacking, hydrogen bonding and van der Waals interactions in the gel[146].

Pyrene derivatives with ester (**54**, **55**, **62**, **63**, **64**), methylene (**56** - **58**) and ether (**59**) linker are two-component organogelators as they form gels only in the presence of 2,4,7-trinitrofluorenone (TNF, **53**). TNF is well known for its ability to form charge transfer complexes. By complexation TNF increases photoconductivity of pyrene derivative 1,4-bis(pyren-1-ylmethylidene)aminomethylbenzene[147] and polymers[148]. Substantial increase in the charge transfer band with pyrene derivatives ($\sim$500 - 600 nm depending on the gelator) was observed by UV-Vis during gelation due to formation of the charge transfer complex with TNF and changes in chemical shifts for the protons of TNF were observed by NMR measurements[85,145].

Two-component organogelators with methylene and ether linker gelate hydroxylic and hydrocarbon solvents but with ester linker only hydroxylic solvents. Amide (**60**) and reverse ester (**61**) linkers result in non-gelators. Compound **65** with urethane linker and bile acid side chain forms gels with TNF in chloroform and hydroxylic solvents. The gelation ability of the bile acid derivatives is also dependent on the position of the pyrene unit in the steroid backbone[6]. It is important to emphasize that the above mentioned

one-component organogelators lose their gelation ability in the presence of TNF. Presumably pyrene-TNF interaction causes improper hydrogen bonding and donor-acceptor interaction geometries which inhibit the gel fiber growth[85]. A two-component system including molar ratio of 1:2 of **66** and TNF (**53**) produced a gel in styrene-divinylbenzene but precipitated as microcrystals within 24 h (Figure 2.14)[149].

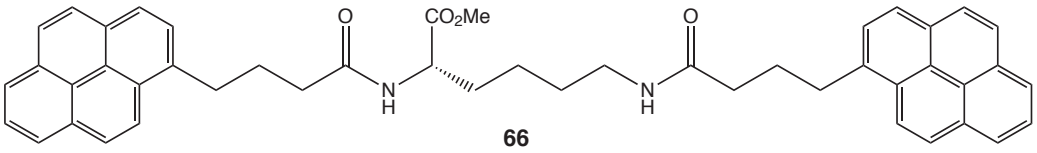

66

Figure 2.14: Two-component organogelator including two pyrene units.

Pyrene substituted dialkyl L-glutamine derivative **67** (Figure 2.15) is able to gelate benzene and cyclohexane[150]. Fluorescence spectroscopy indicated the formation of fibers via π-interaction between the pyrenes in addition to hydrogen bonding among the amide groups. Interestingly in organogel of the binary system with the porphyrin disubstituted dialkyl L-glutamine derivative energy-transfer from the pyrene to the porphyrin was detected. Sugar-pyrene based one-component gelators show interesting gelation properties (Figure 2.15). Compound **68** with glucose residue and sulfonamide linker to pyrene is an ambidextrous gelator and can gelate water and hydroxylic solvents[151]. Hydrogen bonding between the glucose residues is the driving force for gel network formation but also π-π stacking between pyrenes exists.

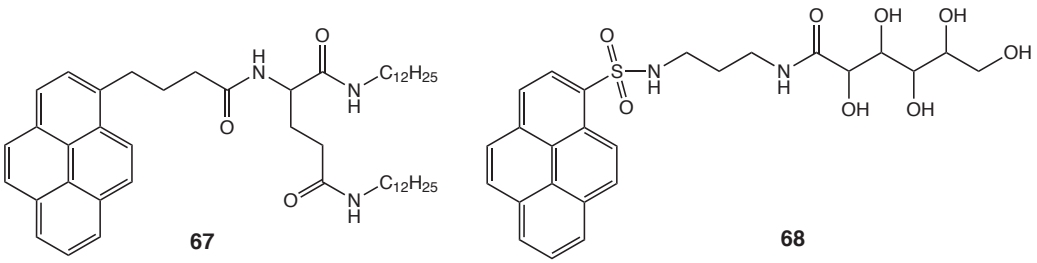

67 **68**

Figure 2.15: Pyrene based one-component organogelators.

Pyrene-containing oligo(glutamic acid) based one-component fluorescent organogelators **69** - **71** (Figure 2.16) were found to gelate hydrocarbon solvents but no gels were observed in alcohols, halogenated or aromatic solvents[152]. The largest of the gelators (**71**) showed the lowest minimum

gelation concentration. The gelator molecules self-assemble to form helical columnar assemblies through intermolecular hydrogen bonding between peptide residues and π-π stacking between the pyrene moieties. Pyrene interaction is a necessity for successful gelation because an analogue compound **72** without pyrene moiety did not form gels in common organic solvents. There is a strong correlation between hydrogen bonding networks of amide groups and the motion of the pyrene moieties. The fluorescence properties depend on the flexibility of the pyrene moieties which can be tuned by using an alkyl spacer between the pyrene and the amino acid moiety (**70**).

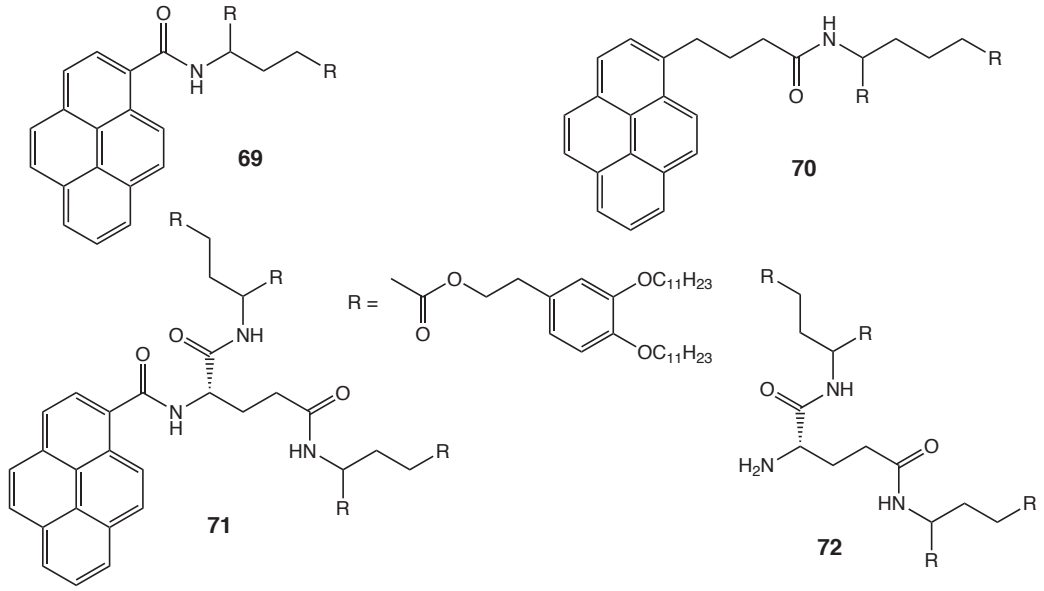

Figure 2.16: Pyrene-oligopeptide organogelators **69** - **71** and non-gelator derivative without pyrene **72**.

Recently a pyrene containing organogelator with ethynyl linker was reported. Pyrene substitution with rigid 4-ethynylphenylaminoacyl derivatives results fluorescent compounds with interesting properties (Figure 2.17). The disubstituted pyrene derivative **73** forms thermoreversible and highly fluorescent gels in cyclohexane, toluene and DMF[153]. Gelation is the result of hydrogen bonding, π-π interactions between pyrenes, and possibly also between the phenyl subunits. In addition, van der Waals interactions of the long alkyl chains play an important role. Morphology of the gels was found strongly dependent on the solvent. However, the tetrasubstituted pyrene derivative **74** is not a gelator, but instead a liquid crystalline material which remains stable up to 200 °C.

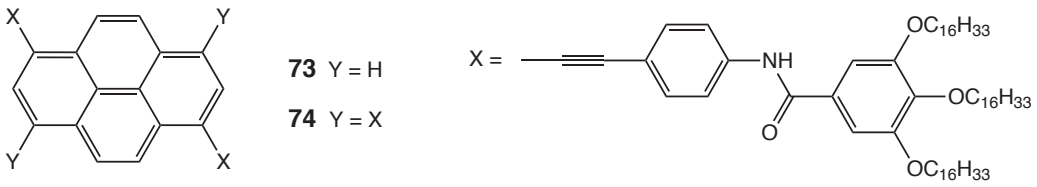

Figure 2.17: Ethynyl-pyrene based disubstituted organogelator **73** and tetrasubstituted liquid crystalline material **74**.

2.4.2 Pyrene containing low molecular weight hydrogelators

Certain pyrene containing LMOGs can gelate also water. Earlier the ambidextrous gelator **68** was already introduced. Bhuniya and Kim[154] developed a series of monosaccharide based one-component hydrogelators using a methylene linker followed by a reverse amide group (Figure 2.18). Compounds **75**, **76**, **80** - **83** and **85** are able to form gels in water and gelation ability is dependent on their amino acid and monosaccharide units. The most efficient hydrogelator **82** is able to gelate water at 1.04 mM concentration (53400 water molecules/gelator molecule), and interestingly the hydrogel of **76** is able to sense insulin at low concentrations. The self-assembly of the gelators is driven by hydrogen bonding and π-π stacking interactions as indicated by FTIR and fluorescence spectroscopy studies.

Vancomycin **88** and its derivatives can act as one- or two-component hydrogelators (Figure 2.19). Vancomycin-pyrene derivative **87** is an efficient hydrogelator and gelates water at 0.36 wt-% concentration ($\sim$23000 water molecules/gelator molecule). Gel fibers are formed via π-π stacking of the pyrene moieties and several hydrogen bonds among the peptide groups[155]. Interestingly, hydrogelator **87** exhibits 8- to 11-fold higher activity against Enterococci than the antibiotic vancomycin **88** itself. Pyrene-alanine derivative **89** forms only a viscoelastic liquid but as a two-component system with vancomycin **88** at least 10^6-fold increase in the storage modulus (G') was observed[156].

A sugar-pyrene gelator **90** with ethyl linker is able to gelate 2:8 mixture of water and DMSO[157]. Butylidene group is responsible for the self-assembly and weak interactions between pyrenes lead to gel formation. No gelation was reported with derivatives **91** - **93**. A hydrogelator **94** composed of pyrene and an amphiphilic three-branched unit gelates a mixture of water and methanol by π-π stacking of pyrenes and hydrogen bonding among reverse amide groups of the linker[158]. In contrast, **95**, with a reverse ester

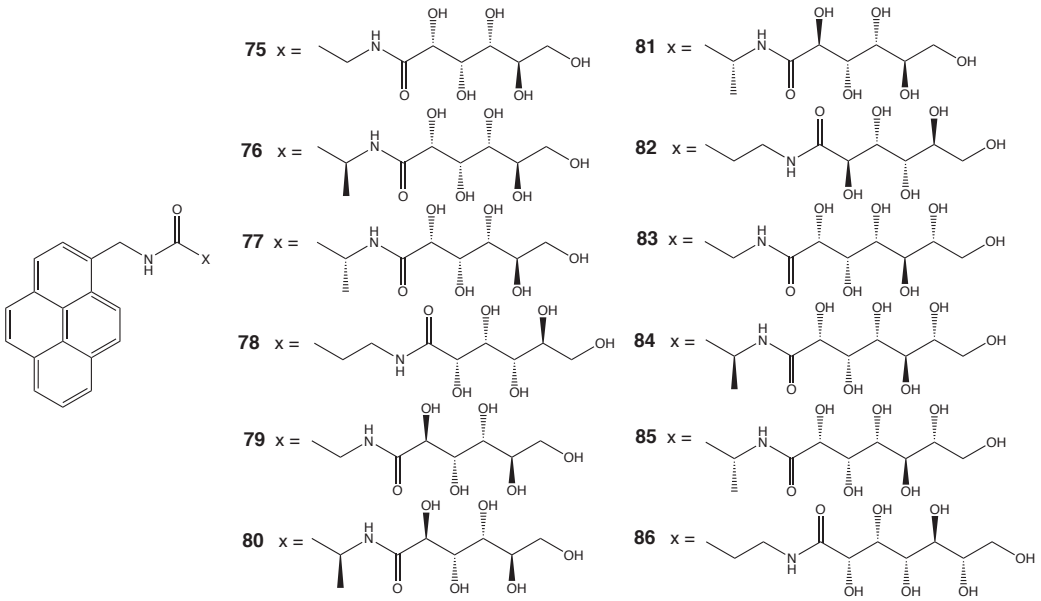

Figure 2.18: Pyrene-monosaccharide based one-component hydrogelators.

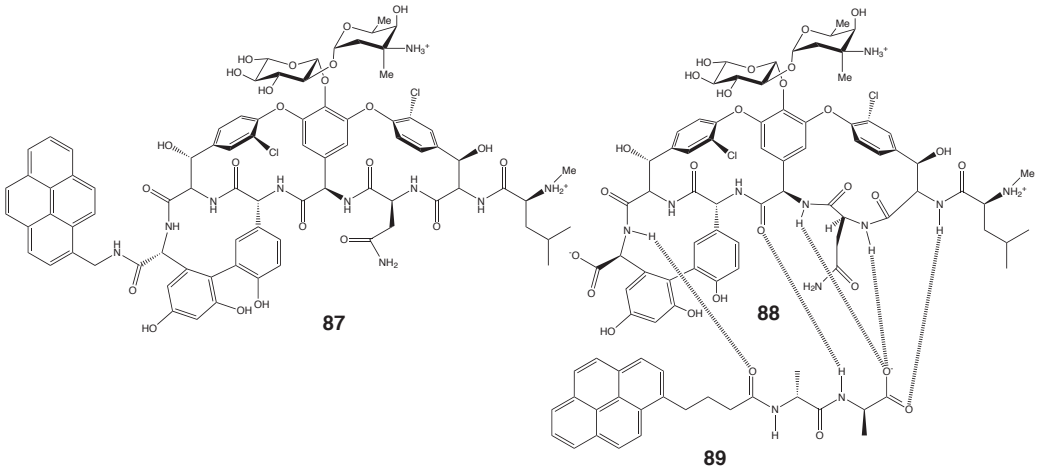

Figure 2.19: One- and two-component pyrene-vancomycin based hydrogelators.

linker did not form gel at the same concentration.

Pentapeptide derivates **96** - **99** (Figure 2.22) are hydrogelators under acidic conditions[159]. For example, compound **96** gelates water when pH is lower than 2.5 and the gel has the gel-sol transition temperature of 88 °C. Corresponding pentapeptides without pyrene are not able to form gel in wa-

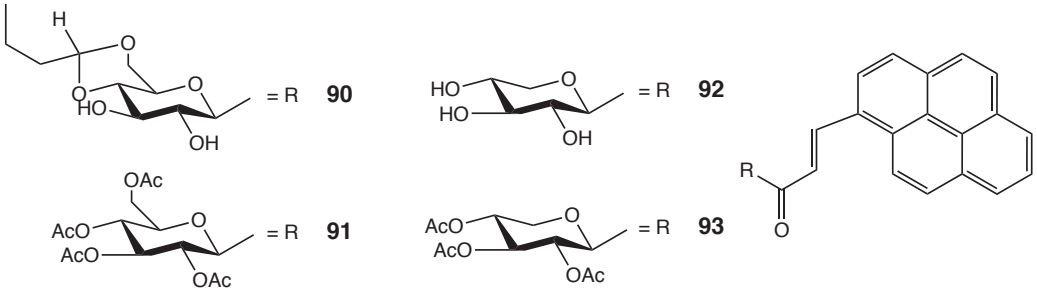

Figure 2.20: Pyrene-sugar based one-component hydrogelators.

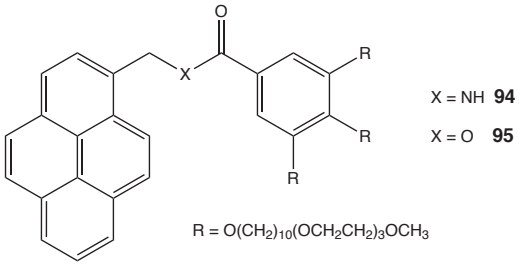

Figure 2.21: One-component hydrogelators composed of pyrene and an amphiphilic three-branched unit.

ter, but also napthalene (in **98** and **99**) or fluorene as an aromatic moiety yields a hydrogelator. Fluorescence and CD spectra indicated that the balance between π-π interactions and hydrogen bonding of the molecules leads to gelation. Compounds **96** and **98** resulted in the mechanically strongest hydrogels according to the rheological measurements. Excellent viscoelasticity is due to the efficient π-π stacking of pyrenes, the least steric bulk of the side chain in **96** and several carboxylic groups in **98**.

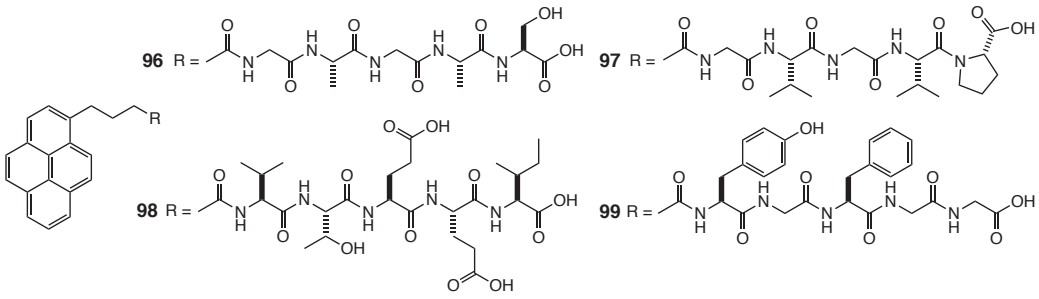

Figure 2.22: One-component hydrogelators composed of pyrene and pentapeptide derivatives.

2.5 Characterization of gels

Gels are very challenging to study due to their relatively disordered nature and structural properties that extend from the molecular to micrometer scale. Various experimental techniques have been applied to study self-assembly and gelation ability of LMOGs, morphology, and thermotropic and rheological properties of the gels. Part of the techniques apply to all types of gels while sometimes the applicability depends on the molecular structure of the gelator and the solvent. Generally, correlations between the structure of the gelators and the bulk properties of the gel can be understood by combining results obtained by several techniques.

2.5.1 Gel formation and phase diagram

The first step is to study the gelation ability of LMOGs in different solvents. The maximum solubility of the LMOGs corresponds to the saturation point of the system. This point is also called the critical gelation concentration (cgc) and self-assembly occurs if the gelator concentration is higher than cgc[160,161]. In partially gelated samples the gelator concentration is above cgc and some gel fibers are formed. In such cases the concentration is below the minimum gelation concentration (mgc) which is needed for sample-spanning gel network. The mgc value takes into account both the dissolved gelators and the self-assembled gelators that form the gel network. Both the cgc and mgc are strongly dependent on temperature and increase with temperature.

Gelation is usually tested by heating a mixture of the gelator or gelators and the solvent, and the hot solution is allowed to stand and cool down to room temperature. Inverted test tube method[162–164] is the simplest and most commonly applied method to evaluate the state of the sample. If the sample does not flow under gravitation it is regarded as a gel. More complex rheological methods can be used to differentiate weak and strong gels from each other (see Chapter 2.5.5).

The solubility of LMOGs and mgc increase with temperature and further characterization of the gels includes determination of the phase diagram, which is a plot of the gel-sol transition temperature T_{gs} vs the gelator concentration (Figure 2.23). The T_{gs} can be determined by the inverted test tube method, dropping ball technique, bubble motion, temperature sweep rheometry, differential scanning calorimetry and different spectroscopical methods (fluorescence, IR, EPR, NMR, UV-Vis, CD)[1,46,165–168]. Instead of T_{gs} the sol-gel transition temperature T_{sg}, as obtained from cooling the sample, can be used; however, this temperature differs from T_{gs} due to hysteresis effects. The T_{gs} corresponds to the temperature at which the gel network is partly

dissolved and the remaining gel fibers are unable to sustain a mechanically stable net

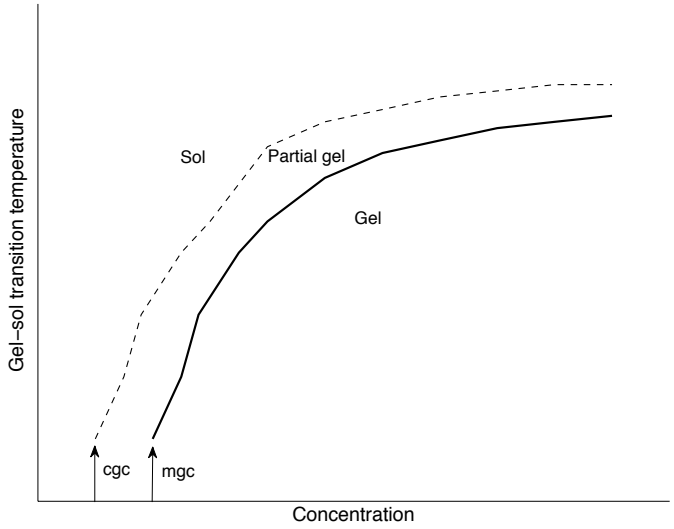

Figure 2.23: Schematic phase diagram for a gelator. The dashed curve represents the solubility curve.

2.5.2 Thermodynamics of gelation

A change in the physical state of the sample such as melting and dissolution can be related to the difference in the heat flow between the sample and reference cell in differential scanning calorimetry (DSC). The peak temperature in a heating curve corresponds to the gel-sol transition temperature T_{gs}. The enthalpy of the gel-sol transition can be determined directly by measuring the amount of heat absorbed in an endothermic phase transition[168,169] and it can provide an insight into the thermodynamics of the gelator-gelator interactions. Both heating and cooling modes can be performed to measure both endothermic and exothermic transitions for thermoreversible gels. However, dilute systems such as gels result often in weak and broad and/or multiple transition peaks and interpretation of the data can be complicated[165,166]. Multiple transition peaks can be due to dissolution of gelators, structural reorganization, conformational rearrangement of the peripheral substituents and various modes of aggregation[157,165,170].

Another common method ascribes gel-sol transition to melting or dissolution of gelator crystals[171] and at a given gelation temperature T_g the gelator concentration (c) corresponds to the solubility of its crystals in an ideal solution:

$$ln\, c = -\frac{\Delta H_m}{RT_g} + constant, \tag{2.1}$$

where ΔH_m is the enthalpy of melting of the neat gelator and R is the gas constant. Elimination of the constant gives

$$ln\, c = -\frac{\Delta H_m}{R}\left(\frac{1}{T_g} - \frac{1}{T_m}\right), \tag{2.2}$$

where T_m is the melting temperature. The ΔH_m values from equation 2.2 are generally slightly higher than values obtained from DSC[46,172]. Equation 2.2 can be used to determine both the enthalpy (ΔH_m) and entropy (ΔS_m) for the gel-sol transition as

$$ln\, c = -\frac{\Delta H_m}{RT_g} + \frac{\Delta S_m}{R}. \tag{2.3}$$

Furthermore, the Gibbs free-energy change and the aggregation constant K at room temperature can be calculated. The aggregation constants are suitable for evaluating gelation properties and aggregation tendencies of LMOGs[173,174].

2.5.3 Supramolecular aggregate formation

Information on the organization of the gelators can be acquired by spectroscopic techniques like UV-Vis, CD, fluorescence, IR and NMR. These methods have generally limited ability to characterize the gel phase due to its solid nature; nevertheless, unique information can be obtained on intermolecular interactions that can not be observed by other techniques. Measurements can be carried out as a function of temperature to obtain information on the gel formation process by studying spectral changes between the solution and the gel phases. UV-Vis and fluorescence spectroscopy can be used to monitor absorption, and fluorescence properties upon gel formation to obtain deeper insight into interactions such as π-π stacking, charge transfer, hydrogen bonding[80,139,175–177]. Increase of the intensity of various bands are generally observed if the stacking of the aromatic units and formation of the charge transfer complex occur upon gelation.

Circular dichroism (CD) is a suitable method to study self-assembly of chiral gelators into helical nanostructures[44,178,179]. Usually a hot sol does not show any CD band, but different enantiomers result bands with opposite signs indicating formation of helical aggregates in the gel state[85,145]. Infrared spectroscopy (IR) is an useful method to provide information on the role of

hydrogen bonding in the process of gelation by studying characteristic peak shifts between dissolved gelators and gelators in the gel phase[180–183].

Information on the gelator aggregate structures and component selection processes can be obtained by NMR spectroscopy by detecting regioselective changes in both line widths and chemical shifts of NMR active nuclei upon gel formation[114,164,184]. Generally, NMR is used in the solution phase prior to gelation because motion of a gelator in the gel is restricted and undetectable by NMR. However, it has been reported that the remaining dissolved gelators and the gelators in the mobile gel fiber regions in the gel phase can be studied[185].

Single crystal X-ray diffraction can be applied on crystals of LMOGs to study organization of the gelators. Single crystal studies[186,187] are limited by the difficulty in obtaining suitable crystals for diffraction and correlation between crystal structure of the gelator and organization in the gel fiber still remains speculative. Powder X-ray diffraction (XRD) of dried gel samples can give more precise information on the molecular packing within the gel. Conformation and packing of the gelator in the gel is known if it matches the crystalline state by single crystal diffraction or other structural analysis for the same morphology[27]. The information is only useful when the molecular packing of the single crystal coincides with the gel fibers[188–190]. The results must be treated with care as there are several studies where the single crystal structures do not match the gel diffraction patterns[27,191,192].

2.5.4 Structure of gels

The structural characterization of the LMOG gels is a compulsory step in the description of gelation. The morphology of the three-dimensional network of gel fibers and the nature of the connections can be studied by several techniques at the 0.1 - 1000 nm scales. An extensive picture on the structural arrangement from the molecular to the supramolecular level can be obtained by combining methods of microscopy, scattering and spectroscopy.

Optical microscopy provides information about the gel structure[164,193–195] but it is less used probably due to insufficient spatial resolution (diffraction limit). More widely used direct imaging techniques include scanning electron microscopy (SEM) and transmission electron microscopy (TEM). A gel sample is first allowed to dry on a substrate and coated under vacuum with a thin metallic layer to enhance image contrast. The dried and coated xerogel is placed in ultra-high vacuum and imaged with an electron beam. Electron micrographs are therefore images of at least partially collapsed gel structures since perturbations can occur during drying and coating. Typically self-assembled fibers, tapes and ribbons are observed.

A gel can been studied in its native state by cryo-electron microscopy techniques (Cryo-EM) where rapid freezing is applied for vitrification of the solvent and to prevent thermal motion of the gelator network causing much less perturbation in the gel sample[19,196]. Cryo-EM micrographs show typically more extended three-dimensional spongelike morphology, in which the solvent is immobilized and observed as cavities within the gel network[120,197]. Atomic force microscopy (AFM) is also suitable to investigate gel fiber thickness and morphological features of the gel and it is often used along with electron microscopy techniques[146,198].

Structural information can also be obtained by indirect scattering techniques such as small angle X-ray and neutron scattering (SAXS, SANS)[199–201]. Radiation scattering is a nonperturbative method utilizing powerful neutron and synchrotron sources, which are advantageous to study diluted systems such as organogels. The scattering depends on the shape of the gel fibers and in contrast to direct imaging methods, interpretation of data is model dependent. Mathematical analysis can be time consuming and complicated for heterogeneous systems and some preliminary knowledge of the size and shape of the gel fibers is required[202]. If the model is correct, scattering techniques provide absolute quantities on the gel fiber diameter and crystallinity of the gel network in the native state of the gel. Gel formation and melting can be studied also in real time and as a function of temperature[203]. The results are a statistical average for the bulk sample, not just for a small area of it.

2.5.5 Rheological properties of gel

Gel rheology is probably the most important feature of a gel[20]. Molecular gels are solid-like materials showing properties of both solids and liquids. These materials can be rheologically described as cellular solids, colloidal systems or soft glassy materials[19,204]. Rheology is the study of deformation and flow of matter under the influence of stress[205]. Rheological experiments provide information about the deformation of solids and the flow behavior of liquids. Rheological properties can be measured with rotational rheometers operating in a rotational or an oscillatory mode. Typical measurement geometries include parallel plates, cone-and-plate and concentric cylinder systems (Figure 2.24)[206].

Viscosity is a property that describes the resistance of a material to flow[205]. The measurement of viscosity of liquids requires definition of parameters which are involved in the flow with the parallel plate model (Figure 2.25). A lateral shearing force F applied to an area A of the liquid leads to a laminar flow (Newtonian flow) in the liquid layer and the shear stress τ

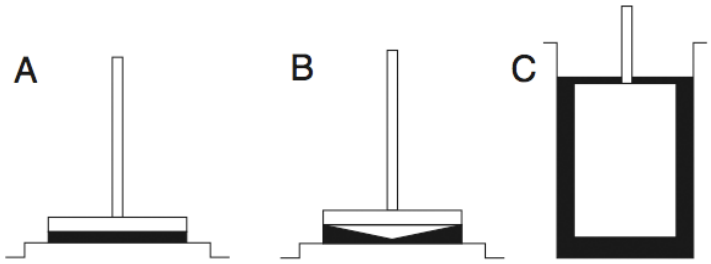

Figure 2.24: Typical measuring systems for rheological experiments include A) parallel plates, B) cone-and-plate and C) concentric cylinder geometries. The black color depicts the sample material.

(Pa) is defined as

$$\tau = \frac{\mathrm{F}}{\mathrm{A}} \tag{2.4}$$

The top layer flows at velocity v and the layer contacting the stationary plate has zero velocity. If the thickness of the liquid is h, then the velocity gradient is defined as shear rate $\dot{\gamma}$ (s^{-1}):

$$\dot{\gamma} = \frac{\mathrm{v}}{\mathrm{h}} \tag{2.5}$$

All materials showing clear flow behavior are referred to as fluids. For ideal viscous fluids the viscosity η (Pas) is defined as the ratio of the shear stress and the corresponding shear rate:

$$\eta = \frac{\tau}{\dot{\gamma}} \tag{2.6}$$

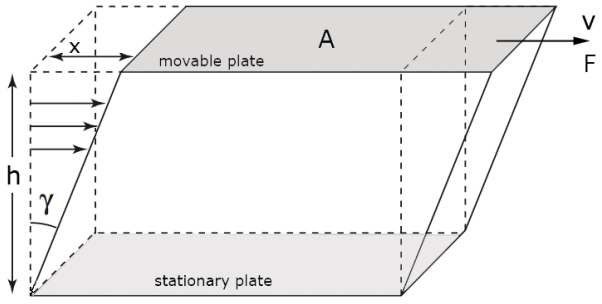

Figure 2.25: Parallel plate model.

The flow behavior of a sample is usually investigated by performing a rotational test at constant temperature to measure the flow curve. The flow curve depicts the relative dependence of the shear stress τ against shear rate $\dot{\gamma}$ and the viscosity curve (η vs $\dot{\gamma}$) is derived from the flow curve using equation 2.6. The viscosity of an ideal viscous (Newtonian) fluid shows no dependency on the shear rate (the flow curve is a straight line) but in many real cases the ratio of $\tau/\dot{\gamma}$ varies with the shear rate and it is called the apparent viscosity. The effect is called shear thinning if the apparent viscosity decreases with increasing rate and shear thickening if the apparent viscosity increases with the increasing shear rate[207]. A few studies on the flow behavior of a gel can be found in the literature[31,183,208–210].

Contrary to viscous fluids, an elastic solid has a definite shape. When lateral force is applied, the elastic solid instantaneously changes its shape, but after removal of the force it returns instantaneously to its original shape. Ideal elastic deformation is described by Hooke's Law:

$$\tau = \mathrm{G}\gamma, \tag{2.7}$$

where G (Pa) is the shear modulus and γ (dimensionless) is the deformation (or strain). The deformation is defined as a ratio of the displacement x and the height of the sample h (Figure 2.25):

$$\gamma = \frac{\mathrm{x}}{\mathrm{h}} \tag{2.8}$$

Gels are soft solids which are considered viscoelastic materials because they show simultaneous behavior of both an ideal viscous fluid and an ideal elastic solid. Viscoelastic properties can be studied by oscillatory tests where the material is subjected to shear stress or strain controlled oscillation. The rate of deformation is determined by the frequency of the oscillation. Generally, a small deformation is used to prevent destruction of the gel structure. When a controlled sinusoidal small strain

$$\gamma(t) = \gamma_o sin(\omega t) \tag{2.9}$$

is applied to a viscoelastic material it causes a stress response

$$\tau(t) = \tau_o sin(\omega t + \delta), \tag{2.10}$$

where γ_o is the strain amplitude, τ_o is the stress amplitude, ω is the angular frequency ($\omega = 2\pi$f, where f is the frequency) and δ is the phase shift angle. The phase shift angle corresponds to the phase shift between γ and τ due to viscoelasticity. Equation 2.10 can be expressed as the sum of in-phase and 90° out-of-phase components with strain[211]:

$$\tau(t) = \mathrm{G}'\gamma_o sin(\omega t) + \mathrm{G}''\gamma_o cos(\omega t), \tag{2.11}$$

where G' is the storage modulus (Pa) and G" is the loss modulus (Pa). The G'-value represents the elastic behavior and is a measure of the deformation energy stored by the sample during the shear process. The G"-value represents the viscous behavior and is a measure of the deformation energy lost during the shear process. For an ideal elastic solid, the strain and the stress are in phase ($\delta = 0°$) and the applied energy is completely stored (G" = 0). For an ideal viscous fluid, the strain and the stress are 90° out of phase and the applied energy is completely dissipated (G' = 0). The lost energy can heat up the sample or it is lost to the surroundings. For viscoelastic materials the behavior is somewhere in between and the phase shift angle is always between 0° and 90°.

The following expressions for the storage and loss moduli are obtained by comparing equations 2.10 and 2.11:

$$\mathrm{G}' = \frac{\tau_o}{\gamma_o} cos\,\delta \tag{2.12}$$

$$\mathrm{G}'' = \frac{\tau_o}{\gamma_o} sin\,\delta \tag{2.13}$$

$$\frac{\mathrm{G}''}{\mathrm{G}'} = tan\,\delta \tag{2.14}$$

The loss tangent $\tan\delta$ is the ratio of the viscous and the elastic portion of the viscoelastic deformation behavior. A sample shows liquid character when $\tan\delta > 1$ (G" > G') and solid character when $\tan\delta < 1$ (G' > G")[205]. Gel formation can be studied by following the loss tangent and the gel point is indicated by the $\tan\delta = 1$ point corresponding to the crossover point G' = G".

As the first oscillatory test an amplitude sweep is carried out to find out a limiting value for linear viscoelastic (LVE) range. The storage (G') and loss (G") moduli are measured at variable amplitudes of controlled shear strain (strain sweep) or shear stress (stress sweep) at constant frequency. Typically a frequency of 1 Hz or an angular frequency of 10 rad/s is used. A sample shows gel character in the LVE range if the elastic behavior dominates the viscous one (G' > G") and liquid character if G" > G'. The LVE range corresponds to a range where both the G' and G" are independent of the applied stress (or strain) and the gel structure remains undisturbed. The limiting value of the LVE range is usually determined as a point where G'-curve begins to deviate noticeably from the LVE plateau indicating that the gel structure is disturbed. The plateau value of the LVE range (G'_{LVE})

describes the rigidity of the gel at rest. The range of the tolerated deviation from the plateau value (e.g. 5 or 10 %) is defined by the user and the values which deviate more are outside of the LVE range[205].

The limiting value of the LVE range corresponds to the yield point τ_y (yield stress) if condition G' > G" holds (Figure 2.26). The gel shows reversible viscoelastic behavior and no significant change in the gel structure occurs at stresses below τ_y. Above the yield point the G' and G" start to decrease which is attributed to partial breakup of the gel that begins to flow. The flow point τ_f corresponds to the crossover point G' = G" where the gel character changes to liquid character and the structure of the gel is breaking to such an extent, that the gel is flowing. The gel character (G' > G") still dominates in the range between τ_y and τ_f and it is called the yield zone[205]. The flow point is still mostly called the yield point in the literature even though τ_y and τ_f usually significantly deviate from each other[76,212].

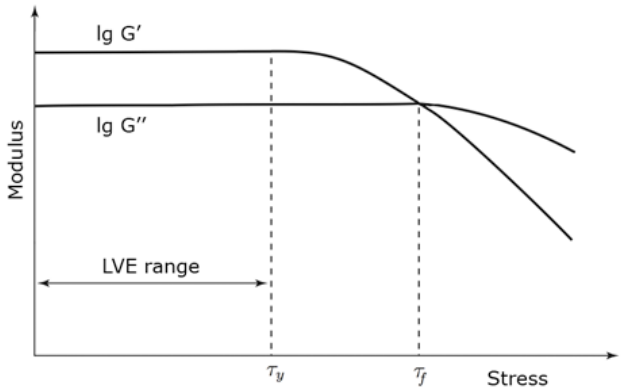

Figure 2.26: Amplitude stress sweep of a gel. The LVE range is limited by the yield point τ_y and the flow point τ_f corresponds to the G' = G" point.

Outside of the LVE range the moduli are decreased rapidly indicating partially collapsed gel network due to shear force, and this behavior is in the most cases non-linear. The non-linear behavior of the rheological parameters can be modeled mathematically but it requires complex calculations and many assumptions. This is why rheological tests are usually carried out only in the LVE range[205].

Gel-like behavior of a sample is usually tested by measuring the magnitudes and ratios of the elastic (G') and loss (G") moduli as a function of frequency. The observed dependence in a frequency sweep provides information about the relaxation and lifetime of the bonds between the gelator molecules[213]. A frequency dependence is observed if the bonds have a tempo-

rary character. An entangled solution shows a viscous fluid character at low frequencies (G' < G"), a cross-over point (G' = G") and an elastic solid character at high frequencies (Figure 2.27 A). This behavior has been observed for solutions of organogel particles[214], wormlike micelles[215], semidilute polymers[216] and polymer melts[217]. Viscoelastic soft solids such as gels show usually only a slight frequency dependence for the whole frequency range (Figure 2.27 B) and the ratio G'/G" is generally 10 or more[31,218–220].

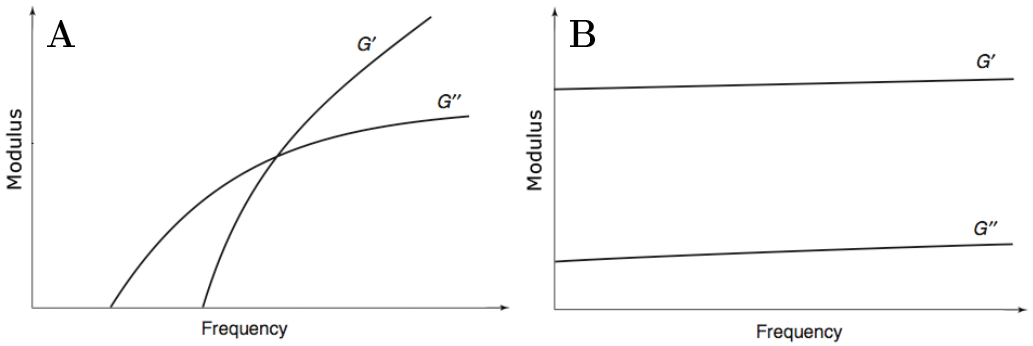

Figure 2.27: Typical frequency sweeps for an entangled solution (A) and a gel (B).

The temperature-dependent behavior of thermoreversible gels can be studied rheologically by performing an oscillatory temperature sweep. The intersection of the curves of G' and G" (G"/G' = $\tan\delta = 1$) has been extensively used as the sol-gel transition temperature T_{sg} (gelation temperature) during cooling and the gel-sol transition temperature T_{gs} (melting temperature) upon heating even though this point is known to be frequency, strain and cooling/heating rate dependent[205,216,221–223].

Chambon and Winter[224–226] developed a more advanced way to determine the gelation temperature or time by using the point at which both G' and G" scale with angular frequency ω^n (n is a relaxation exponent) so that the ratio of G" to G' is frequency independent. This method is more laborious and therefore many researchers still use the crossover point[222,227–229]. The T_{gs} was not affected if a low shear stress (0.2 - 2 Pa) and heating rate ($\leq$ 1 °C min^{-1}) were used[166] and the difference in the T_{sg} value between Winter-Chambon and the crossover point methods was only 0.5 °C when an angular frequency under 2 rad s^{-1} was used[222].

2.6 Applications of LMOGs

The LMOGs have received particular interest since they enable reversible gelation, highly ordered structure of the three dimensional gel network, easy tunability of the molecular gelator structure and the gel properties. While some industries are already making use of organogel technology, many of its potential applications are still in the research and development phase.

The lubrication industry has long used metal salts of 12-hydroxystearic acid to gelate oil- and grease- based lubricants to restrict their mobility[1]. Organogelators can be applied to bind spilled oil and solidification and safer disposal of used oil[13,230]. Crude oil recovery can be enhanced by pumping gel into oil wells[8] and napalm is prepared by gelating fuel for destructive purposes[231]. Organogels have been used in cosmetics[232,233] and in conservation of artwork by cleaning oil paintings[234].

Organogels can be used for molecular recognition which can be applied in enantioselective catalysis, separation techniques and in the formation of supramolecular systems[235]. Chiral recognition has been demonstrated through cooperative interactions between aggregates and gels of bis(ureido)-cyclohexane derivatives with a coaggregating derivative including azobenzene chromophore[235]. Glutamic acid derivatives form functionalized organogels which can be used for enantioselective separation[236]. Irradiation[47], pH[237,238] and humidity[239] -sensitive organogels can be exploited in sensors.

Organogels have been utilized in preparation of reversed and polymerized aerogels for molecular imprinting[240]. Organogel fibers have been employed as template structures to prepare various nanofibrous inorganic materials such as hollow silica[55,241] and TiO_2[242]. Organogels have been extensively used to synthesize and stabilize nanoparticles into the gel structure creating promising materials for potential applications in optics, electronics, ionics, mechanics, biology, fuel and solar cells, catalyst and sensors[3]. Organogels of cholesterol based perylene[243] and oligo(p-phenylenevinylene)[244] derivatives are examples of light harvesting systems which can mimic photosynthesis and may be used in electronic applications. Liquid crystalline behavior has been also shown with organogels. The combination of self-assembled organogelator fibers and liquid crystals may lead to design of new anisotropic phase separated functional materials such as electro-optical displays and organic electro-active materials[245].

Organogel fibers containing electron-conducting groups enable formation of molecular wires[213] which have potential applications in the areas of sensor technology, materials science and catalysis. Several organogel electrolytes based on LMOGs have shown almost identical conductivity as liquids[246,247]. Ionic liquid gels with carbon nanotubes are both ion and elec-

troconductive and have potential for electrochemical applications such as solar cells, sensors and capacitors[248]. Bis-ureathiophene[249,250] and perylene bisimide[83,251] derivatives are both organogelators and organic semiconductors and efficient charge transport within the organogels has been shown. An isooctane gel including ferrite becomes superparamagnetic under applied field of 1000 G and may be used as a precursor for microsensors[252].

Organogels have been utilized as reaction medium for photoreactions[253], esterifications[254], fluorescence quenching[255] and preparation of new gelators[256]. Dye-doped organogels offer suitable medium for lasing and other optical applications[257]. Lecithin, amino acid and fatty acid derivatives are examples of large variety of LMOGs showing potential for drug delivery applications[258,259]. However, relatively few are actually applied in practice due to the lack of information on the biocompatibility and toxicity of LMOGs and their degradation[258]. Organogelation has been applied in structuring transdermal pharmaceuticals[260]. The edible oil organogels have been demonstrated potential applications in both the food and pharmaceuticals industries including the restriction of oil mobility and migration, the replacement of saturated and trans fats, the stabilization of emulsions, and the ability to control the rate of nutraceutical release[261].

3 Results and discussion

3.1 Syntheses

In this study, fifteen pyrene derived low molecular weight organogelator molecules **I** - **XV** were prepared (Figure 3.1). Two of the compounds, **III** and **V**, were known prior to this study. The compounds were synthesized according to a modified known route[85,145]. Synthesis procedure for 1-decylpyrene **II** is presented as an example (Scheme 3.1). The decanoyl chloride was prepared by mixing decanoic acid with excess of thionyl chloride ($SOCl_2$). It should be noted that the acid must be chosen in advance to have carboxylic or ester functionality if a functional group was desired as the end group in the alkyl side chain. The decanoyl chloride was mixed with pyrene in 1,2-dichloroethane and addition of titanium tetrachloride ($TiCl_4$) in ice bath resulted Friedel-Crafts acylation reaction and formation of 1-(pyren-1-yl)decan-1-one.

Molecules containing a keto group next to pyrene were not able to form gels and therefore the keto group was reduced to methylene group by the Wolff-Kishner method. The 1-(pyren-1-yl)decan-1-one and KOH were mixed in diethylene glycol and heated to 180 °C before hydrazine monohydrate was added slowly keeping temperature at 190 - 200 °C under nitrogen atmosphere for 12 h. The temperature was slowly raised to 220 °C and after cooling down 1-decylpyrene **II** was isolated as yellow powder with 88 % yield. All the new compounds were characterized by elemental analysis and spectroscopic techniques (IR, ^{1}H NMR, ^{13}C NMR and MS). Full synthesis procedures and characterization data for all intermediate and end products can be found in the section *Experimental* (Chapter 5.3).

The general procedure for the preparation of pyrene derived LMOGs is simple in principle, but the purification of the compounds to achieve the end product in gram scale can be laborious. The purification of compounds containing functional groups required chromatographic techniques. However, non-functional gelators can be readily recrystallized from hexane after filtration through a column of silica.

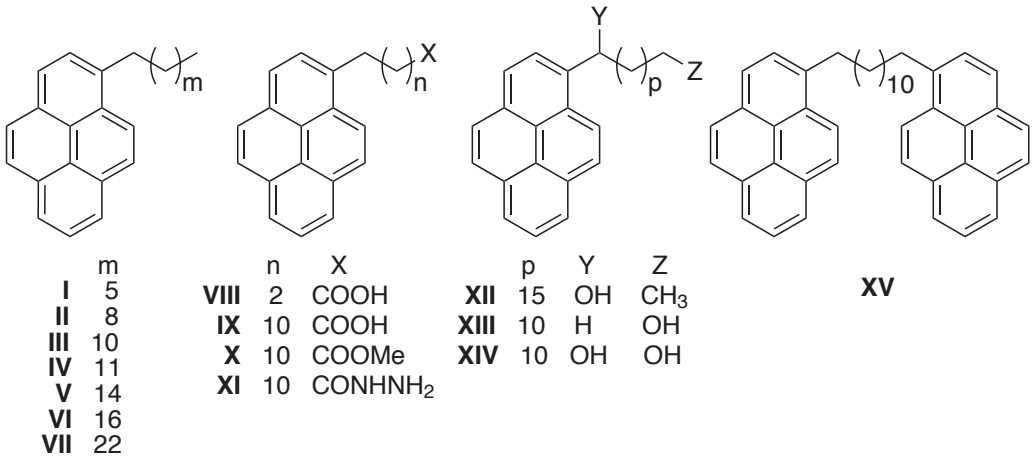

Figure 3.1: Pyrene based LMOGs **I** - **XV** prepared in this work. Previously known compounds **III** (**56**) and **V** (**57**).

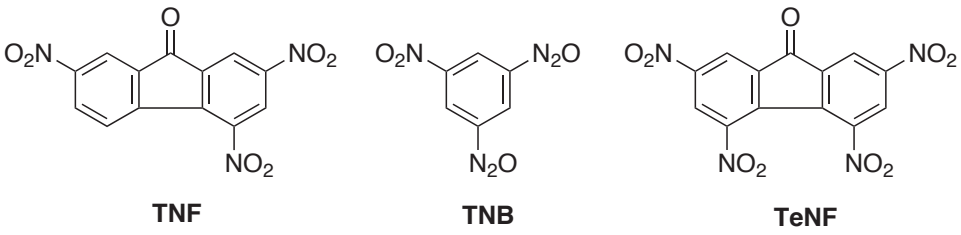

Figure 3.2: Coupling reagents 2,4,7-trinitrofluorenone (TNF, **53**), 1,3,5-trinitrobenzene (TNB) and 2,4,5,7-tetranitrofluorenone (TeNF) used in this work.

3.2 Gelation with two-component gelator system

Gel samples were prepared by adding equimolar amounts of a gelator and 2,4,7-trinitrofluorenone (TNF, **53**) into a vial before adding a solvent. The vial was sealed and the sample was heated up to boiling point of the solvent to maximize solubility. The sample was stored for 24 hours in the dark at room temperature before the gelation test result was observed (Figure 3.3).

Gelation tests with a two-component gelator system of pyrene derivatives **I** - **XV** and TNF indicated that one component can be present in isotropic solution but only in the presence of the second component complexation and subsequent self-assembly into gel fibers is possible. Gelation occurs

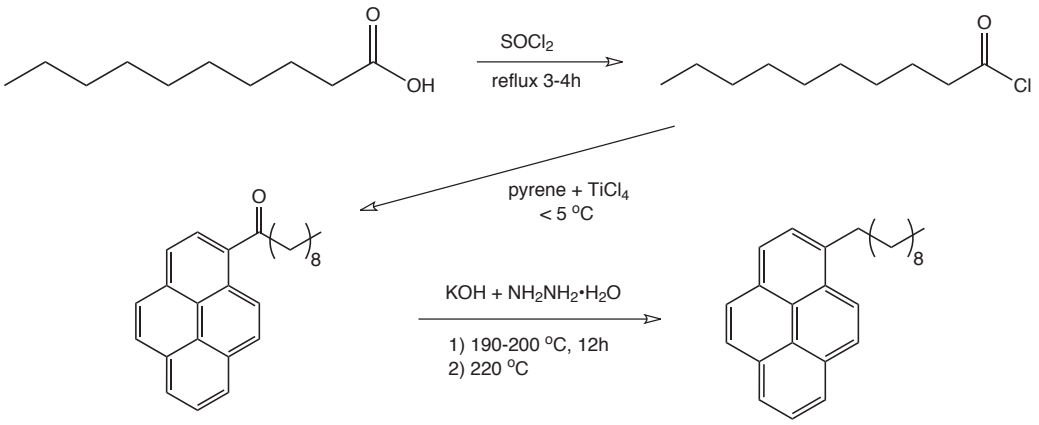

Scheme 3.1: Synthesis of 1-decylpyrene **II**.

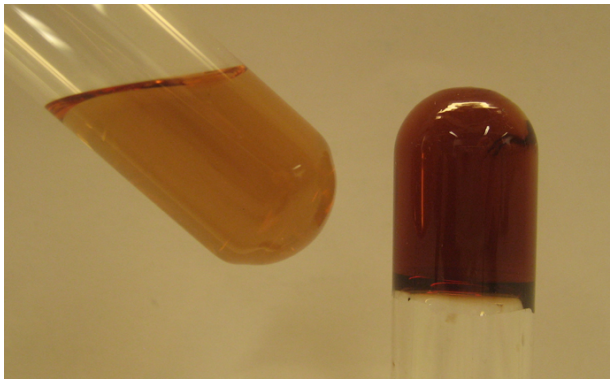

Figure 3.3: Samples of **II** with TNF at 15 mmol kg^{-1} in 1-octanol as a hot sol (left) and as a gel after cooling down to room temperature (right).

only when both components are soluble enough showing that the system is a true two-component system. The results from the gelation experiments are listed in Table 3.1. Gelation with **II** was studied more in detail and the results will be discussed in Chapter 3.3.2.

Compounds **I** - **XV** did not form a gel in hexane due to the poor solubility of the polar TNF. The samples remained transparent and insoluble yellow TNF was observed at the bottom of the vial. Aromatic solvents and chloroform were not gelated but the samples were dark red colored solutions indicating the presence of the charge transfer complex of the gelators. These solvents were not gelated because of too high a solubility of the components. All compounds formed gels in higher alcohols. Gelators **I** - **VII** including alkyl side chain without functionality formed the strongest gels. Inverted test

Table 3.1: Visual observations of gelation tests with TNF[a]

Gelator	Hexane	$CHCl_3$	C_6H_6	Toluene	Octanol	Decanol	Dodecanol
I-VII	I	S	S	S	SG	SG	SG
VIII	I	S	S	S	WG	WG	WG
IX	I	S	S	S	WG	SG	SG
X	I	S	S	S	WG	SG	SG
XI	I	S	S	S	WG	WG	SG
XII	I	S	S	S	WG	WG	SG
XIII	I	S	S	S	WG	G	SG
XIV	I	S	S	S	WG	WG	G
XV	I	S	S	S	WG	WG	WG

a) 15 mmol kg^{-1} gelator and 15 mmol kg^{-1} TNF. SG = strong gel (a spatula does not sink under its own weight), G = gel (sample does not come out of a test tube by knocking), WG = weak gel (sample collapses partially by knocking or shaking), S = solution, I = insoluble or solubility too low.

tube method showed that the gelation takes place usually in a few minutes at room temperature. If a hot sample was placed on a thermostated plate at 20 °C gelation occurred in seconds indicating that gelation process is mostly limited by the cooling rate and not by the molecular self-assembly. A gel melts upon heating to form an isotropic solution and forms a gel again upon cooling. This process can be repeated arbitrarily many times indicating that the gel formation is thermoreversible.

The exact mechanism for the gelation of pyrene analogs in the presence of TNF is not completely understood. TNF acts as a coupling reagent in the self-assembly and has a key role in the one dimensional growth of the gel fibers by forming a charge transfer (CT) complex with the pyrene nucleus. Compounds form red CT gels as depicted in Figure 3.4.

Gelation was also tested by using other coupling reagents than TNF resulting different charge transfer complexes in color (Figure 3.4). Rather weak, opaque and bright orange gels were formed when 1,3,5-trinitrobenzene (TNB, Figure 3.2) was used in 2:1 molar ratio to the gelator. Aliphatic hydrocarbons can be more readily gelled due to much better solubility of TNB. Dark green gels were formed with 2,4,5,7-tetranitrofluorenone (TeNF, Figure 3.2) but the gels precipitated within a few days indicating the complexation was too strong. Aromatic hydrocarbons could not be gelled with any combination as they dissolved the CT complex too well or prevented the gelation by complexing to the CT agent themselves.

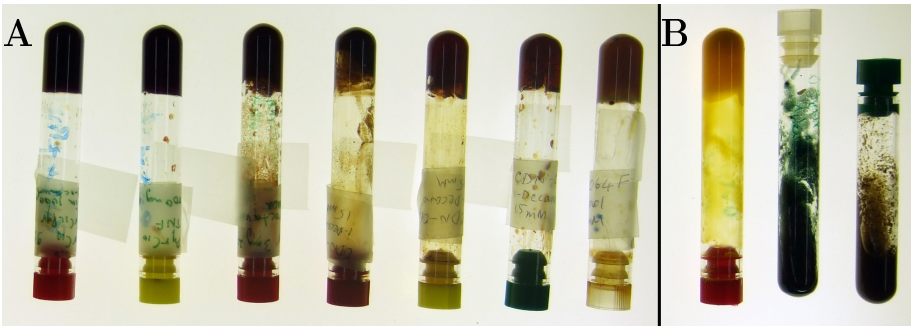

Figure 3.4: Gel samples in 1-decanol with background lightning. The gelator concentration was 30 mmol kg^{-1} including both a pyrene derivative and TNF. The order of the gelators in set A are from left **II**, **III**, **VI**, **IX**, **XI**, **X** and **XIII**. Set B shows the samples of **II** with TNB, **II** with TeNF and **IV** with TNB.

Pyrene forms a bright red CT complex with TNF, but no gelation was observed in organic solvents. This result demonstrates that an alkyl chain on the pyrene moiety is essential for gelation. An alkyl chain prevents the free movement of the solvent molecules by binding them to the backbone of the gelator chain and increases solubility of the gelator into aliphatic solvents.

3.3 Explanation of gelation using various solvent parameters

The solubility parameters are widely used for selecting appropriate solvents for given solutes[262]. They have been applied to characterize the solubility of coating materials[263], polymers[264,265] and drug molecules[266] in solvents. Absorption of drug molecules[267] and solvent uptake by crosslinked polymers[268] can be predicted by solubility parameters. In recent years the dispersibility of single-walled carbon nanotubes[269,270] and graphene[271] have been correlated with solubility parameters.

The solvent-gelator interactions play a key role in gel formation and determine the properties of the gel. According to a recent report the thermodynamic driving force for gelation is solution saturation and the solubility of the gelator controls the gel formation[160]. Moreover, the solvent effect on gelation has been described by correlating the gel-sol transition temperature[59,120,272], minimum gelation concentration[65] and gelation number[273] with solubility parameters and solvent polarity parameters. The complexation and stability of pyrene complex has been described with solvent polarity and solubility pa-

rameter[274]. Visual observations indicated that gelation ability of the pyrene based two-component system was limited mostly because of poor solubility of TNF. This led to attempts to correlate gelation results with different solvent and solubility parameters and the results are discussed in this chapter.

3.3.1 Solubility parameters by group contribution methods

The definition of the Hildebrand solubility parameter[262] is given in terms of the molecular cohesive energy (E_{coh}) per molar volume V:

$$\delta = \sqrt{\frac{E_{coh}}{V}} = \sqrt{\frac{\Delta H_{vap} - RT}{V}} \tag{3.1}$$

The molar cohesive energy is the energy associated with all molecular interactions in one mole of the material, i.e. it is the energy of a liquid relative to its ideal vapor at the given temperature. Solubility parameters are useful in selection of a solvent for a solute. The use of Hildebrand solubility parameter δ is restricted to nonpolar components[7,262]. For the polar components Hansen[7] developed a three dimensional solubility parameter model by expressing the cohesive energy (E_{coh}) as a sum of energies from dispersion (E_d), dipole-dipole (E_p) and hydrogen bonding (E_h) interactions:

$$E_{coh} = E_d + E_p + E_h \tag{3.2}$$

By dividing with molar volume it can be expressed in terms of total solubility parameter δ_{tot} as a sum of dispersion, polar and hydrogen bonding solubility parameters, δ_d, δ_p and δ_h, respectively as follows

$$\delta_{tot}^2 = \delta_d^2 + \delta_p^2 + \delta_h^2 \tag{3.3}$$

To enable two-dimensional plots combined solubility parameters δ_v and δ_a have been defined[275] as

$$\delta_v = \sqrt{\delta_d^2 + \delta_p^2} \tag{3.4}$$

$$\delta_a = \sqrt{\delta_p^2 + \delta_h^2} \tag{3.5}$$

The partial Hansen solubility parameters (HSP) describe the ability of a molecule to interact with an another one via intermolecular forces. Hildebrand solubility parameter (δ) and Hansen total solubility parameter (δ_{tot}) are theoretically the same but their numerical values may differ as they are obtained by different methods. The solubility parameters of non-volatile

compounds can only be determined indirectly. Inverse gas chromatography[276,277], swelling measurements[7,278], intrinsic viscosity measurements[7,279] and group contribution are examples of methods applied to estimate unknown HSPs for an organic compound.

The simplest technique for the determination of solubility parameters is the group contribution method. No experimental data are needed as the method is based on the molecular structure of the compounds. Several group contribution methods have been proposed by Van Krevelen and Hoftyzer[280,281], Fedors[282], Hoy[283,284], Beerbower[263] and Stefanis and Panayiotou[285,286]. Example calculations of the Hildebrand and Hansen solubility parameters of gelators **II** and TNF can be found in Appendix A. Results of the calculations of applicable methods are summarized in Table 3.2. Results for pyrene are also included for comparison as the experimental value for the total solubility parameter of pyrene was found from the literature[287,288].

Table 3.2: Solubility parameters for **II**, TNF and pyrene obtained by the various group contribution methods. $[\delta]$ = $MPa^{1/2}$

	δ	δ_{tot}	δ_d	δ_p	δ_h
II					
Fedors	21.0				
Hoy		19.6	17.3	7.4	5.6
Stefanis (2004)	18.7				
Stefanis (2008)		22.5	22.5	-0.2	0.1
TNF					
Fedors	27.4				
Stefanis (2008)		33.5	24.8	21.9	5.1
Pyrene					
Fedors	24.1				
Hoy		21.1	16.6	10.1	8.1
Stefanis (2004)	20.0				
Stefanis (2008)		24.0	23.1	4.5	4.4
Internet source[289]		23.2	22.8	4.2	1.7
Experimental[287,288]	21.7				

δ = Hildebrand solubility parameter, δ_{tot} = total solubility parameter, δ_d = dispersion parameter, δ_p = polar parameter and δ_h = hydrogen bonding parameter

Application of both van Krevelen-Hoftyzer and Beerbower methods was not possible as they do not include aromatic carbon and NO_2 group contribu-

tions. Hildebrand solubility parameter δ can be evaluated using Fedors group contribution method[282]. Theoretically the method is valid only for liquids but it is sometimes applied for non-volatile materials as the results compare well with values obtained by other methods[290]. The method can give satisfactory results for relatively simple molecules but appers to be unsuitable for complex molecules such as gelator molecules in this work.

The method of Hoy contains additive molar functions, auxiliary equations and expressions for solubility parameters (Table A.2) and gives prediction for HSP's of **II**. On the contrary, calculation for TNF fails due to the missing NO_2 group contribution. For more detailed information regarding this method, refer to reference 281.

There are two group contribution methods by Stefanis and Panayiotou. One of them is used for predicting the total solubility parameter δ[285], and the method published later is suitable for predicting the Hansen solubility parameters[286]. Both methods use two classes of characteristic groups: first-order groups that describe the molecular structure of the compounds and second-order groups, which are based on the conjugation theory and improve the accuracy of the predictions. Prediction of δ for TNF fails due to the missing >C=O group contribution, and the extended method was found to be the only group contribution method able to evaluate HSP's for both **II** and TNF. The extensive use of second-order contributions provides better description of complex molecular structures including multiring, heterocyclic or aromatic compounds, which supports the use of solubility parameter values from this method.

The Stefanis-Panayiotou methods were originally developed for polar compounds including hydrogen bonding and they may not predict correctly HSP's of **II**, which is a nonpolar compound without polar or hydrogen bonding groups. This can be one reason for the negative δ_p value of **II** even though the δ_p and δ_h of the nonpolar **II** are expected to be close to zero. Theoretically, the solubility parameters cannot be negative as they were defined for volatile compounds by Equation 3.1. However, there should be no objection to negative values, if it is accepted that gelator's HSP's are only a set of empirical parameters used to characterize the interactions affecting solvent-gelator solubility and to establish correlations rather than thermodynamic constants. Negative solubility parameter values have been reported for example for natural rubber[291] and polymers[263]. It can also be thought that negative values represent repulsive forces, which is a physically feasible explanation.

The solubility parameters were estimated for the CT complex by using a linear combination $\delta_i(\text{complex}) = \phi(\mathbf{II})\delta_i(\mathbf{II}) + \phi(\text{TNF})\delta_i(\text{TNF})$, where $i = d$, p and h and ϕ = molar fraction = 0.5. The Hansen solubility parameters

applied in this study are presented in Table 3.3.

Table 3.3: The Hansen solubility parameters for gelator **II** and TNF and their CT complex. $[\delta]$ = $MPa^{1/2}$

	δ_{tot}	δ_d	δ_p	δ_h
II	22.5	22.5	-0.2	0.1
TNF	33.5	24.8	21.9	5.1
complex	26.2	23.7	10.9	2.6

3.3.2 Correlations between gelation and parameters of the solvent and gelators

Gelation was tested with **II** and TNF in various organic solvents ranging from highly nonpolar to highly polar (Table 3.4). No gel is formed if both components are very soluble (eg. aromatic solvents), instead the sample remains as a strongly colored sol. Due to limited amounts of gelators available, aromatic solvents were not tested for gelation at very high gelator concentrations.

A single parameter scales for solvent polarity are the dielectric constant ϵ and E_T. The E_T scale is constructed by using the solvatochromic behaviour of the Reichardt's dye[293,295]. The values of these parameters for different solvents are presented in Table 3.5. Gels were formed in solvents with ϵ between 5.8 - 25.3. In highly polar (ϵ = 41.4) or nonpolar (1.9 - 2.2) solvents the low solubility of at least one of the gelator components restricted or prevented gelation. However, ϵ values of the solvents in which the result was solution or partial gel overlapped with the gel range. The correlation between the dielectric constant and gelation is not clear indicating that dielectric constant of the solvent alone does not take into account specific interactions between the solvent and the gelators.

The correlation between gelation and solvent polarity parameter E_T was found to be more clear. The order of E_T values follows an order of I $<$ S $<$ G $<$ PG $<$ I from the gelation test results. The only exception in order were the cycloalkanes. The E_T values were 34 - 40 kcal mol^{-1} in case of solutions and 47 - 52 kcal mol^{-1} for gelated solvents. The correlation between gelation and the solvent polarity parameter E_T is not ideal but it can give at least an estimation on gelation ability in other than nonpolar solvents.

Unfortunately, the solubility parameters for gelators were not available in the literature and the values from group contribution method have been

Table 3.4: Gelation test result of **II** + TNF, solvent polarity parameters (ϵ and E_T) and solubility parameters (δ_{tot}, δ_d, δ_p and δ_h) of organic solvents

solvent	sample[(a)]	ϵ[(b)]	E_T[(c)]	δ_{tot}	δ_d[(d)]	δ_p[(d)]	δ_h[(d)]
benzene	S	2.28	34.3	18.5	18.4	0.0	2.0
toluene	S	2.38	33.9	18.2	18.0	1.4	2.0
chloroform	S	4.81	39.1	19.0	17.8	3.1	5.7
MIAK	S	13.53	N/A	17.4	16.0	5.7	4.1
cyclohexanone	S	16.1	39.8	19.6	17.8	6.3	5.1
THF	S	7.52	37.4	19.5	16.8	5.7	8.0
ethyl acetate	S	6.08	38.1	18.2	15.8	5.3	7.2
ethylene glycol	I	41.4	56.3	33.0	17.0	11.0	26.0
hexane	I	1.89	31.0	14.9	14.9	0.0	0.0
dodecane	I	2.01	31.1	16.0	16.0	0.0	0.0
cyclohexane	PG	2.02	30.9	16.8	16.8	0.0	0.2
decalin	G	2.20	31.2	18.0	18.0	0.0	0.0
2-methoxyethanol	PG	17.2	52.0	24.8	16.2	9.2	16.4
methanol	PG	33.0	55.4	29.6	15.1	12.3	22.3
ethanol	G	25.3	51.9	26.5	15.8	8.8	19.4
1-propanol	G	20.8	50.7	24.6	16.0	6.8	17.4
1-butanol	G	17.84	49.7	23.2	16.0	5.7	15.8
1-pentanol	G	15.13	49.1	21.6	15.9	4.5	13.9
cyclohexanol	G	16.4	47.2	22.4	17.4	4.1	13.5
1-octanol	G	10.3	48.1	21.0	17.0	3.3	11.9
2-octanol	G	8.13	N/A	20.1	16.1	4.9	11.0
1-decanol	G	7.93	47.7	20.4	17.6	2.7	10.0
1-dodecanol	G	5.82	47.5	18.7	16.0[(e)]	2.3[(e)]	9.4[(e)]

(a) 7.5 mmol kg^{-1} of **II** and 7.5 mmol kg^{-1} of TNF after 24 h storage at 25 °C, S = solution, G = gel, PG = partial gel, I = one or both components insoluble at solvent reflux temperature. ϵ = dielectric constant, E_T [kcal mol^{-1}] = solvent polarity parameter, δ_{tot} = total solubility parameter, δ_d = dispersion parameter, δ_p = polar parameter and δ_h = hydrogen bonding parameter, [δ] = $MPa^{1/2}$, *(b)* Ref 292, *(c)* Ref 293, *(d)* Ref 7 and *(e)* Ref 294. MIAK = 5-methyl-2-hexanone.

applied here. If the Hansen solubility parameters in Table 3.3 are correct, then the solvents with HSP's close to these values should be good solvents. Moreover, solubility of gelators in a given solvent should decrease the more solvent's HSP's deviate from those of the gelators. This can be easily tested by calculating the distance in Hansen space, R_a, from the the point repre-

Table 3.5: Solvent polarity parameters ϵ and E_T, hydrogen bonding solubility parameter δ_h of the solvent and Hansen distances R_a of the gelators for different gelation test results. Results in highly nonpolar solvents ($\epsilon \leq 2.2$) are separated and marked with a star (*). N = occurrence

Result	N	ϵ	E_T kcal mol^{-1}	δ_h MPa$^{1/2}$	R_a(**II**) MPa$^{1/2}$	R_a(TNF) MPa$^{1/2}$
I*	2	1.9 - 2.0	31.0 - 31.1	0	6.5 - 7.6	24.1 - 24.6
PG*	1	2.0	30.9	0.2	5.7	23.8
G*	1	2.2	31.2	0	4.5	23.5
S	7	2.3 - 16.1	33.9 - 39.8	2.0 - 8.0	4.5 - 11.4	17.1 - 23.0
G	9	5.8 - 25.3	47.5 - 51.9	9.4 - 19.4	11.4 - 22.3	20.0 - 21.9
PG	2	17.2, 33.0	52.0, 55.4	16.4, 22.3	19.8, 26.5	19.2, 22.0
I	1	41.4	56.3	26.0	28.7	24.8

senting the solvent HSP's to that representing the gelator or CT complex HSP's. The Hansen distance is given by

$$R_a = \sqrt{(\delta_{d2} - \delta_{d1})^2 + (\delta_{p2} - \delta_{p1})^2 + (\delta_{h2} - \delta_{h1})^2} \tag{3.6}$$

where the indices 1 and 2 are used to represent solvent and solute. In fact, Hansen has written the expression with a factor 4 in the first term of equation to double the dispersion component scale and create a spherical volume of solubility[7]. The factor 4 is supported by extensive empirical data but it has no theoretical foundation. Therefore, the equation 3.6 without the factor 4 was applied in this work. However, all the analysis described below was also carried out using the factor 4 and the same trend was found in both cases.

Highly different solubility behavior can be expected for the components in the gelator system. TNF is a polar and hydrogen bonding capable molecule and pyrene based component **II** is a nonpolar molecule which does not form hydrogen bonds. Their charge transfer complex should be somewhere in between in polarity. Hansen distances of gelators and their complex were calculated for all 23 tested solvents (Table 3.6) by using solubility parameters in Table 3.3 and Table 3.4. The R_a represents the solubility of a compound or a complex and the smaller the R_a the better the solubility. Table 3.5 summarizes different gelation behavior as a function of ranges of the solvent parameters and R_a of the gelators.

The Hansen distances of TNF are long (R_a = 17.1 - 24.8 MPa$^{1/2}$) and R_a(TNF) > R_a(**II**) except in ethylene glycol, methanol, 2-methoxy ethanol

Table 3.6: Gelation test result of **II** and **TNF** and Hansen distance R_a of the gelators and their complex **II**+**TNF**. The R_a values are calculated without the factor 4. $[R_a] = MPa^{1/2}$

solvent	R_a(**II**)	R_a(**TNF**)	R_a(**II**+**TNF**)
benzene	4.5	23.0	12.1
toluene	5.1	21.8	11.1
chloroform	8.0	20.1	10.3
MIAK	9.6	18.5	9.4
cyclohexanone	9.5	17.1	7.9
THF	11.4	18.3	10.2
ethyl acetate	11.2	19.0	10.7
ethylene glycol	28.7	24.8	24.3
hexane	7.6	24.6	14.2
dodecane	6.5	24.1	13.6
cyclohexane	5.7	23.8	13.1
decalin	4.5	23.5	12.6
2-methoxy ethanol	19.8	19.2	15.8
methanol	26.5	22.0	21.5
ethanol	22.3	21.4	18.7
1-propanol	19.8	21.4	17.2
1-butanol	18.0	21.4	17.2
1-pentanol	16.0	21.4	15.1
cyclohexanol	15.0	21.0	14.3
1-octanol	13.5	21.3	13.8
2-octanol	13.6	20.0	12.8
1-decanol	11.4	21.1	12.6
1-dodecanol	11.6	21.9	13.4

and ethanol, which are the most polar solvents according to the E_T-scale. This shows that TNF is the limiting factor for gelation in general due to its low solubility. The solubility of **II**, TNF and their complex as a function of solvent polarity parameters ϵ and E_T are presented in Figure 3.5. The solubility of **II** and the complex decrease when ϵ or E_T increase and correlation is rather linear but not ideal. There is no correlation between either polarity parameters and the solubility of TNF. The E_T scale separates the different gelation results more clearly indicating that it takes better account of the solvent-gelator interactions on the molecular level.

The solubility of the gelators and their complex as a function of the

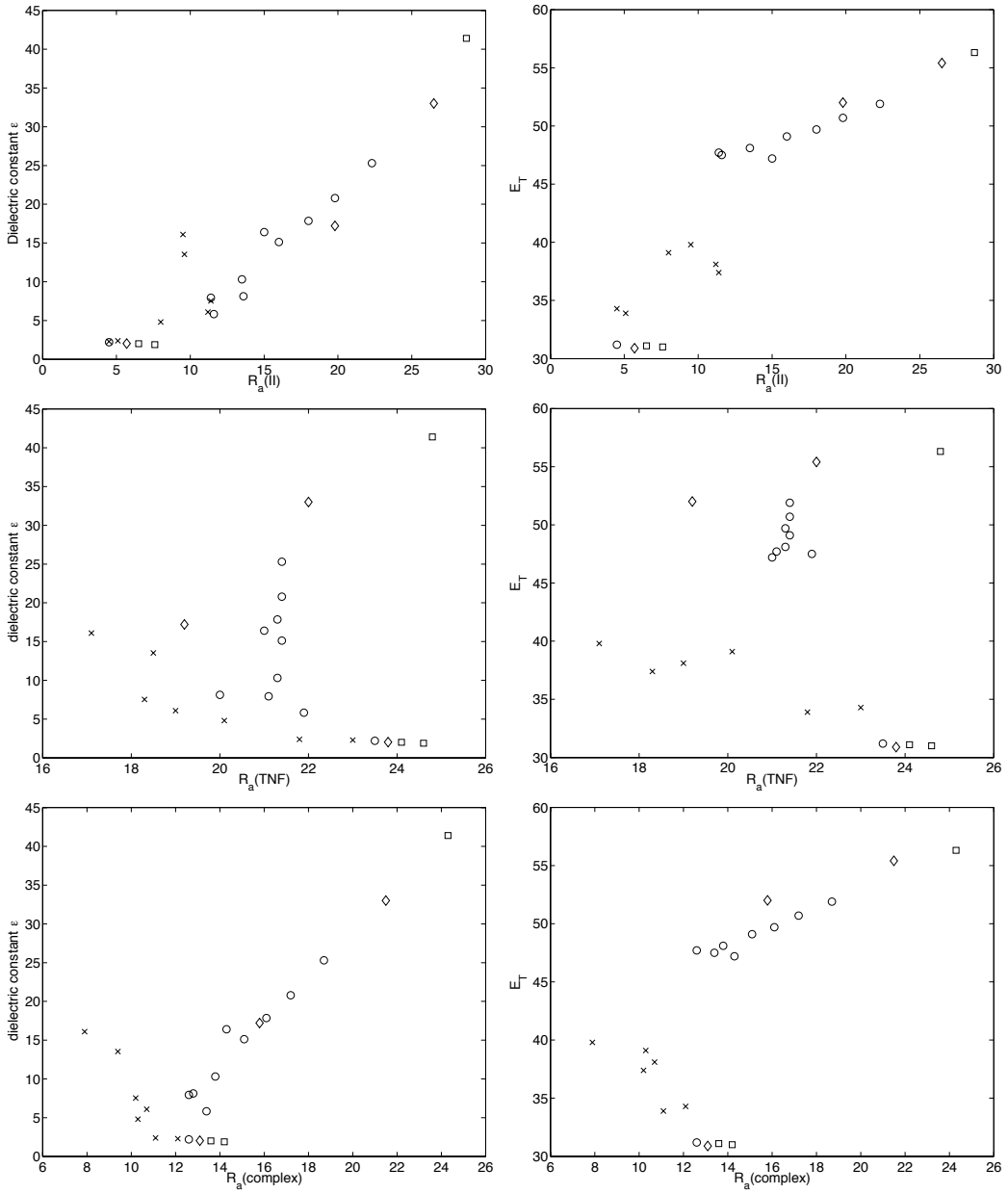

Figure 3.5: Effect of polarity of the solvent on the solubility of the gelators **II** and TNF and their complex. Polarity scale of dielectric constant ϵ presented on the left and E_T on the right. Gelation test results: $\circ$ = gel, $\diamond$ = partial gel, $\times$ = solution and $\square$ = insoluble.

solubility parameters of the solvent are presented in Figure 3.6 and Figure 3.7.

There is no correlation between the dispersion solubility parameter δ_d and the solubility of the gelators or the complex. Generally, the solubility of **II** and the complex decrease when δ_p and δ_h increase. There is a clear linear correlation with δ_h indicating that the solubility is mostly governed by the hydrogen bonding. Some correlation is also observed between R_a(**II**) and the polarity solubility parameter δ_p. The correlation is even more linear than in the case of ϵ or E_T. No correlation between R_a(TNF) and any of the Hansen solubility parameters of the solvent is observed. However, a range of solvent δ_h (9 - 20 $MPa^{1/2}$) results to gels regardless of R_a(TNF) to the solvent. Thus, the solubility of TNF seems to only depend on the solvent δ_h, but not on the HSP-distance. This is supported by the observation, that in gelated alcohols solubility of TNF remains rather constant even if δ_p increase.

The solubility of the gelators do not follow above described correlations in highly nonpolar solvents ($\epsilon < 2.4$, $E_T < 35$ kcal mol^{-1}). These solvents are on the x-axis or close to it because δ_p and δ_h of the solvents are zero or close to zero. Application of HSP's and Hansen distances seems to work only in solvents with δ_p and δ_h values exceeding 2.0 $MPa^{1/2}$. Hansen[7] developed his solubility parameters for polar components, thus problems with highly nonpolar solvents may be expected. The gelation in these solvents can be better understood by using the Hildebrand solubility parameter δ which will be discussed later.

The solubility of **II** and the complex follow the order of I < PG < G < S of the gelation results if highly nonpolar polar solvents are excluded. The solubility increases in the opposite order than the solvent parameters E_T, δ_h and the combined polar solubility parameter δ_a showing that there is a correlation between gelation and the solubility of the gelators and solvent parameters. The only exception to this order is 2-methoxy ethanol. The solubility of TNF has the same trend but S and G ranges are partially overlapped.

The higher solubility of the gelators and the complex means less preference for self-assembly and gel network formation and a higher gelator concentration is required for gelation. Partial gel may be observed even though the applied gelator concentration is above mgc if poor solubility of one or more gelator components lower the actual complex concentration below mgc. In highly nonpolar or polar solvents the solubility of one or both gelators is so poor that no red complex or gelation were observed and the samples remained transparent.

The samples having the lowest R_a(complex) values have the best complex solubility and produced red colored solutions. In these solvents the effective solubilization of the complex prevents the self-assembly process and no gel fibers are observed because the gelator concentration 15 mmol kg^{-1} ($\sim$0.5

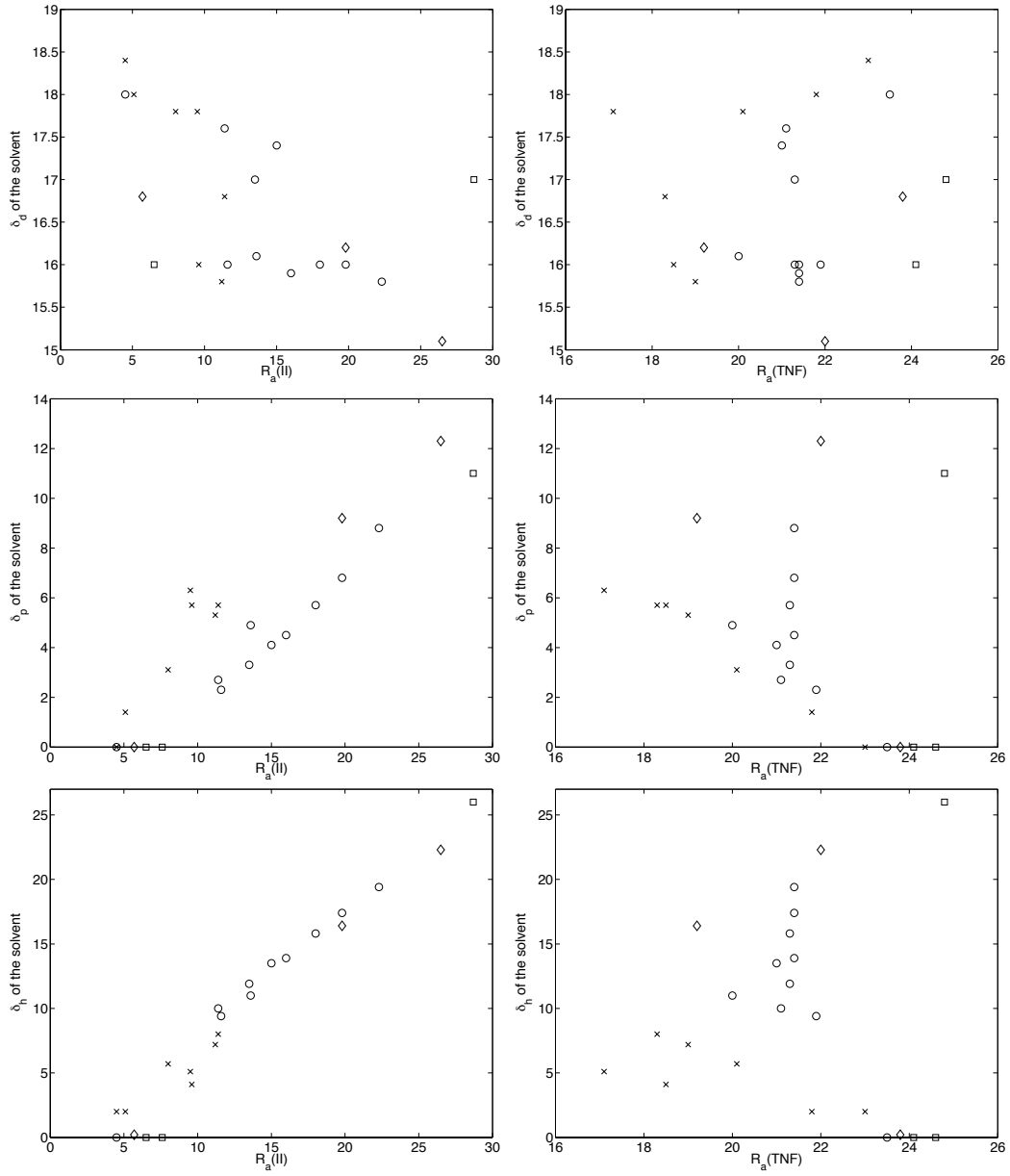

Figure 3.6: Effect of the solubility parameters of the solvent on the solubility of **II** and TNF. Gelation test results: ○ = gel, ◇ = partial gel, × = solution and □ = insoluble.

% w/w), is below cgc. Charge transfer and π-π interaction are still present as the solutions are red colored due to complexation[296], but solvophilic attraction between the complexes and the solvent overcome the effect of van der

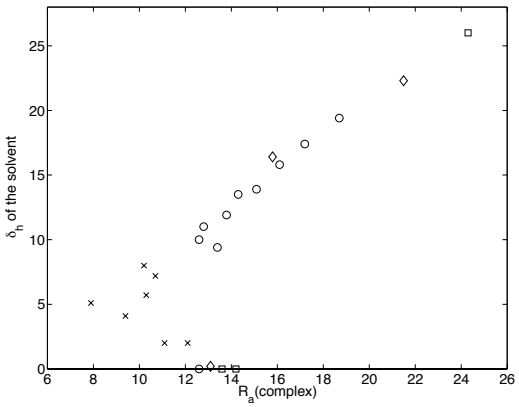

Figure 3.7: Effect of the hydrogen bonding parameter δ_h of the solvent on the solubility of the complex of **II** and TNF. ○ = gel, ◇ = partial gel, × = solution and □ = insoluble.

Waals forces necessary for gelation. In MIAK gelation occurred when gelator concentration was increased up to 6 % w/w and in ethyl acetate a partial gel was observed at 9 % w/w. These solvents were not studied further due to limited amount of gelators available. Also, it was not of interest to study solvents, which require large amount of gelator to form a gel, but instead to choose some other, more suitable gelator for these solvents.

For successful gelation the solubility of the gelators and the complex must be somewhere between too low and too high. It is possible to find requirements for the gelation by using Hansen distances covering all tested solvents. Requirements for gelation in two-component gelator system includes solubility ranges for both gelator components and their complex:

1. $R_a(\mathbf{II}) \leq 22.3$ MPa$^{1/2}$
2. 20.0 MPa$^{1/2} \leq R_a(\text{TNF}) \leq 23.5$ MPa$^{1/2}$
3. 12.6 MPa$^{1/2} \leq R_a(\text{complex}) \leq 18.7$ MPa$^{1/2}$

It is noteworthy that R_a(complex) can be within the gelation range but gelation does not occur if the other requirements are not fulfilled. For example in aliphatic hydrocarbons the solubility of the complex is within the required range but poor solubility of polar TNF ($R_a > 24$) prevents gelation. Requirements for solubilities form a window which is presented in Figure 3.8.

The minimum gelation concentrations (mgc) of the two-component gelator system of **II** and TNF at 25 °C were 9, 11, 13 and 15 mmol kg^{-1} in 1-butanol, 1-pentanol, 1-octanol and 1-dodecanol, respectively. Figure 3.9 A

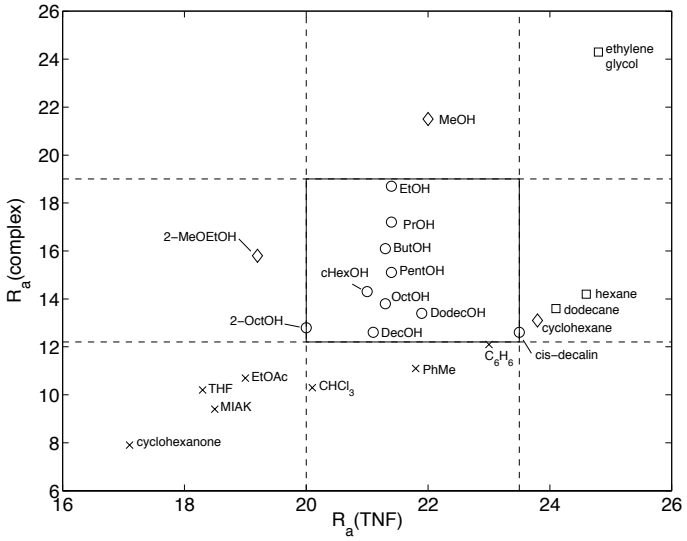

Figure 3.8: The solubility of TNF and complex of **II** and TNF depicted by Hansen distance form a window of solubility for gelation. ○ = gel, ◇ = partial gel, × = solution and □ = insoluble.

shows that the dispersion solubility parameter δ_d of the alcohol has no effect on the mgc but there is a linear correlation between the mgc and the polar solubility parameter δ_p, the hydrogen bonding solubility parameter δ_h and the combined polar solubility parameter δ_a. The mgc of the two-component gelator system falls as the δ_p, δ_h and δ_a increase. A correlation between δ_a and mgc has been observed also with cyclo(dipeptide)s[65] but the mgc was found to increase with δ_a. The opposite behavior can be due to different interaction forces as gelation of the cyclo(dipeptide)s is based on intermolecular hydrogen bonding between the amide groups.

Figure 3.9 B indicates that lower solubility of the complex of **II** and TNF results to a lower mgc. In lower alcohols solvophobic forces increase and enhance the self-assembly process. In methanol very low mgc is expected but not enough complex is formed due to poor solubility of nonpolar **II** (R_a = 26.5 $MPa^{1/2}$) and only a partial gel is observed. It is clear that solvophobic interaction is necessary for gelation but too low a solubility and too strong a repulsion precipitate the gelators out of the solvent.

The Hildebrand solubility parameter δ was developed primarily for nonpolar solvents. Compounds with comparable solubility parameters are likely to be miscible. More precisely, compounds with $\Delta\delta < 7$ $MPa^{1/2}$ are likely to be miscible whereas compounds with $\Delta\delta > 10$ $MPa^{1/2}$ are likely to be

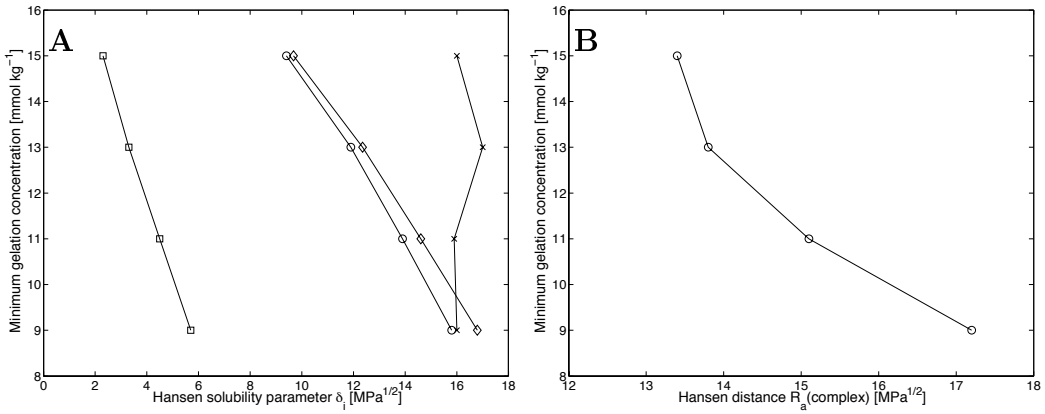

Figure 3.9: Effect of δ_d (x), δ_p (□), δ_h (○) and δ_a (◇) of the solvent (A) and the solubility of the complex (B) on minimum gelation concentration of the two-component gelator system of **II** and TNF in primary alcohols.

immiscible[290,297]. The $\Delta\delta$ were determined for **II**, TNF and the complex in nonpolar solvents which have δ_p and δ_h values of 2 MPa$^{1/2}$ or less (ϵ = 1.9 - 2.4, E_T = 30.9 - 34.3 kcal mol^{-1}). The $\Delta\delta$ values in Table 3.7 indicate that **II** is likely to be soluble but TNF is very likely to be insoluble in nonpolar solvents.

The solubility of the complex is the major factor for gelation. In hexane and dodecane the complex and TNF are probably immiscible and the samples remained as transparent solutions indicating insolubility. A red colored solution was observed in toluene and benzene in which $\Delta\delta$(complex) $\leq$ 8 MPa$^{1/2}$. In cyclohexane and decalin the $\Delta\delta$(complex) values are between the given limits. Decalin was gelated, but in cyclohexane TNF is not soluble enough and it was only partially gelated.

The results indicate that gelation behavior of the two-component gelator system in nonpolar solvents is as follows: solutions (S) with $\Delta\delta$(complex) $\leq$ 8 MPa$^{1/2}$ and insoluble (I) with $\Delta\delta$(complex) $>$ 10 MPa$^{1/2}$. Gelation is possible if 8 MPa$^{1/2}$ $<$ $\Delta\delta$(complex) $<$ 10 MPa$^{1/2}$ and partial gel behaviour can be expected if $\Delta\delta$(TNF) $>$ 16 MPa$^{1/2}$.

Application of both Hildebrand and Hansen solubility parameters approaches can provide an useful description of the two-component gelator system. The Hildebrand solubility parameter δ should be applied only to nonpolar solvents where the application of the Hansen solubility parameters does not give any benefit over δ because δ_p and δ_h of nonpolar solvents are zero or close to zero. However, it was possible to determine requirements for gelation including solubility ranges for the components and the complex

Table 3.7: Gelation test results in highly nonpolar solvents and the difference of the Hildebrand solubility parameter ($\Delta\delta$) between a gelator component and a nonpolar solvent. $[\Delta\delta] = \mathrm{MPa}^{1/2}$

Solvent	Result*	$\Delta\delta$(**II**)	$\Delta\delta$(TNF)	$\Delta\delta$(complex)
hexane	I	7.6	18.6	11.3
dodecane	I	6.5	17.5	10.2
cyclohexane	PG	5.7	16.7	9.4
decalin	G	4.5	15.5	8.2
toluene	S	4.3	15.3	8.0
benzene	S	4.0	15.0	7.7

(*) 7.5 mmol kg^{-1} of **II** and 7.5 mmol kg^{-1} of TNF after 24 h storage at 25 °C, S = solution, G = gel, PG = partial gel, I = one or both components insoluble at solvent reflux temperature.

covering the whole solvent range by using only Hansen's approach.

The solvophobic forces have an important role in gelation and the self-assembly is strongly influenced by solvent polarity, polar and hydrogen solubility parameters of the solvent. Overall, the bonding between molecules can be more complex and multidimensional than the solubility parameters suggest since hydrogen bonding, π-π and donor-acceptor interactions also alter the solubility and the gelation and these are not taken into account in the solubility parameters. Charge transfer mechanism and π-π interaction are essential for the alignment of the gelator components but the main binding occurs through the van der Waals forces[106].

3.4 Influence of the gelator and xerogel structure of the gel

The properties of the 1-octanol gels of **II**, **VI** and **IX** were studied by rheology. The **II** and **VI** formed strong gels with TNF in 1-octanol (Table 3.1) and the effect of a functional group on the gel properties was studied by using **IX**. The frequency sweep measurements of the samples showed gel character (G' > G") over three orders of magnitude of frequencies and both G' and G" were relatively independent on the frequency in the linear viscoelastic range (Figure 3.10). In Figure 3.10, the G'/G" at 1 Hz frequency is ∼10 as expected for a soft viscoelastic solid like a gel. The G'- and G"-curves were almost parallel throughout the entire frequency range showing a little slope

indicating that the samples were clearly gels. A slight frequency dependency of G' and G" is common for physical gels and is consistent with a viscoelastic behavior[213,298,299].

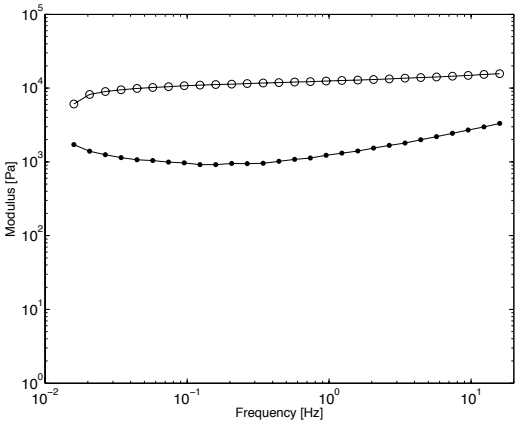

Figure 3.10: Example of a frequency sweep curve for a 1-octanol gel of **II** and TNF at 30 mmol kg^{-1} (1 wt-%) gelator concentration (G' ∘ and G" •).

Figure 3.11 shows typical temperature dependencies of the shear storage modulus, loss modulus and loss tangent ($\tan\delta$) for the gels of **II** and **VI**. The storage modulus (G') represents elastic behaviour of a material and below the gel-sol transition temperature (T_{gs}) the higher G' indicates the more elastic gel network[31,205]. The loss modulus (G") represents viscous behavior of a material and the loss tangent ($\tan\delta$ = G"/G') describes the ratio of viscous and elastic properties of the gel[205]. The G' and G" are fairly insensitive to temperature at low temperatures but at high temperatures a sharp decrease of both moduli is observed, which is attributed to the melting of the gel network. According to $\tan\delta$, the gels remain stable below 60 °C indicating that no relaxation or other material changes occur until the gels start to melt above 60 °C. The T_{gs} was defined as the crossover point of the elastic and the loss moduli (G' = G"), which corresponds to phase angle of 45° or $\tan\delta$ = 1 value.

The largest G', the lowest $\tan\delta$ and thereby the highest gel elasticity were observed for the gel of **II** (Table 3.8). The length of the alkyl side chain had a large effect on the elasticity of the gel network. Gelator **VI** has eight carbons longer alkyl chain than **II** and the gel elasticity was almost three times lower. Complexation of TNF and **IX** leads to formation of gel fibers including free functional groups which are able to bind for example nanoparticles into the gel structure. However, the functionalized gelator **IX** formed a weak gel indicating that a functional group disturbs gel formation probably

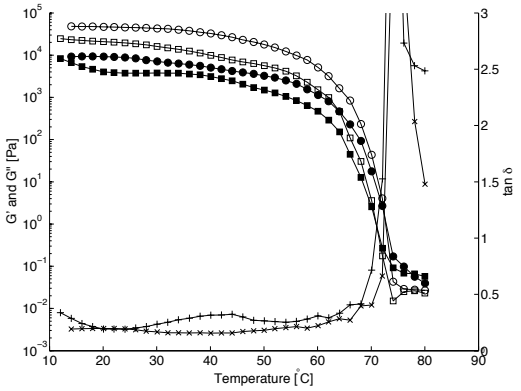

Figure 3.11: Temperature dependency of the storage modulus G' (○ **II**, □ **VI**), loss modulus G" (● **II**, ■ **VI**) and tan δ (× **II**, + **VI**) of 1-octanol gels of **II** and **VI** during heating.

due to a competing hydrogen bonding through the functional groups. The elasticity of the gel is significantly reduced by functionality as the G' was only 0.22 kPa for gel of **IX**. Also the loss tangent values showed that viscous properties become more dominant if the gelator has longer alkyl chain or functionality.

Table 3.8: The storage modulus (G') and the loss tangent (tan δ) at 30 °C and the gel-sol transition temperature (T_{gs}) as obtained from temperature sweep runs and the viscosities at 1, 10 and 100 s^{-1} shear rates.

	II	**VI**	**IX**	**II:IX**, 9:1
G', kPa	44 ± 4	16.2 ± 1.5	0.22 ± 0.09	24.7 ± 1.2
tanδ	0.17 ± 0.03	0.21 ± 0.03	0.22 ± 0.06	0.171 ± 0.007
T_{gs}, °C	69 ± 3	68 ± 3	66 ± 5	68.3 ± 1.2
η_1, Pa s	28 ± 7	20 ± 3	1.9 ± 0.4	14.3 ± 0.6
η_{10}, Pa s	2.4 ± 0.2	1.6 ± 0.3	0.38 ± 0.09	1.6 ± 0.2
η_{100}, Pa s	0.67 ± 0.04	0.42 ± 0.04	0.16 ± 0.03	0.41 ± 0.03

The T_{gs} values were 69, 68 and 66 °C for gels of **II**, **VI** and **IX**, respectively. The length of the alkyl chain does not have a significant effect on the thermal stability of the gel when the chain length is between C_{10} - C_{18}. Similar results have been achieved for gels of pyrene derived LMOGs also by inverted test tube method[85]. However, the alkyl chain length affects significantly thermal stability when the length is shorter than C_{10} or longer than C_{18} (Chapter 3.5.3). Functionality in **IX** lowers thermal stability only

slightly even though the elasticity was substantially low. The viscosities at 1, 10 and 100 s^{-1} shear rate (Table 3.8) followed the same order of **II** > **VI** > **IX** as the elasticity and the thermal stability of the gel.

The adverse effects of the gelator functionality can be prevented with a three-component system by mixing non-functionalized and functionalized gelators or pyrene with TNF to keep the functional groups apart from each other. A strong functionalized gel was achieved by mixing functionalized and non-functionalized gelators. High gel elasticity and thermal stability were observed when a gel was prepared from **II** and **IX** at 9:1 ratio. The loss tangent value indicated that the three-component system had similar ratio of elastic and viscous properties than the gel of the two-component system including **II** and TNF. Functionality had the greatest impact on viscosity as 5 mol-% of **IX** in the gel of **II** and TNF resulted to a 30 - 50 % lower viscosity.

The morphology of the gels were studied by electron microscopy to gain insight into the gelator effect on the gel structure. Figure 3.12 shows the micrographs of 1-octanol gels of **II**, **VI**, **IX** and **II** with pyrene. Micrographs showed that all gelators with TNF self-assemble into gel fibers and form an entangled network, which immobilizes the solvent. Examination at high magnification indicated that regardless of the gelator the smallest resolved gel fibers were 70 - 80 nm on average which is 10 - 20 times larger than the molecular dimensions of the gel fiber. Estimated maximum molecular gel fiber thicknesses were 3.9 and 5.9 nm in gels of **II** and **VI** which were calculated by using molecular length of 0.85 nm for pyrene and 1.5 and 2.5 nm for decyl and octadecyl, respectively. Single fiber thickness did not significantly depend on the gelator but the micrographs at lower magnification showed clearly that thicker fibers are composed of thinner fiber bundles. The thickest gel fiber bundles were up to two magnitudes larger than gelator molecules themselves.

The gel of **II** shows thin gel fibers as well as homogenous and dense gel network. The occurrence of fiber bundles and regularity of the gel network increased when **VI** with longer alkyl chain was used. Even greater gaps between large bundles and the most regular gel network were observed in the gel of **IX**. The more dense the gel network the stronger and more elastic the gel structure was observed. The more fiber bundles and the more regular gel network was found by SEM, the weaker the gels and the lower the viscosity. Addition of small amount of pyrene increases the density and irregularity of the gel network (Figure 3.12, c).

The results indicate that the length of alkyl side chain or pyrene do not significantly affect the gel fiber thickness but they both have an influence on the fiber bundle formation. Thick bundles in gel of **IX** suggest

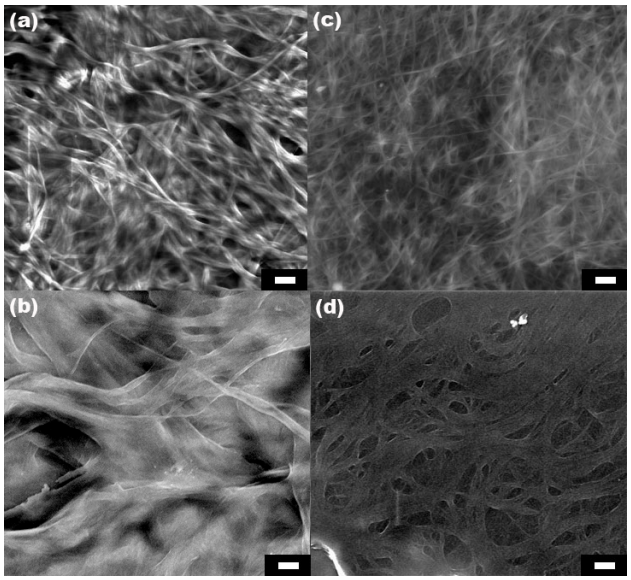

Figure 3.12: Electron micrographs of xerogels of (a) **II**, (b) **VI**, (c) **II** with pyrene at 9:1 ratio and (d) **IX** in 1-octanol. Scale bar 1 μm.

that the gel structure is mostly determined by solvent-gelator interaction. Functional group of **IX** results high solvent-gelator interaction in 1-octanol and the gelator molecules are likely to aggregate to form thicker fiber bundles. Lower solvent-gelator interaction results less bundles and more dense gel network. More elastic gels were observed when solvent-gelator interaction was decreased by using a gelator with shorter alkyl chain or pyrene was added. The effect of pyrene on the gel properties is discussed in more detail in Chapter 3.7.

3.5 Solvent and alkyl chain length effects in primary alcohols

3.5.1 Minimum gelation concentration and gelation number

The pyrene derived organogelators **I**, **II**, **V**, **VI** and **VII** with alkyl side chains of 7, 10, 16, 18 and 24 carbon atoms, respectively, form strong gels in higher primary alcohols (Table 3.1, page 48). This shows that the solubility of the pyrene derivatives or TNF does not restrict the gel network formation in primary alcohols.

Below the minimum gelation concentration (mgc) no sample-spanning

gel is formed because the concentration is insufficient to immobilize the solvent. The amount of the gelators in the gel fibers is always lower than the total amount added as part of the gelators stay dissolved. This indicates that poor solubility of the gelators is favorable to the self-assembly and low mgc whereas high solubility leads to high mgc. A sample-spanning gel network is formed and a sample is regarded as a gel when the gelator concentration is higher than mgc.

Figure 3.13 illustrates the mgc as a function of alkyl chain length of the pyrene derivative in primary alcohols at 25 °C. The mgc values were 9 - 15 mmol kg^{-1} corresponding to 0.4 - 0.5 wt-% depending on the gelator. The mgc values were determined by inverted test-tube method in steps of 1 mmol kg^{-1} by diluting the sample until gelation was not observed within 24 h. Usually no difference could be found in the mgc if the chain length was altered by 2 - 3 carbon atoms. The mgc was not determined for **VII** (C_{24}) due to precipitation. The mgc was very sensitive to temperature. Gelator concentration of 1 mmol kg^{-1} lower than the mgc did not result to a gel at 25 °C but all samples were gelated at room temperature (21 °C). The gelation number of the gelators represents the maximum number of solvent molecules that get entrapped per gelator molecule[273]. The gelation number was calculated by using the mgc value at 25 °C and the data are listed in Table 3.9.

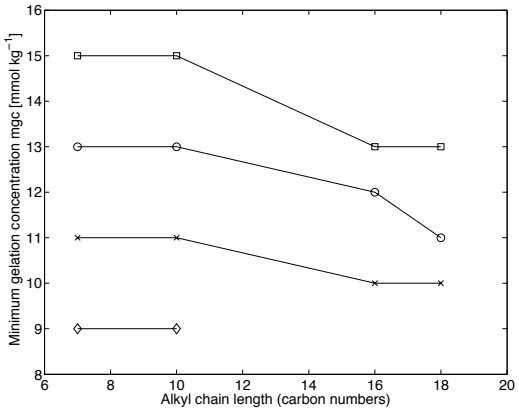

Figure 3.13: Effect of the solvent and alkyl chain length of the pyrene derivative on the minimum gelation concentration. ♢ = 1-butanol, x = 1-pentanol, ○ = 1-octanol and □ = 1-dodecanol.

The mgc decreases and gelation number increases with elongation of the alkyl chain in all solvents. Clearly, the longer the alkyl chain, the lower the solubility and the more efficiently the two-component system gelates polar alcohols. The interaction of pyrene derived gelator with polar solvent

Table 3.9: Gelation number of the gelators **I**, **II**, **V** and **VI** with TNF in primary alcohols at 25 °C. Corresponding total gelator concentration in mmol kg^{-1} is given in parentheses.

Gelator	1-pentanol	1-octanol	1-dodecanol
I, C_7	530 (11)	590 (13)	360 (15)
II, C_{10}	530 (11)	590 (13)	360 (15)
V, C_{16}	1130 (10)	640 (12)	410 (13)
VI, C_{18}	1130 (10)	700 (11)	410 (13)

is weakened more in case of gelators containing longer hydrophobic alkyl chains, which enhances the gelator assembly leading to higher gelation numbers. Zhu and Dordick[273] observed similar behavior in gelation number in primary alcohols with one-component trehalose derivatives with C_8 - C_{13} long alkyl chains. The alkyl chain length had a similar effect also with *L*-tryptophan based hydrogelators[300]. An increase in gelator efficiency with alkyl chain length as well as the loss of gelation ability beyond a certain chain length has been observed with carbamate derivatives[301]. Higher gelation ability can be related also to stronger van der Waals stabilization with compounds having longer alkyl chains. Generally a long alkyl chain is preferred for compounds which form organogels[32,51,53,302]. Gelator efficiency of simple alkanes[16], triphenylene[303], cyclohexane bis-urea[304] and tris-amide[305] compounds increase with alkyl chain length. However, an increase of the alkyl chain length did not increase the gelator efficiency but favored gelation in more nonpolar aliphatic solvents with tripodal tris-urea derivatives[71].

Solubility of the pyrene derivatives and the mgc of the two-component system decrease with the solvent polarity. For example, the mgc of **I** and **II** were 15, 13, 11 and 9 mmol kg^{-1} in 1-dodecanol, 1-octanol, 1-pentanol and 1-butanol, respectively. Gelator solubility is strongly dependent on the nature of the solvent, thus a minor change in the polarity of the solvent affects mgc and the self-assembly of the gelator molecules. Higher polarity leads to lower mgc and linear correlation was observed between the mgc, dielectric constant ϵ and solvent hydrogen bonding parameter δ_h (Figure 3.14).

A higher gelation number results in lower mgc as can be seen in Table 3.9. The gelation number increases with the polarity of the solvent but decreases when the molecular size of the solvent increases. This indicates that not only the solvent polarity but also the molecular size of the solvent has an effect on the gelation number and mgc. These results are in accordance with a recent report where the self-assembly process of π-conjugated

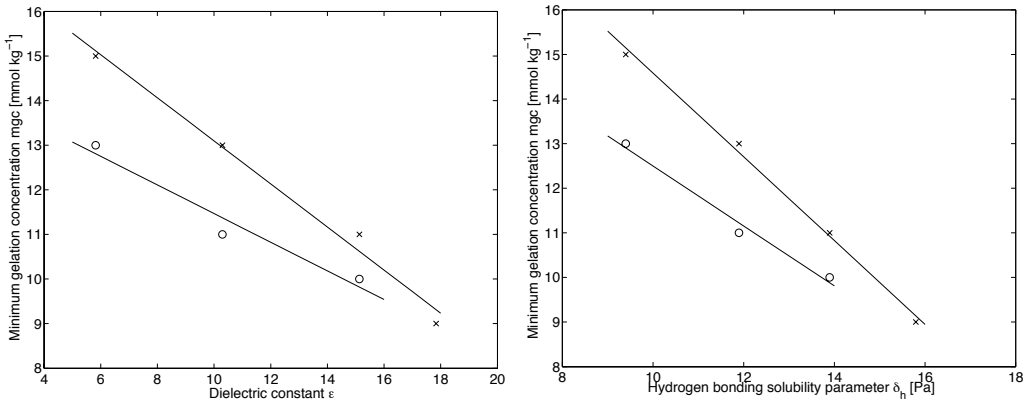

Figure 3.14: Correlation between minimum gelation concentration and dielectric constant ϵ and hydrogen bonding solubility parameter δ_h of the solvent. x = **I** and **II**, ∘ = **VI**.

oligo(*p*-phenylenevinylene) derivatives was found to depend strongly on solvent structure and the solvent molecules at periphery of the aggregates played an explicit role in rigidifying the aggregates and formation of bundles and gels[306].

3.5.2 Yield and flow points

An efficient way to characterize gel stability is to measure the oscillation stress amplitude sweep where a wider linear viscoelastic (LVE) range indicates a more stable gel. The LVE range is frequency dependent and a frequency of 1 Hz was used in this work. A gel shows reversible viscoelastic behavior as long as the applied stress is below the yield point τ_y (yield stress). Flow points τ_f (flow stress) were determined as the crossover point where behavior changes to a liquid character (G' < G") and the sample starts to flow. Usually for viscoelastic materials like gels, G' is an order of magnitude greater than G" in the LVE range, demonstrating the dominant elastic behavior of the system. The transition between the LVE range and the flow range occurs gradually in gels and the range between the yield and the flow points is called the yield zone. In the yield zone the gel character is dominant but also some irreversible gel network breakage occurs[205].

The gels of **I**, **II** and **V** - **VII** showed yield points between 3 - 160 Pa and the flow points were 5 to 10 times higher than the yield points (Table 3.10). It should be noted that the yield point was determined as a point where 5 % deviation from the G'$_{LVE}$ was observed. As the yield point is an user defined

value, it should be regarded as a comparative quantity between different gels showing wide yield zones.

Table 3.10: Storage modulus of the linear viscoelastic range G'$_{LVE}$, the yield point τ_y and the flow point τ_f of the gels of **I**, **II**, **V** - **VII** in primary alcohols. Total gelator concentration was 30 mmol kg^{-1}.

	G'_{LVE} [kPa]	τ_y [Pa]	τ_f [Pa]
1-Pentanol			
I, C_7	14.1 ± 0.4	28 ± 4	200 ± 30
II, C_{10}	13 ± 3	14.9 ± 0.8	300 ± 130
V, C_{16}	15.8 ± 1.2	21 ± 2	200 ± 40
VI, C_{18}	24 ± 3	30 ± 5	120 ± 4
VII, C_{24}	73 ± 8	160 ± 40	500 ± 50
1-Octanol			
I, C_7	8.7 ± 0.7	16 ± 4	150 ± 8
II, C_{10}	6.7 ± 1.4	11 ± 3	170 ± 40
V, C_{16}	2.9 ± 1.0	5 ± 3	40 ± 13
VI, C_{18}	3.4 ± 1.1	3.6 ± 0.9	20 ± 8
VII, C_{24}	42 ± 4	61 ± 4	340 ± 50
1-Dodecanol			
I, C_7	7.5 ± 0.5	16 ± 4	120 ± 30
II, C_{10}	6.6 ± 0.5	15.7 ± 1.0	370 ± 80
V, C_{16}	0.8 ± 0.2	3.0 ± 0.4	30 ± 11
VI, C_{18}	0.67 ± 0.10	3.7 ± 0.3	20 ± 3
VII, C_{24}	11.6 ± 0.5	35 ± 4	140 ± 9

The yield points were 15 - 160 Pa in 1-pentanol, 4 - 60 Pa in 1-octanol and 3 - 35 Pa in 1-dodecanol. The gels in 1-pentanol showed the highest yield and flow points whereas the lowest values were observed in 1-dodecanol. Both the yield and flow point follow the order 1-pentanol > 1-octanol > 1-dodecanol which corresponds to the order of solvent polarity or hydrogen bonding solubility parameter δ_h of the solvent. The yield point is the larger the longer the alkyl chain and the more polar the solvent is (Figure 3.15 A). In 1-octanol and 1-dodecanol the yield point decreases with the alkyl chain length up to C_{18} but C_{24} (**VII**) showed the highest τ_y. This indicates that in polar alcohols the van der Waals interaction between the alkyl chains is pronounced as the length of the alkyl chain increases resulting to a stronger gel network, higher yield point and wider linear viscoelastic range. In 1-pentanol the solvophobic forces towards nonpolar alkyl chains are the strongest and

an increase in the yield point is observed already from shorter chain length C_{16} onwards.

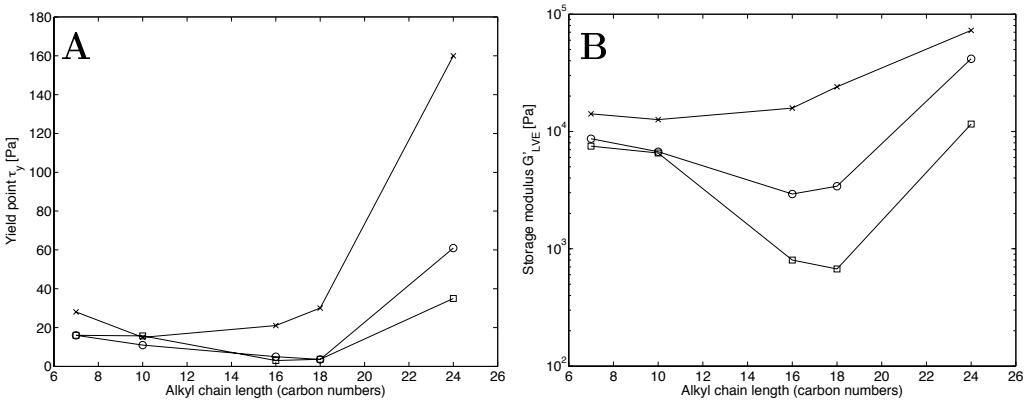

Figure 3.15: Effect of alkyl chain length on the yield point τ_y (A) and the linear viscoelastic region G'$_{LVE}$ (B). x = 1-pentanol, ∘ = 1-octanol and □ = 1-dodecanol.

The G'$_{LVE}$ describes the gel elasticity[205] and the gel network strength[166]. The effect of the solvent and the alkyl chain length are similar on the structural stability than on the yield point (Figure 3.15 B). The G'$_{LVE}$ follows the order of the solvent polarity and the effect is greater with longer alkyl chains. The lowest G'$_{LVE}$ values, and hence structurally weakest gels, were obtained with **VI** (C_{18}) in 1-dodecanol, **V** (C_{16}) in 1-octanol and **II** (C_{10}) in 1-pentanol showing that the effect of the alkyl chain length on structural stability is pronounced in more polar solvents.

Compound **VII** (C_{24}) resulted to the most structurally stable gels with the highest τ_y and G'$_{LVE}$ values in all solvents. However, it seems that at certain chain length solvophobic forces dominate as gels of **VII** precipitate within a few days after their preparation. All the other gels remained visually stable at least two years when stored in sealed vials at room temperature. Some carbamate derivatives also lose their gelation ability beyond a certain chain length[301].

3.5.3 Thermal and structural stability of the gel

The gels of **I**, **II** and **V** - **VII** melted thermoreversibly showing gel-sol transition temperatures (T_{gs}) in the range of 51 - 131 °C. Thermally the most stable gels were obtained in 1-pentanol. The T_{gs} values were 79 - 129 °C in 1-pentanol, 54 - 81 °C in 1-octanol and 51 - 69 °C in 1-dodecanol (Table 3.11).

The highest T_{gs} of 129 °C was observed with 1-pentanol gel of **I** (C_7) and the 1-dodecanol gel of **VII** (C_{24}) resulted the lowest T_{gs} of 51 °C. Thermal stability increases in the order 1-dodecanol < 1-octanol < 1-pentanol, corresponding to increasing polarity. Figure 3.16 A illustrates the correlation between T_{gs} and the dielectric constant of the solvent. The correlation is similar also with the polarity parameter E_T, and hydrogen bonding solubility parameter δ_h (not shown here). Apparently, the higher thermal stability is due to restricted solvent-gelator interaction and stronger solvophobic interaction which can be attributed to the long alkyl chains of the gelators. In less polar solvent the solvent-gelator interactions are stronger resulting to a less thermally stable gel.

Table 3.11: The storage (G') and loss (G") moduli at 30 °C and the gel-sol transition temperature T_{gs} determined from temperature sweep measurement*.

	G'_{30} kPa	G''_{30} kPa	T_{gs} °C
1-Pentanol			
I, C_7	51.6	3.9	128.6 ± 0.6
II, C_{10}	34.0	3.6	84.7 ± 1.3
V, C_{16}	29.6	3.0	91 ± 3
VI, C_{18}	36.6	4.2	85.3 ± 0.9
VII, C_{24}	69.7	10.6	79.2 ± 0.4
1-Octanol			
I, C_7	41.0	4.2	80.6 ± 0.6
II, C_{10}	38.5	3.1	68.4 ± 0.4
V, C_{16}	25.5	2.6	70.2 ± 1.1
VI, C_{18}	26.6	3.6	69 ± 2
VII, C_{24}	24.9	2.5	54 ± 2
1-Dodecanol			
I, C_7	42.1	5.6	69 ± 2
II, C_{10}	25.3	3.0	60.9 ± 1.3
V, C_{16}	12.6	1.4	64 ± 3
VI, C_{18}	7.0	1.5	62.2 ± 0.8
VII, C_{24}	11.1	1.2	51.0 ± 1.3

* The G' and G" were determined from merged data of three measurements by interpolating 10 measurement points around 30 °C. The T_{gs} was determined from each measurement and the given result is mean ± standard deviation.

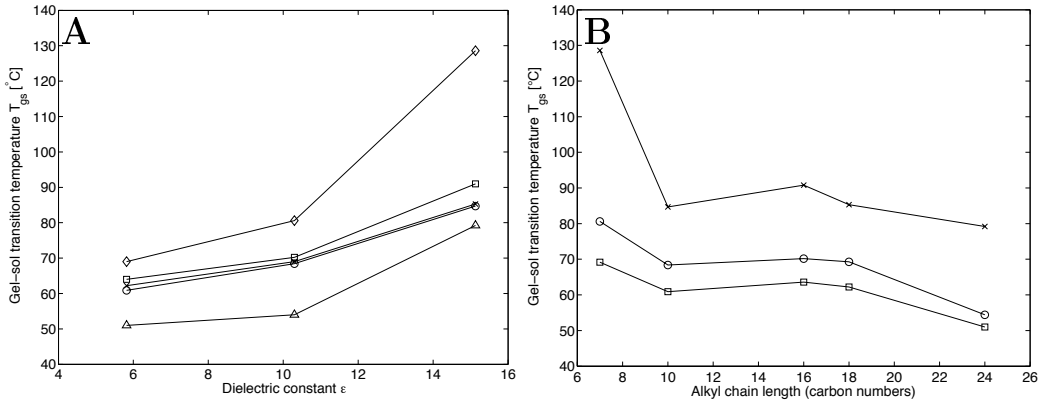

Figure 3.16: Effect of the solvent polarity ϵ (A) and alkyl chain length (B) on the gel-sol transition temperature T_{gs}. In A: $\diamondsuit$ = **I**, $\circ$ = **II**, $\square$ = **V**, x = **VI** and $\triangle$ = **VII** and in B: x = 1-pentanol, $\circ$ = 1-octanol and $\square$ = 1-dodecanol.

Brinksma *et al.*[218] found similar correlation for thermal stability in primary alcohol gels of bis-urea cyclohexane derivative. The gelation was based on hydrogen bonding in less polar solvents in which thermal stability decreased with increasing solvent polarity. The unexpected opposite behavior of T_{gs} in polar alcohols was reasoned by solvophobic forces between the two dodecyl chains in the gelator that become dominant over H-bonding. Also opposite behavior has been observed as the thermal stability of gels of bis(amino acid)oxalyl amides decreased linearly with increasing dielectric constant in lower alcohols than heptanol[59].

Solvophobic forces have more significant role in stabilization of gels in more polar solvents. Percentually T_{gs} was roughly 10 % higher in 1-octanol and 40 % higher in 1-pentanol compared to 1-dodecanol regardless of the alkyl chain length. The only exception to this was 1-pentanol gel of **I** (C_7); however the value obtained is probably slightly overestimated due to solvent evaporation during the measurement. A comparable increase in the solvent polarity increases the thermal stability of the gel more in high polarity range than in low polarity range.

The influence of the alkyl chain on the thermal stability is not straightforward. Figure 3.16 B indicates that the length of the alkyl chain affects the T_{gs} similarly in different solvents. Generally, T_{gs} follows the order $C_7 > C_{16} > C_{18} \approx C_{10} > C_{24}$ in all solvents. The gelator with shortest alkyl chain C_7 (**I**) resulted the highest T_{gs} and the gelator with longest alkyl chain C_{24} (**VII**) resulted the lowest T_{gs}. The gel-sol transition temperature seems to decrease with the elongation of the alkyl chain length but gels of **II** (C_{10})

are exceptions. This is due to an interesting result that gelators with chain length of 10 (**II**) and 18 (**VI**) carbon atoms resulted identical thermal stability regardless of the solvent even though a large difference in the structural stability was observed (Figure 3.17). An explanation for this peculiar result has not been found.

Actually, the length of the alkyl chain does not have a significant effect on the thermal stability of the primary alcohol gels if the chain length of the pyrene derivative is between C_{10} - C_{18}. This alkyl chain length range (C_{10} - C_{18}) is similar to the findings of the Maitra group[85] but contrary to their conclusion it is clear that there are cases for which T_{gs} depends on the alkyl chain length. The thermal stability increases if the alkyl chain length is shorter than C_{10} and decreases if the chain length is longer than C_{18}. The effect of alkyl chain length is more significant for shorter alkyl chains than for the longer ones.

At elevated temperatures eventually a breakdown in storage (G') and loss (G") moduli was observed indicating the loss of interconnections of the gel fibers. At T_{gs}, part of the gel network is dissolved and the remaining part is incapable to self-support[160]. The cgc and mgc increase with the temperature and dissolution of the entire gel network occurs when the cgc equals the gelator concentration. From the temperature sweep measurements the storage (G'_{30}) and loss ($G"_{30}$) moduli at 30 °C were determined (Table 3.11). The chosen temperature is well under the melting range as the lowest T_{gs} values were 50 °C or higher. The highest G'_{30} values and thus the mechanically strongest gels were found in 1-pentanol while the weakest gels were obtained in 1-dodecanol. The G'_{30} values were between 7 and 70 kPa and also followed the solvent polarity order of 1-pentanol > 1-octanol > 1-dodecanol (Figure 3.17 A).

The effect of the alkyl chain length on the structural stability was found to be partially solvent dependent (Figure 3.17 B). The strength of the gels decreased with the elongation of the alkyl chain until C_{16} in all solvents as G'_{30} followed the order of $C_7 > C_{10} > C_{16}$. But with chain lengths C_{18} - C_{24} the G'_{30} value increased in 1-pentanol ($C_{16} < C_{18} < C_{24}$), remained the same in 1-octanol ($C_{16} \approx C_{18} \approx C_{24}$) and decreased further in 1-dodecanol ($C_{16} < C_{24} < C_{18}$). This indicates that solvophobic forces enhance the structural stability of the gel the more the higher the polarity of the solvent but too high solvophobic forces can lead to precipitation as observed with **VII** (C_{24}) a few days after the gel was prepared.

The solvent effect on T_{gs} is much larger than the effect of the alkyl chain length and more significant with shorter alkyl chain gelators. The Hansen distance R_a illustrates the solubility of the compound and higher R_a value indicates lower solubility. For example, R_a of the complex of **II** + TNF were

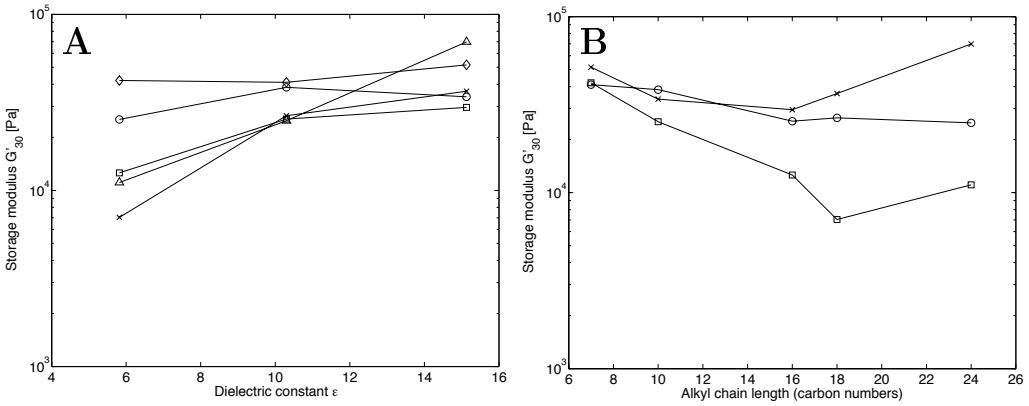

Figure 3.17: Effect of the solvent polarity ϵ (A) and the alkyl chain length (B) on the storage modulus G' at 30 °C in primary alcohols. In A: ♢ = **I**, ○ = **II**, □ = **V**, x = **VI** and △ = **VII** and in B: x = 1-pentanol, ○ = 1-octanol and □ = 1-dodecanol.

15.1, 13.8 and 13.4 in 1-pentanol, 1-octanol and 1-dodecanol, respectively (Table 3.6). The solubility of the complex decreases with solvent polarity resulting in lower mgc and higher gel-sol transition temperature. However, the alkyl chain effect on the thermal stability is counterintuitive because the elongation of the alkyl chain resulted to lower solubility and mgc as expected but also to a *lower* gel-sol transition temperature. This indicates that stronger van der Waals interaction between longer alkyl chains weakens the non-covalent bonding between pyrene moiety and TNF inducing lower thermal stability of the gel. Decrease in thermal stability with the elongation of the alkyl chain length has not been observed with organogelators before to my knowledge. The opposite behavior is much more common as observed with alkanes[16], carbamates[301], fatty acid derivatives[58] and ethylenediamine derivatives[307].

The effect of the gelator concentration on the gel-sol transition temperature (phase diagram) was not studied in this work as it was already shown for pyrene derivatives by others[85,149]. It is common behavior for LMOGs that the gel-sol and sol-gel transition temperatures increase with increasing gelator concentration up to a certain plateau level[101,165,308]. The effect of concentration is more significant at low concentration. In this work temperature sweeps were measured at 70 mmol kg^{-1} gelator concentration and the gelation systems were considered at least in a region well above their mgc 10 - 15 mmol kg^{-1} values if not in the plateau region of their thermal profiles to minimize the effect of possible minor small error in concentration. As

a comparison the gel-sol transition temperature of 1-octanol gel of **V** was 64 °C at 70 mmol kg^{-1} in this work and others have observed the sol-gel transition temperature 52 and 64 °C at 20 and 50 mmol kg^{-1} concentration, respectively[85].

The effect of the gelator concentration on the structural stability can be estimated by comparing the G'_{30} value from temperature sweeps and the G'_{LVE} value from oscillatory stress amplitude sweeps. The temperature sweep measurements were carried out at 2.3 times higher gelator concentration than stress amplitude sweeps (70 vs 30 mmol kg^{-1}). The higher gelator concentration resulted to a 2 - 4 -fold increase of the storage modulus in 1-pentanol, a 5 - 9 -fold increase in 1-octanol and a 4 - 16 -fold increase in 1-dodecanol, if **VII** (C_{24}) is excluded. The increase of the gelator concentration enhances the structural stability more in less polar solvents. Surprisingly, the structurally strongest gels at 30 mmol kg^{-1} were the gels of **VII** but at 70 mmol kg^{-1} no increase was observed in storage modulus or even lower value was observed in 1-octanol. The storage modulus increased the most with chain lengths C_{16} - C_{18} in 1-octanol and 1-dodecanol but with chain lengths C_7 - C_{10} in more polar 1-pentanol.

3.5.4 Viscosity

A region of shear-rate-independent viscosity could not be observed at the shear rates used for gels at 30 mmol kg^{-1} gelator concentration including equimolar amount of pyrene derivative and TNF. The viscosity (η) of all gels decreased with the increase in the applied shear rate, showing a similar shear thinning behavior (Figure 3.18). A sharp drop in viscosity at high shear rates indicates sample slippage, which restricted the maximum shear rate that could be applied.

The effect of the solvent and the alkyl chain length on the viscosity were investigated by measuring flow curves and determining the viscosity values at 1, 10 and 100 s^{-1} shear rate (Table 3.12).

The viscosity at 1 s^{-1} shear rate was 30 - 190 Pa s in 1-pentanol and 10 - 50 Pa s both in 1-octanol and 1-dodecanol. The solvent effect was observable and viscosity followed solvent polarity order 1-pentanol > 1-octanol > 1-dodecanol (Figure 3.19 A). The solvent effect was significant between 1-pentanol and 1-octanol but only small difference in viscosity between 1-octanol and 1-dodecanol was found. Gelator side chain lengths C_7 - C_{16} showed no effect on the viscosity but the viscosity was increased with longer alkyl chains C_{18} - C_{24}.

Figure 3.19 B illustrates the viscosity at ten times higher shear rate, $\dot{\gamma}$ = 10 s^{-1}. The solvent effect on viscosity was clearly observed only for gels

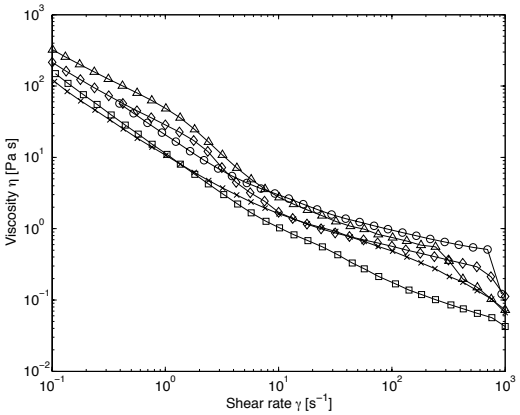

Figure 3.18: Flow curves for 1-dodecanol gels of **I** (♢), **II** (○), **V** (□), **VI** (x) and **VII** (△) at 25 °C.

Table 3.12: Viscosity η at 1, 10 and 100 s^{-1} shear rate from flow curves.

	η_1 Pa s	η_{10} Pa s	η_{100} Pa s
1-Pentanol			
I, C_7	41 ± 12	3.4 ± 0.3	0.46 ± 0.02
II, C_{10}	40 ± 20	2.0 ± 0.5	0.25 ± 0.04
V, C_{16}	30 ± 10	1.9 ± 0.6	0.21 ± 0.03
VI, C_{18}	60 ± 20	6 ± 2	0.095 ± 0.012
VII, C_{24}	190 ± 30	23 ± 5	0.81 ± 0.11
1-Octanol			
I, C_7	27 ± 7	3.1 ± 0.9	0.61 ± 0.11
II, C_{10}	28 ± 7	2.4 ± 0.2	0.67 ± 0.04
V, C_{16}	8 ± 2	1.21 ± 0.13	0.454 ± 0.005
VI, C_{18}	20 ± 3	1.6 ± 0.3	0.42 ± 0.04
VII, C_{24}	49 ± 7	5.5 ± 0.7	0.509 ± 0.014
1-Dodecanol			
I, C_7	23 ± 7	1.74 ± 0.09	0.61 ± 0.06
II, C_{10}	20.8 ± 0.8	3.0 ± 0.3	0.91 ± 0.06
V, C_{16}	10.7 ± 0.7	0.97 ± 0.07	0.22 ± 0.05
VI, C_{18}	11.7 ± 1.0	1.6 ± 0.1	0.46 ± 0.04
VII, C_{24}	46 ± 5	2.7 ± 0.3	0.75 ± 0.03

of **VII** (C_{24}). The viscosity values for gel of **VII** were 23, 5.5 and 2.7 Pa

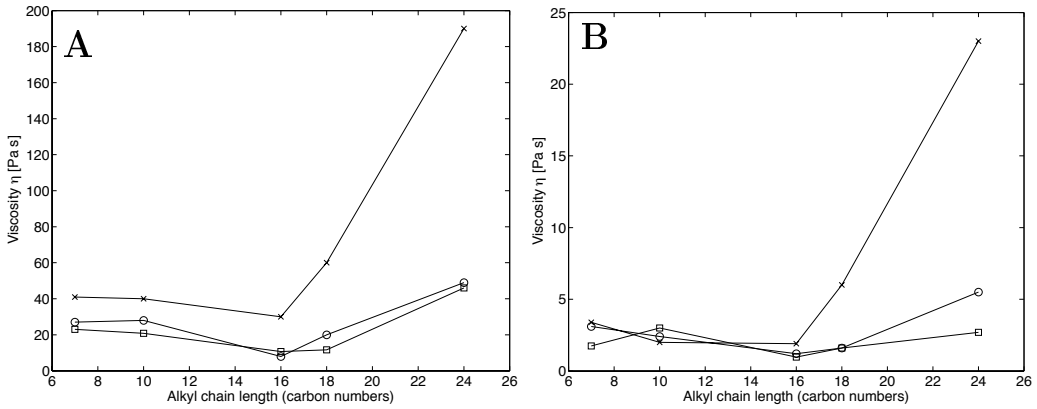

Figure 3.19: Effect of alkyl chain length and the solvent on the viscosity at 1 s^{-1} (A) and 10 s^{-1} (B) shear rates in primary alcohols. x = 1-pentanol, ∘ = 1-octanol and □ = 1-dodecanol.

s in 1-pentanol, 1-octanol and 1-dodecanol, respectively. A small deviation between solvents can be found in gels of **VI** (C_{18}) but generally no significant solvent or alkyl chain length effect on the viscosity at 10 s^{-1} shear rate could be observed with alkyl chains C_7 - C_{18}. At 100 s^{-1} shear rate the viscosity was 0.1 - 0.9 Pa s regardless of the solvent or the alkyl chain length of the pyrene derivative. The results indicate that the solvent and the alkyl chain length effect decrease with increasing shear rate. More gel fibers are broken down at higher shear rates and the viscosity of the gel approaches the viscosity of the solvent.

The downward shear-rate flow behavior of 1-octanol gel of **II** was measured under programmed down-shear rate from 10 - 10^{-6} s^{-1}. The shear stress τ decreased to 20 Pa at 2 s^{-1} shear rate showing a flow behavior but increased exponentially reaching 650 Pa at 10^{-6} s^{-1}. This behavior is due to yield stress (yield point) and gives an approximate shear rate range where the gel starts to show solid-like behavior. Flow behavior started to occur at higher than 1 - 5 s^{-1} shear rate depending on the gel. Flow curves were modeled in the flow range ($\dot{\gamma}$ = 1 - 1000 s^{-1}) according to Herschel-Bulkley (HB) model function $\tau = \tau_{HB} + k\dot{\gamma}^n$. In the HB-model τ is the shear stress, τ_{HB} is the yield point, k is the consistency coefficient and the exponent n is dimensionless flow behavior index. In the model n $<$ 1 corresponds shear thinning behavior, n $>$ 1 corresponds shear thickening behavior and n = 1 corresponds to Newtonian behavior. The Herschel-Bulkley model function is suited for flow curves including yield point[205] and high regression values of 0.995 - 0.999 in the flow range were obtained. Application of Ostwald-de

Waele power-law model function $\tau = k\dot{\gamma}^n$ for flow curves without a yield point resulted to lower regression values indicating, that the gels cannot be modeled without taking a yield point into account.

The calculated flow factors are presented in Table 3.13. All gels had flow index (n = 0.6 - 0.9 Pa) showing shear thinning behavior. The consistency coefficients (k = 1.2 - 3.3 Pa s) were equal in 1-octanol and 1-dodecanol but lower (k = 0.2 - 0.8 Pa s) in 1-pentanol. The yield points τ_{HB} were of the same order of magnitude but generally lower than the yield points τ_y from oscillatory stress amplitude sweep measurements (Table 3.10). No clear correlations between τ_{HB} and solvent parameters or alkyl chain length of the pyrene derivative could be found.

Table 3.13: Herschel-Bulkley model parameters when fitting of the flow curves was done between 1 - 1000 s^{-1} shear rate range.

	τ_{HB} [Pa]	k [Pa s]	n	R^2
1-Pentanol				
I, C_7	25.2 ± 0.8	0.5 ± 0.2	0.82 ± 0.09	0.999
II, C_{10}	8 ± 3	0.8 ± 0.2	0.69 ± 0.03	0.997
V, C_{16}	8 ± 4	0.6 ± 0.2	0.75 ± 0.06	0.999
VI, C_{18}	6 ± 7	0.19 ± 0.04	0.84 ± 0.03	0.996
VII, C_{24}	47 ± 5	0.5 ± 0.7	0.9 ± 0.2	0.996
1-Octanol				
I, C_7	23 ± 8	1.15 ± 0.07	0.76 ± 0.05	0.995
II, C_{10}	10 ± 3	3.3 ± 0.3	0.62 ± 0.03	0.999
V, C_{16}	3 ± 2	2.8 ± 0.3	0.582 ± 0.013	0.997
VI, C_{18}	5.5 ± 0.8	1.9 ± 0.4	0.65 ± 0.03	0.998
VII, C_{24}	12 ± 6	2.1 ± 0.9	0.65 ± 0.07	0.999
1-Dodecanol				
I, C_7	6 ± 2	2.2 ± 0.5	0.70 ± 0.05	0.999
II, C_{10}	16 ± 2	2.3 ± 0.4	0.74 ± 0.02	0.999
V, C_{16}	7 ± 4	1.3 ± 1.4	0.6 ± 0.2	0.995
VI, C_{18}	6.2 ± 1.3	2.9 ± 1.1	0.58 ± 0.08	0.997
VII, C_{24}	17 ± 3	1.8 ± 0.6	0.76 ± 0.08	0.998

3.6 The effect of TNF equivalency

The T_{gs} and G' at 30 °C were determined as a function of molar ratio of TNF : **II** and TNF : **VI** (Figure 3.20). In general, both thermal stability and elasticity of the gel network are weakened if the ratio is altered from 1:1 indicating the optimum ratio 1:1 for self-assembly and gelation. An alteration in the gelator ratio has a larger effect on the gel elasticity than on the thermal stability. An excess of TNF has a greater weakening impact on the gel properties. This observation is in accordance with results of Moffat and Smith[149] but differs from Maitra's group's result as they did not find any significant effect on the thermal stability in case of excess TNF[85].

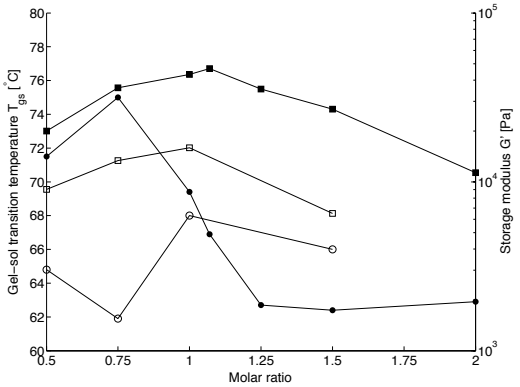

Figure 3.20: The gel-sol transition temperature T_{gs} (• **II**, ∘ **VI**) and the storage modulus G' (■ **II**, □ **VI**) versus molar ratio of TNF/**II** and TNF/**VI** in 1-octanol. Total gelator concentration 70 mmol kg^{-1}.

An exceptional behaviour was observed in the thermal stability of the gel of **II**. The highest T_{gs} of 75 °C was observed at 0.75 molar ratio and even at 0.5 ratio T_{gs} was slightly higher than that of 1:1 gel. The storage modulus indicates the 1:1 ratio to be the optimal molar ratio but different behaviour in T_{gs} can be due to chain length dependent effect. At some point there must be a limit for gel fiber growth as fibers can not grow further in one-dimension if there is only one component remaining in the solution. Shorter gel fibers form weaker gels but shorter fibers can apparently withstand more heat. Shorter gel fibers can move more freely and excess molecules of **II** can be entangled into gel fibers by van der Waals interaction between alkyl chains increasing the thermal stability. Different behavior is observed with longer alkyl chain (**VI**) indicating the effect to be pyrene side chain length dependent. The effect of shorter gel fibers caused by excess TNF is limited as the T_{gs} of gel of **II** decreases with an increase of TNF until 1.25 molar ratio and remains constant thereafter.

3.7 The effect of pyrene

Pyrene (pyr) is the starting material for the LMOG syntheses and some residual pyrene tends to remain in the end product. Hence, it is of interest to know, how detrimental the pyrene impurity is for the gel formation i.e. how well the pyrene has to be removed from the product. The gelation tests showed that pyrene forms a bright red complex with TNF but the complexes precipitate and no gelation occurs. An alkyl chain in the pyrene is a necessity for gelation. The alkyl chains stabilize the gel structure through van der Waals forces and inhibit the solvent flow. The effect of pyrene on the gel stability was tested by substituting part of the gelators with pyrene. The second half of the total gelator concentration was always TNF.

The mechanical strength of the gel network increased and the thermal stability remained constant in gels containing up to 10 mol-% of pyrene but both G' and T_{gs} decreased if the pyrene concentration was increased further (Figure 3.21). The higher gel elasticity is due to more dense and more irregular gel network as seen in the micrographs (Figure 3.12). In case of **VI**, the G' was greater than that for the unsubstituted gel even if more than 10 mol-% pyrene was used but it was clearly seen by eye that the solvent binding ability decreased at high pyrene concentration. Solvent started to exude out from the gel when the measuring plate of the rheometer squeezed the sample before the measurement. This caused the gel to be somewhat concentrated before the measurement, which partially explains the higher observed G' values. At low (< 10 mol-%) pyrene concentrations this effect was not observed.

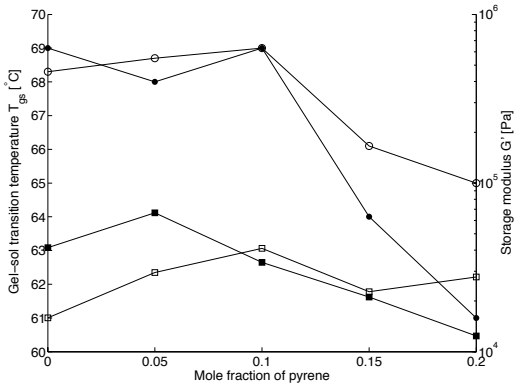

Figure 3.21: Effect of substituted pyrene on the gel-sol transition temperature T_{gs} (• **II**, ○ **VI**) and the storage modulus G' (■ **II**, □ **VI**) of 1-octanol gel. The mole fraction of TNF is 0.5.

In self-assembly the alkyl side chains come in close contact with each

Table 3.14: Influence of pyrene on the storage modulus of the LVE range (G'_{LVE}), the yield point (τ_y) and the flow point (τ_f) of the gels of **II** in the oscillation stress amplitude sweep test (n = 5). The total gelator concentration was 30 mmol kg^{-1} (1 wt-%)

ϕ(pyr)	G'_{LVE} [kPa]	$\tan\delta$	τ_y [Pa]	τ_f [Pa]
0	6.7 ± 1.3	0.15 ± 0.03	16 ± 2	170 ± 30
0.05	9.8 ± 0.03	0.135 ± 0.006	20 ± 3	300 ± 60
0.10	11 ± 2	0.118 ± 0.003	20 ± 5	190 ± 70
0.20	2.9 ± 1.3	0.113 ± 0.008	7 ± 3	170 ± 20

other and steric effect reduces the possible degrees of freedom of the molecules. By adding pyrene, complexation with TNF still occurs but steric effect is reduced, since pyrene creates gaps in the gelator chain (no alkyl group with steric hindrance present). The gelator molecules can assemble more freely and gel fibers are less sterically restricted. Steric hindrance is greater with longer alkyl side chains and the elasticity of gels is improved more with pyrene when longer chain pyrene derivative **VI** was used. At high pyrene concentration the gels of **VI** (C_{18}) were weakened less than the gels of **II** (C_{10}).

A similar behavior was seen in the oscillation stress amplitude sweep measurements of gels of **II** and pyrene at lower gelator concentration (Table 3.14). Examples of stress amplitude sweeps are presented in Figure 3.22. The more elastic behavior of the gels containing pyrene can be seen from the loss tangent values. The loss tangent ($\tan\delta$) is the ratio of moduli which characterize the viscous and the elastic behaviour of the material: the lower the loss tangent value the more elastic the material. All samples showed gel character G' > G" ($\tan\delta < 1$) in the linear viscoelastic range. The maximum values of the G' of the LVE range (G'_{LVE}), the yield (τ_y) and the flow points (τ_f) were obtained at 0.05 - 0.1 pyrene mole fractions. Interestingly, the G'_{LVE} and τ_y decreased when the fraction of pyrene was increased from 10 to 20 mol-% even though according to the loss tangent value the gel became more elastic. This inconsistent result is due to slipping of the rheometer probe because of the exuded solvent.

The flow points were at least 10 times greater than the yield points showing that gel character and elastic properties are still dominant at much higher shear stresses than the yield points indicate. At high stresses a collapse of G' and G" are observed indicating partial breakup of the gel network. However, at higher stresses the slipping of the rheometer probe is more prob-

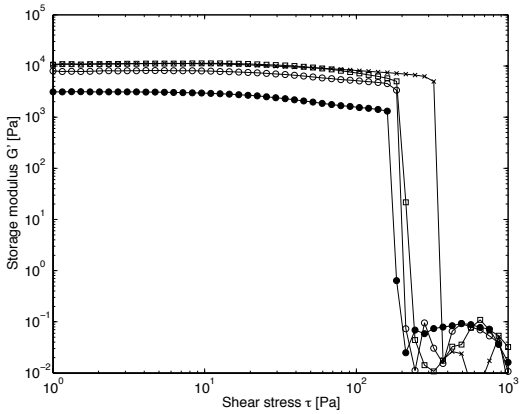

Figure 3.22: Influence of pyrene on stress amplitude sweep of the gels of **II**. Mole fraction of pyrene 0 (○), 0.05 (×), 0.1 (□) and 0.2 (●).

able which explains why flow point decreased already when more than 5 % pyrene was used. The results show clearly that it is possible to enhance the elasticity of the gel with a small amount of pyrene not affecting the thermal stability significantly. A small excess of pyrene can be used in the synthesis of LMOGs and if higher gel stability is desired, complete purification of the pyrene from the synthesis end product is not necessary.

3.8 The effect of crosslinker

In polymers the mechanical properties of the material depend strongly on the crosslinker concentration. It is well known that even low crosslinker concentrations raise the viscosities of polymer melts. Gummy polymers can be transformed into elastomeric and high strength materials by using intermediate crosslinker concentrations[309]. The effect of a crosslinker (**XV**) on gelation was tested by substituting a fraction of **II** with **XV**. In the crosslinker synthesis the alkyl chain was chosen to be longer than in **II** in order to reduce the steric hindrance. Both pyrenes of **XV** are available for complexation which enables a covalent link between separate gel fibers. The desired effect of crosslinker modification is to provide a gel network that imparts elastic stability at higher temperatures which is also indicated by a decrease in the loss tangent. Formation of metastable organogel with TNF and hydrogen bonding capable crosslinker including two pyrene units has been previously reported[149].

The oscillatory stress amplitude sweep measurements showed that the crosslinker increases the stability of the gel (Table 3.15). The storage modulus

of the linear viscoelastic range (G'_{LVE}) and the yield point (τ_y) are good indicators of elastic and mechanical stability. The τ_y determines the end point of the LVE range and no significant change in the gel structure occurs at stresses inside the LVE range.

Table 3.15: Influence of the crosslinker **XV** on the properties of gel of **II**. The storage modulus G', the yield point τ_y and the loss tangent $\tan\delta$ of the LVE range and the flow point τ_f in the oscillation stress amplitude sweep tests and the viscosity (η) at 1, 10 and 100 s^{-1} in the flow curve measurements (n = 6). Corresponding values for the gel without crosslinker can be found in Table 3.8 and Table 3.14.

ϕ(**XV**)	0.25	0.625	1.25	2.5
G'_{LVE}, kPa	8.7 ± 1.2	11.6 ± 1.2	9 ± 2	12 ± 2
τ_y, Pa	24 ± 5	31 ± 2	28 ± 7	31 ± 3
τ_f, Pa	250 ± 90	180 ± 60	160 ± 50	250 ± 60
$\tan\delta$	0.084 ± 0.010	0.075 ± 0.010	0.079 ± 0.012	0.09 ± 0.02
η_1, Pa s	26 ± 6	19 ± 4	11 ± 3	12.8 ± 0.6
η_{10}, Pa s	1.7 ± 0.5	1.55 ± 0.05	1.26 ± 0.09	1.7 ± 0.2
η_{100}, Pa s	0.36 ± 0.05	0.34 ± 0.03	0.324 ± 0.007	0.39 ± 0.04

Gels with a crosslinker had wide LVE ranges. Only 0.25 mol-% crosslinker in the gel increased the τ_y from 16 to 24 Pa and the G'_{LVE} from 6.4 to 8.7 kPa. The gel containing 0.625 mol-% crosslinker had the highest G'_{LVE} and τ_y but no further increase in gel stability was observed at higher crosslinker concentration. There was no clear trend in the flow point with crosslinker concentration but the elastic properties were dominant up to 5 to 10 times higher stress values compared to a noncrosslinked gel. Wider LVE range is a sign of the ability of structure to resist greater external stresses. Lower loss tangents ($\tan\delta$) in the LVE range show that the elastic properties become more dominant than the viscous properties if crosslinker is used. The addition of a crosslinker to a gel decreases the loss tangent value significantly, meaning that the crosslinker brings elasticity to the base gel as expected. The lowest $\tan\delta$ value was observed with 0.625 crosslinker mole fraction and interestingly the $\tan\delta$ slightly increased at higher crosslinker concentration. Even small amount of the crosslinker hardens the gel to a great extent. However, slippage of the sample may have affected the measurements at higher crosslinker concentrations.

According to the temperature sweep measurements, the gel of **II** had the T_{gs} of 69 °C. The T_{gs} was increased by 2 and 5 °C when 0.625 and 1.25

mol-% crosslinker were used, respectively. Unfortunately the sample with 2.5 mol-% crosslinker was so rubbery that reliable data could not be obtained due to slippage. However, the addition of the crosslinker does improve the thermal stability of the gel and better thermal stability is more obvious at higher crosslinker concentration than increase in elasticity in the oscillation stress amplitude sweep measurements.

All the gel samples showed a strong shear thinning behavior, however, a region of shear-rate-independent viscosity could not be reached. The structural and thermal stability increase with crosslinker concentration but, interestingly, the observed viscosity values at 1, 10 and 100 s^{-1} were reduced when higher crosslinker concentration was applied. With 1.25 mol-% crosslinker the viscosity values were roughly half of the values obtained in gels with no crosslinker. The crosslinker effect on the viscosity is just the opposite than observed in polymers and can be explained only by increasing slippage of the rheometer probe.

3.9 Gel stability

The stabilities of the gels of **II** and **VI** were examined during one year period. Gels were stored in closed vials in the dark at room temperature and the measurements were carried out one day after gel preparation (0-sample), and then after 2, 4 and 8 weeks and finally one year after the gel preparation. The stability during storage was examined by determining the gel-sol transition temperature T_{gs} and the storage modulus at 30 °C (Figure 3.23).

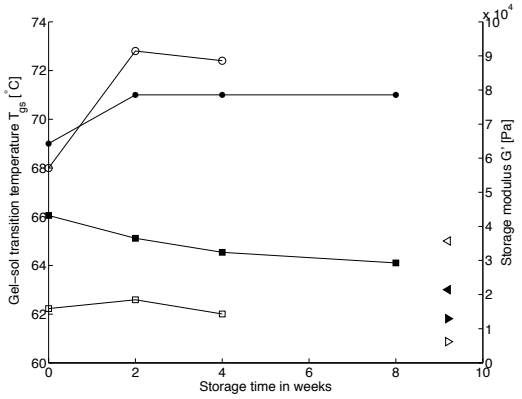

Figure 3.23: Gel-sol transition temperature T_{gs} (● **II**, ○ **VI**) and storage modulus G' (■ **II**, □ **VI**) of the 1-octanol gel as a function of storage time. Values after one year: T_{gs} (◀ **II**, ◁ **VI**) and G' (▶ **II**, ▷ **VI**) of the gel.

The 0-sample storage moduli after 1 day (G'_o) were 43.2 and 15.9 kPa

for gels of **II** and **VI**, respectively. During the first 8 weeks the storage modulus of the gel of **II** followed well the kinetics of G'(n) = $0.9^{n/2}G'_o$ where n is storage time in weeks. The G' of the gel of **VI** was slightly increased after 2 weeks but decreased thereafter. The gel network of **II** was more elastic and is presumed to maintain structural stability and resistance to external forces longer. The T_{gs} of the 0-samples were 68 - 69 °C showing similar thermal stability. After two weeks the T_{gs} of gels of **II** and **VI** gels were increased by 2 and 4 °C, respectively. The T_{gs} remained stable afterwards even if lower G' were observed. The loss tangent ($\tan\delta$) was 0.17 for gel of **II** and 0.23 for gel of **VI** and the values remained stable during the first 8 weeks.

The properties of the gels were examined next time after one year. After prolonged storage the G' were 12.7 and 6.1 kPa for gels of **II** and **VI**, respectively. The G' and $\tan\delta$ values were ~35 % of the 0-sample indicating that weakening of the gel network occurs slower after 8 weeks than during the first 8 weeks after gel preparation. After one year the T_{gs} was 63 and 65 °C for **II** and **VI**, respectively. The T_{gs} were 3 - 5 °C lower than 0-samples and 6 - 10 °C lower than the maximum T_{gs} values during the first 8 weeks. Two weeks after the gel preparation T_{gs} of the gel of **VI** was slightly higher than the gel of **II** but after one year the gel of **VI** had lower thermal stability. Generally, the gels were structurally and thermally very stable for the 8 week period. By visual inspection no change in the gel structure or exuded solvent were observed even after one year. By rheometry the gels remain thermally stable even though the gels are weakened more in terms of structural stability. Percentually the thermal stability decreased less than 10 % and the structural stability decreased 30 - 40 % during one year.

The gels of pyrene derived LMOGs proved to be extremely stable against the effects of acceleration when sedimentation of the sample was tested with a centrifuge. Only one droplet of solvent was released by centrifuging a 2 ml 1-octanol gel of **II** and TNF at 30 mmol kg^{-1} concentration under 1000 g acceleration for one hour. For comparison 40 % of the kerosene was released from jet fuel gel gelled with 5 wt-% fumed silica (Figure 3.24).

3.10 Spectroscopic properties and gelation kinetics

Gelator molecules **I** - **XV** are highly UV and fluorescence active and show characteristic UV-visible absorption bands of pyrene. A very strong absorption band between 360 - 560 nm was observed when TNF was added to solutions of pyrene derivatives in 1-decanol (Figure 3.25 A). Wavelengths

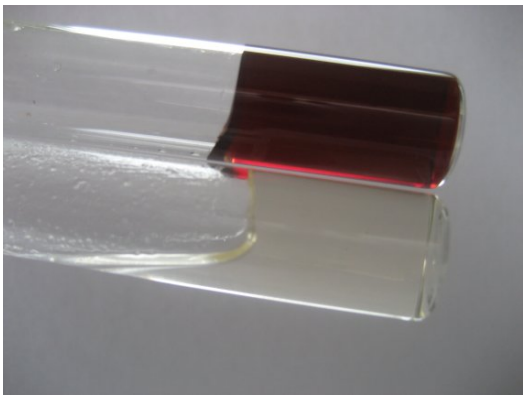

Figure 3.24: Gels of **II** and TNF in 1-octanol (top) and 5 wt-% Aerosil 200 in kerosine JET A1 (below) after 1h under 1000g acceleration.

below 550 nm are very strongly absorbed in the gel where a broad absorption band causes the red colour of the gels resulting from the charge transfer complex in analogy to light harvesting antennas in bacteria and plants. The hot sols were transparent over the entire range. UV-Vis spectra of the gels exceeded the device range indicating too high a sample concentration (∼15 mmol kg^{-1}). However, lower gelator concentration could not be applied because no gel network is formed and no appreciable change in the spectrum is observed.

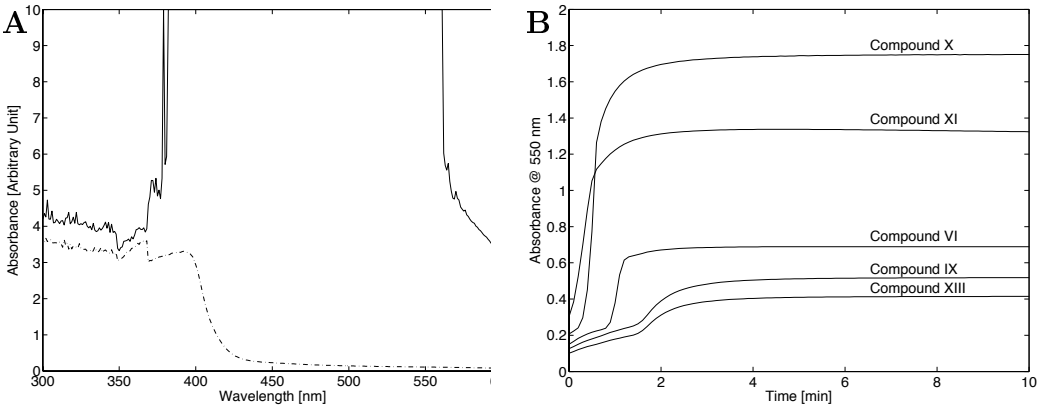

Figure 3.25: (A) UV-Vis spectrum of 1-decanol gel of **IX** at 25 °C (solid curve) and hot sol at 80 °C (dashed curve). (B) Gelation kinetics of gelators **VI**, **IX** - **XI** and **XIII** in 1-decanol by UV-Vis. The gelator concentration was 16 mmol kg^{-1} (A) and 30 mmol kg^{-1} (B) including equimolar amounts of pyrene derivative and TNF.

The spectral data is shown here for pyrene based LMOGs including various functional groups to illustrate the effect of the functional group. The absorption and fluorescense maxima for the gel were at 480 nm which could not be used in the kinetic measurements due to excessive absorption. Thus, the gelation kinetic measurements for gels of **VI**, **IX** - **XI** and **XIII** (Figure 3.25 B) were carried out at 550 nm in order to avoid saturation of the measurement.

The absorbance at 550 nm increased strongly directly from the start of the cooling process of a hot sol for gels of **X** and **XI**. The rapid increase in absorbance for gels of **VI**, **IX** and **XIII** was observed but it occurred after 40 - 90 s after the measurement started. The charge transfer band is very sensitive to temperature and the absorbance reached the maximum steady state value at the gelling point within 3 - 5 min for all gels. All gelators form thermoreversible gels very fast unlike polymeric gelators, where re-equilibration can take weeks. The effect of finite cooling rate is negligible on this time scale because there was only a few seconds setup time before the measurement was started. A kinetic plot showed that the fastest CT gel formation occurs with gelators **VI**, **X** and **XI** ($\sim$3 min to steady maximum absorption). The gel formation is somewhat slower (4 min) with gelators **IX** and **XIII** containing hydroxyl groups at the alkyl chain end. The results indicate that strong solvent-gelator interaction slows down CT gel formation and such an interaction is generally more pronounced with gelators containing functionality.

The absorbance of 1-decanol gel of **X** at 550 nm was followed during both the heating and the cooling cycles and a systematic hysteresis was observed (Figure 3.26 A). The hysteresis curve showed that upon cooling the self-assembly of the gelator molecules enhances at 55 °C whereas melting of the gel network begins at 35 °C during the heating. The hysteresis can be ascribed to the rate of the sol-gel and gel-sol transitions, and its magnitude depends on the cooling and heating rates. Small hysteresis effect was observed despite of the fast cooling and heating rate (10 °C min^{-1}) showing the gels form and equilibrate fast. The hysteresis results are in accordance with rheological temperature sweep experiments in which storage moduli started to decrease generally around 40 °C (Figure 3.11).

The pyrene ring fluoresces strongly and shows five emission bands at low concentrations. The third and first bands are highly sensitive to the polarity of the solvent. At higher concentrations pyrene is expected to show an excimer band at 480 nm due to the formation of an excited state dimer. A broad fluorescence band was observed at 450 - 520 nm with excitation wavelength 336 nm. The UV-Vis and fluorescence experiments can give general idea about gel properties even though measurements at higher concentra-

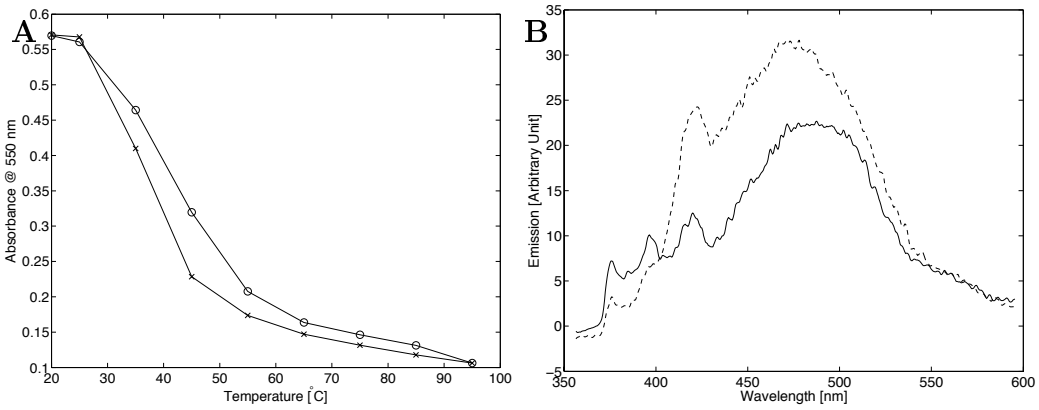

Figure 3.26: (A) Gelation hysteresis of gelator **X** in 1-decanol by UV-Vis using 10 °C min^{-1} heating (○) and cooling (×) rate. (B) Fluorescence spectra of 1-decanol gel of **IX** at 25 °C (solid curve) and hot sol at 80 °C (dashed curve) at 30 mmol kg^{-1} total gelator concentration. The excitation wavelength was 336 nm.

tions are not recommended. The emissive properties of both sols and gels were studied and showed a strong fluorescence (λ_{max} at 480 nm) resulting from the excited state complex with TNF (Figure 3.26 B). The fluorescent intensity of the gels was temperature dependent. According to the fluorescence the 1-decanol gel of **IX** melts completely before 75 °C which agrees with the UV-Vis and rheology results.

3.11 Thermoanalysis

The phase transitions of the 1-decanol gels of **VI**, **IX** and **XI** were studied by differential scanning calorimetry (DSC). The pyrene based LMOGs included an alkyl chain without functionality (**VI**) and alkyl chains containing different functionalities (**IX** and **XI**) to study the effect of the functional group. The DSC profiles of the gels (Figure 3.27) show several exothermic transitions along with the endothermic transition showing, that many structural changes take place in the material during heating and the determination of the transition enthalpy can be complicated. All gels showed gel-sol transition in the range of 60 - 80 °C. The shape of the DSC profile and the gel-sol transition temperature depend on the functional group of the pyrene derivative.

Gel of **XI** and TNF (1:1) in 1-decanol showed repeatable endothermic

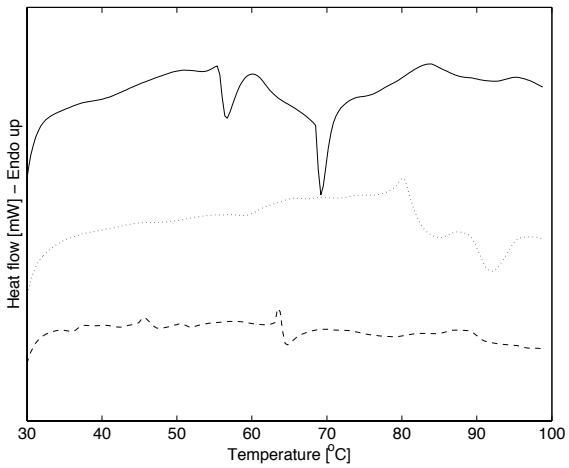

Figure 3.27: DSC of 1-decanol gels of **VI** (solid curve), **IX** (dashed curve) and **XI** (dotted curve) at 30 mmol kg^{-1} total gelator concentration.

peak with transition enthalpy of +0.6 kJ mol^{-1} which is significantly less than the melting enthalpy of the neat gelator molecules, which were about 40 - 50 kJ mol^{-1} for the pyrene based LMOGs. The small enthalpy value indicates that the observed endothermic transition corresponds to dissolution of the gelators. This low enthalpies were at the limits of the instrument but the measurements were reproducible. The thermal profiles shown are an average of three separate measurements. The reasons for the exothermic phase transitions are unclear and the gel-sol transition enthalpies for gels of **VI** and **IX** could not be determined due to unexplained phase transitions. The gel-sol transition temperature for the gels were determined by rheology instead of DSC due to the unclear phase transitions of the DSC profiles. Multiple phase transitions may be due to various modes of aggregation and structural rearrangement.

As the energy changes by DSC are measured only at the end of the transitions, the gel has completely turned into a sol at the temperature where the enthalpy changes are recorded. Hence, DSC is less suitable for investigating structural changes in a gel. Rheology, inverted test tube and viscosity measurements can detect much more subtle changes than a complete melting. Consequently, the gel-sol transition temperatures by these methods are lower than those obtained from DSC.

3.12 Xerogel and supramolecular structure

A dual structure was observed at larger scale in the electron micrograph of the xerogel of **XI** and TNF (Figure 3.28). A dense gel network included uniformly 50 nm thick gel fibers and evenly sized spherical clusters of 1.5 μm in diameter. All gels showed fibrous structure but the diameter of the gel fibers varied between 20 - 300 nm depending on the pyrene derivative. The micrographs at higher resolution showed that the thicker gel fibers consist of multiple thin fibers. A dual structure was observed in gels of gelators including functional group in the alkyl chain, e.g. in gels of **IX** - **XI** and **XIII**.

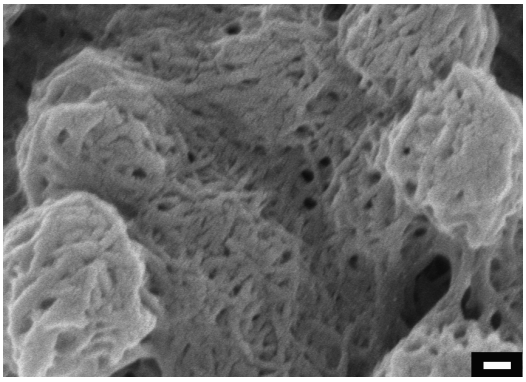

Figure 3.28: Electron micrograph of the xerogel of **XI** and TNF in 1-decanol. Scale bar 200 nm.

The enthalpy of formation of the charge transfer complex of **XI** and TNF was calculated at PM3 level of theory using Gaussian 03[310] in gas phase at 0 K. The energy of formation for a linear chain structure was -7.4 kJ mol^{-1} (Figure 3.29). Another structure included hydrogen bonding between >C=O and -$NHNH_2$ groups had very similar energy of formation (ΔH_f = -7.6 kJ mol^{-1}). In this structure the hydrogen bonds twist the chain structure into a spherical or helical configuration and the π-π interaction between pyrene and TNF is broken. The calculated minimum energy structures indicate that the gelator chain can have two possible structures in the gel. This supports the observation of the dual structure by SEM.

The calculated energy of formation is an order of magnitude greater than measured gel-sol transition enthalpy of the CT gel of **XI** and TNF (+0.6 kJ mol^{-1}) by DSC. This suggests that the solvation enthalpy of the gelator is almost as large as the enthalpy of formation of the chain, since the DSC can only detect the difference of the two. Another possibility is, that the entropy change is from gel to sol is relatively large causing a positive

heat release and a smaller detected change of enthalphy than the calculations suggest. As both mechanisms can be present simultaneously, it is not possible to evaluate the magnitude of each of them. The magnitude of the measured change of enthalpy is similar to a typical heat of solvation of organic molecules into organic solvents, which indicates the gel to sol transition resembles a dissolution of the components.

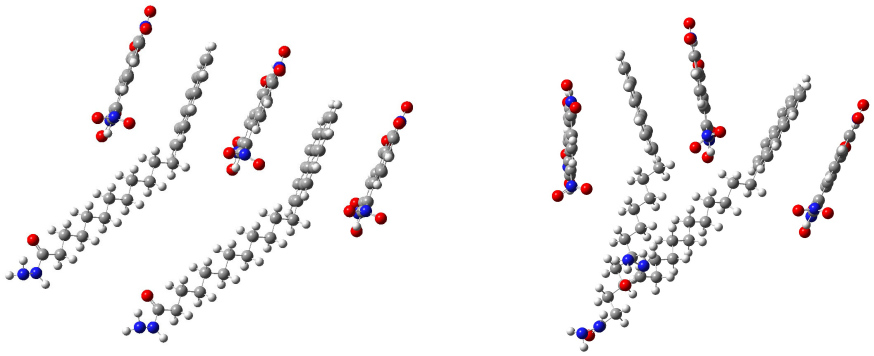

Figure 3.29: Calculated minimum energy structures of **XI** and TNF: linear π-π- configuration (left) and hydrogen bonded spheroid or helix (right).

Calculations on larger than dimeric aggregates were unsuccessful due to the very flat potential energy surface and numerous local minima in these systems. Crystallization attempts of the CT complexes failed and information on the crystal structure is not available so far.

The atomic charges were fitted to reproduce the molecular electrostatic potential at a number of points around the molecule using the Merz-Kollman-Singh[311] (MKS) method. In the twisted structure the sum of atom charges on TNF by MKS method was zero indicating that charge transfer does not occur. In the linear chain structure the sum was -0.0055 electron charges showing only a weak CT mechanism. Less than 5 % of the bonding energy in the linear chain structure can be attributed to CT interaction the rest being due to van der Waals bonding. According to the calculations, the CT mechanism cannot be responsible for gelator chain formation nor the gel-sol transition enthalphy observed. Generally, aromatic complexes show CT bands but theoretical calculations indicate that charge transfer plays only a minor role in the stability of the ground state of molecular complexes[296].

However, it may be necessary for self-assembly to first align the molecules by π-π interactions so that the short range multipolar field coulombic interactions between individual atoms in the pyrene derivative and TNF can take over. Atomic charges of TNF ($\pm$0.5 electron charges) and pyrene derivative (up to $\pm$0.3 electron charges) create much larger bonding energies than

0.0055 total electron charge over the entire molecule despite of the larger surface area. Atomic charges have a short effective range due to the multipolar electric field of the system while the π-π interactions have much longer range.

In order for ideal atom-to-atom van der Waals bonding to occur, the atoms have to be aligned in a way that a positively charged atom always matches a negatively charged counterpart in the adjacent molecule. This also explains why any even weakly electronegative substituent on the pyrene inhibits gelation since it changes the order of negative and positive atoms in the pyrene system. The match with TNF at the optimal CT complex geometry is lost in addition to reduction of the π-electron density. Without any alignment by the π-π mechanism, atoms could form van der Waals bonds to each other at a random locations of the molecule and no ordered chains of the molecules would be formed. If there is a longer range π-π interaction available first guiding the molecules into a correct position, then every atom can find a pair and the atom-to-atom forces can lock the pyrene and TNF into a minimum energy configuration, which is otherwise difficult to attain due to numerous other local energy minima in the system. If a solvent is present, the van der Waals bonding energy will be even higher since there is bonding between the alkyl chains via solvent molecules. The calculations were carried out without solvent molecules present while DSC was carried out with solvent producing approximately an order of magnitude lower enthalpy than the calculations indicated.

The bonding energy of the twisted structure originates from hydrogen bonding only unless the solvent is present generating van der Waals bridges between the alkyl chains. This configuration alone cannot form gel fibers as it has only one binding site but it can alter the linear gel fiber formation. Hydrogen bonding at the end of the alkyl chain twists the pyrenes apart despite of the flexibility available in the alkyl chain (Figure 3.29). Hydrogen bonding between the functional groups of the alkyl chains must be prevented to allow a π-π interaction and subsequent van der Waals bonding in the gel fiber while the functional groups are needed for binding other materials. The hydrogen bonding could be avoided by adding non-functionalized pyrene derivative or pyrene to the gel to separate the hydrogen bonding groups preventing mutual interactions as discussed in the Chapter 3.4.

3.13 Nanoparticles in gels

In recent years interest in nanoparticle-gel composites has increased due to their possible applications as new materials with novel properties[312]. In many

cases, the attention has been on gel network templated metal nanoparticle synthesis in which low molecular weight gelator with functional group acts as a capping agent and binds metal nanoparticles into the gel[313–318].

The effects of nanomaterial incorporation into the gel of pyrene derived low molecular weight gelator was examined by mixing aluminum nanoparticles with gelators. Vigorous sonication to disperse 100 nm aluminum nanoparticles (AlNP) heated the sample and additional heating to dissolve the gelator components was not needed. It was found that **II** and TNF did not form a gel in 1-octanol in the presence of uncoated AlNP's. The self-assembly of the gelators was prevented because the polar TNF was adsorbed on the surface of the AlNP's.

A strong gel was formed when AlNP's were coated with decanoic or stearic acid before mixing with the gelator components. Electron micrograph showed that aluminum nanoparticles remained dispersed in the gel structure (Figure 3.30). The rheological properties of the gels, including 1 wt-% of the gelators, were altered only slightly when 10 wt-% coated AlNP's were added to the gel (Table 3.16). A minor decrease was observed in the viscosity at 1, 10 and 100 s^{-1} shear rates. The yield point of the gel was 14 - 17 Pa with or without AlNP's in the gel. The flow points were 70 % lower but 20 - 40 % higher G'_{LVE} values indicated that the strength of the gel network was enhanced by AlNP's. The gel of 1-decylpyrene (**II**) was structurally more stable when AlNP's were coated with decanoic acid so it may be beneficial to use the same alkyl chain length in the coating agent as in the pyrene based gelator.

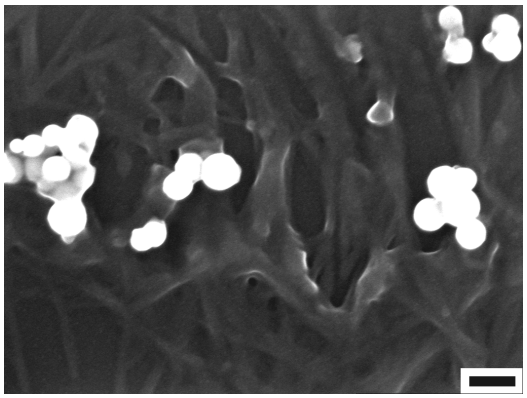

Figure 3.30: SEM image of 1-octanol gel of **II** and TNF including 10 wt-% decanoic acid coated 100 nm aluminum nanoparticles. Scale bar 200 nm.

These results suggest that nanoparticles can be bound into the organogel of pyrene derivatives if nanoparticles are first coated with functionalized

Table 3.16: Influence of decanoic and stearic acid coated Al nanoparticles (10 wt-%) on the storage modulus of the LVE range (G'_{LVE}), the yield point (τ_y), the flow point (τ_f) and the viscosity (η) at different shear rate of the gel of **II**. The total gelator concentration was 30 mmol kg^{-1} (1 wt-%)

	no metal	Al/Decanoic acid	Al/Stearic acid
G'_{LVE}, kPa	6.7 ± 1.3	9.6 ± 1.0	7.9 ± 0.9
τ_y, Pa	16 ± 2	17 ± 3	14 ± 3
τ_f, Pa	170 ± 30	60 ± 9	49 ± 12
η_1, Pa s	28 ± 7	24.7 ± 1.4	35 ± 11
η_{10}, Pa s	2.4 ± 0.2	2.13 ± 0.13	1.7 ± 0.3
η_{100}, Pa s	0.67 ± 0.04	0.504 ± 0.002	0.45 ± 0.03

pyrene derivative, such as **IX**, and TNF is added afterwards to achieve gelation. In the preliminary tests the non-functionalized gelator **II** had to be used due to the low amount of functionalized gelators available.

4 Conclusions

In this work, fifteen pyrene based functionalized and non-functionalized low molecular weight organogelators were synthesized and characterized by spectroscopic techniques and elemental analysis. The gelation ability of the compounds at room temperature were studied in various organic solvents and the properties of the gels were investigated by rheometry, scanning electron microscopy, differential scanning calorimetry, UV-Vis and fluorescence spectroscopy.

The compounds **I** - **XV** formed thermoreversible gels in the presence of 2,4,7-trinitrofluorenone (TNF) in alcohols due to non-covalent interactions. The majority of the gels remained visually stable at least for two years. In chloroform, ketones and aromatic solvents no gelation was observed at practically useful gelator concentrations and gelation in these solvents was not studied further due to limited amount of gelators available. Aliphatic hydrocarbons were not gelated due to the poor solubility of TNF. The polarity of the solvent and the gelator solubility were found to govern the gelation ability of the two-component gelator system. The minimum gelation concentration decreased linearly when the polarity or the hydrogen bonding solubility parameter δ_h of the solvent increased. Theoretical calculations indicated that the self-assembly of the two-component gelator system is primarly driven by π-π and charge-transfer (donor-acceptor) interactions between a pyrene derivative and TNF, but most of the intramolecular binding energy can be accounted to van der Waals forces.

The results suggest that it is possible to estimate the gelation ability of a multi-component gelator system without experimental work. The previously unknown solubility parameters of the gelator components and their charge transfer complex were estimated by group contribution method. The solubility of the components were further estimated by calculating their Hansen distances to the solvent which showed that the polar TNF restricts the gelation ability of the two-component gelator system in general. The gelation abilities of the pyrene based LMOGs are closely related to the hydrogen bonding solubility parameter of the solvent. The range of Hansen distances

of **II**, TNF and their complex were determined for cases when a gelation occurred. Any solvent or solvent mixture fulfilling requirements of R_a(**II**) $\leq$ 22.3 $MPa^{1/2}$, 20.0 $MPa^{1/2} \leq R_a$(TNF) $\leq$ 23.5 $MPa^{1/2}$ and 12.6 $MPa^{1/2} \leq R_a$(complex) $\leq$ 18.7 $MPa^{1/2}$ should form a gel, provided no unaccounted other effects are present such as π-π complexation with the solvent. Application of the Hansen solubility parameters and distance can give a good estimation for gelation behavior of the two-component gelator system including both nonpolar and polar solvents. However, it seemed that gelation behavior in highly nonpolar solvents can be better understood by using the Hildebrand solubility parameter because of the restrictions of the Hansen model in such solvents.

Rheological measurements indicated that the gels were viscoelastic soft materials showing a shear thinning behavior and a yield point. The effect of the solvent and the alkyl side chain length of the pyrene based LMOGs were studied by preparing gels in primary alcohols with pyrene derivatives with C_7 - C_{24} alkyl side chain lengths. The mechanical strength, viscosity and thermal stability of the gel depended strongly on the solvent polarity. The thermal and structural stability of the gels increased with polarity and hydrogen bonding solubility parameter δ_h of the solvent. The solvent effect was more significant with shorter alkyl side chain than longer ones.

The effect of the alkyl side chain length was found to be solvent dependent. Generally, the mechanical strength of the gel decreased with an increase in the length of the alkyl chain between C_7 - C_{18}. However, the strongest gels were obtained with alkyl chain length C_{24} but these gels precipitated within a few days. At 1 and 10 s^{-1} shear rates the viscosity was independent of the alkyl chain between C_7 - C_{16} but increased with longer alkyl chains. At higher shear rates the alkyl chain length effect disappeared and generally the solvent and the alkyl chain length effect on viscosity decreased with increasing shear rate. The gel-sol transition temperature was independent of the alkyl chain length between C_{10} - C_{18} but increased below C_{10} and decreased above C_{18}. Remarkably, the thermal stability of the gels decreased with elongation of the alkyl chain length. This result is opposite to what has commonly been observed with low molecular weight organogelators.

New insights into relationship between the structure of the pyrene based organogelators and the rheological properties of the gel were obtained by combining SEM and rheological studies. Electron microscopy showed that gel formation is due to self-assembly of the gelators into long fibers, which in turn stick together to an entangled gel network structure. Solvent-gelator interaction and the structure of the pyrene based gelator component affect the structure of the gel network. Single gel fiber thickness was relatively independent on the gelator but formation of gel fiber bundles and regularity of the gel

network were gelator dependent. Gels with less gel fiber bundles and denser gel network were more elastic and had higher viscosities. A gelator including a functional group formed less elastic and thermally less stable gel and had lower viscosity indicating that competing mechanisms over functional groups disturb the gel network formation. The rheological properties of the functionalized gels could be significantly improved by mixing them with a non-functionalized gelator resulting to a three-component gelator system. A small concentration of pyrene or a crosslinker as a third gelator component was also found to increase both the elasticity and the thermal stability of the gel. The gels were extremely stable to the effects of acceleration. During one year the thermal stability of the gels decreased less than 10 % and the structural stability 30 - 40 %.

Preparation of the aluminum nanoparticle doped gels showed that functionalized pyrene based LMOGs can be used to stabilize and disperse metal nanoparticles into the gel matrix. The results presented here show that pyrene based organogelators in two- and three-component gelator systems open wide possibilities to controlling the gel properties.

5 Experimental

5.1 Preparation of the gels

The pyrene based gelators were synthesized as described in Chapter 5.3 and 2,4,7-trinitrofluorenone (TNF) was purchased from Apin Chemicals Ltd, UK. All solvents were of analytical grade and were used as received. The gels were prepared by weighing equimolar amounts of a gelator and TNF into a vial before the solvent was added. Molality was used to prepare gel samples instead of widely used molarity. The determination of molality only requires a good scale, because masses of both solvent and solute can be obtained by weighing. Molality is independent of physical conditions like temperature and pressure, providing advantages over molarity. By determining the gel concentration based on molality makes the preparation of the gel samples easier and more accurate.

A small magnet stirrer was added to samples prepared for the rheology measurements before closing the vial and the solution was stirred and heated in a oil bath, if necessary, up to the boiling point of the solvent, until preferably both components were fully dissolved. The gel was formed when the solution was allowed to cool down to room temperature.

5.2 Characterization of the gels

5.2.1 Rheology

Rheological properties were determined using a Haake Rheostress1 and Anton-Paar Physica MCR-301 rheometers using a cone-plate (angle 2°, diameter 25 and 35 mm) and a plate-plate (diameter 50 mm) configurations. A minimum of three parallel measurements were performed and the average of these was used as the result and the standard deviation as error limits. The gel samples were placed on the measuring plate with a Pasteur pipette as a hot solution and after 5 min the measurement was started. Only exception to this sample preparation procedure were the gel samples tested for gel stability. These

samples could not be melted and they were placed on the measuring plate with a spatula. The tests performed were oscillation frequency, stress amplitude and temperature sweeps and flow curve measurement. The frequency sweep experiments were carried out at a constant stress of 1 Pa. In the stress amplitude sweep test the stress was increased from 1 to 1000 Pa using a constant 1 Hz frequency at 25 °C. From stress amplitude sweep the linear viscoelastic (LVE) region, the yield and flow points were determined. The limiting value of the LVE region in terms of the shear stress corresponds to the yield point and it was determined by using 5 % tolerance in the storage modulus G' value. The flow point corresponds the crossover point G' = G".

The thermal stability of the gels was determined by sweeping the temperature from 10 to 80 °C at a rate of 1.2 °C min^{-1} in oscillation mode using a 1 Hz frequency and stress of 1 Pa. A cover was placed over the measurement head and the gel-sol transition temperature (T_{gs}) was determined by sweeping the temperature upwards to minimize adsorption of moisture and loss of solvent. The viscosity was determined by sweeping the shear rate from 0.001 to 1000 s^{-1}) in 1 min at 25 °C. The total gelator molality of 70 mmol kg^{-1} (2.2 - 3.0 wt-% depending on the gelator) was used for temperature sweeps and 30 mmol kg^{-1} (1.1 - 1.3 wt-%) for stress amplitude sweeps and flow curves. The different gel concentration in the temperature sweeps was used in order to improve the signal to noise ratio in each case.

5.2.2 Scanning electron microscopy

Gel samples (1 - 3 mg) were melted on pieces of silicon wafers and dried at room temperature for 3 days. Prior to imaging the samples were coated with a thin layer of gold using Jeol Fine Coat Ion Sputter JFC-1100. A sputtering time of 30 seconds was used with 1 kV voltage, 10 mA of current and 5 mbar air as the gas medium producing an about 1 nm thick gold coating.

Micrographs were recorded with RAITH E-Line high resolution field emission scanning electron microscope operating at 6 kV using 30 µm aperture, 6 mm working distance and using ultra high vacuum ($< 4 \times 10^{-7}$ Torr) with an Everhart Thornley in-lens detector.

5.2.3 Spectral characterization

UV-Vis and fluorescence spectra were measured with a Shimadzu UV-2100 UV-Vis spectrophotometer using a thermostated quartz cuvette with 10 mm path length at 25 °C. The hysteresis studies were carried out with a heating and cooling rate of 10 °C per minute.

The kinetic experiments by UV-spectroscopy were carried out by transferring a 80 °C hot solution consisting of a gelator and TNF at 2:1 ratio into a UV cuvette with path length of 1 mm maintained at 25 °C . Less TNF than 1:1 ratio was used to prevent precipitation of any substance and to reduce the very high absorbance level. Absorbance at 550 nm was monitored against time. Fluorescence spectra were measured using Perkin-Elmer LS-50B luminescence spectrometer with a 10 mm path length quartz cuvette at 25 °C using 336 nm excitation wavelength.

5.2.4 Thermoanalysis

Thermal transitions for the gels were determined on power compensation type Perkin-Elmer Pyris Diamond DSC. The measurements were carried out under nitrogen atmosphere (flow rate 50 ml min^{-1}) using 50 μl sealed aluminum sample pans. The gel samples were melted with a hot-air blower and placed as a hot solution on a sample pan. Samples were allowed to cool down to room temperature before sealing the sample pan. The temperature calibration was made using indium and n-decane standards and energy calibration by an indium standard (28.45 J g^{-1}). Each sample (10 - 20 mg) was heated from 25 to 100 °C with a heating rate of 20 °C/min. The uncertainty for measured temperatures was less than 0.8 °C.

5.3 Syntheses and characterization data

All chemicals and solvents were used as received from sealed containers. ^{1}H and ^{13}C NMR NMR spectra were recorded on a Bruker Avance DRX 500 (500 and 126 MHz). The solvent peak for $CDCl_3$ was adjusted to 7.26 ppm in ^{1}H NMR and to 77.0 ppm in ^{13}C NMR at 30 °C. The IR spectra were recorded on a Mattson Satellite FTIR spectrometer by using KBr pellets. The melting points were determined in open capillaries with a Stuart Scientific SMP3 melting point apparatus and are uncorrected. Mass spectra were measured with Micromass LCT (electrospray MS) or with VG Autospec (electron impact MS). The reference material used for high resolution mass spectroscopy (HRMS) was leucine enkephalin acetate hydrate for ESI-MS and perfluorokerosene for EI-MS. The elemental analyses were carried out with a VarioEL III CHN elemental analyzer by using sample weights of 1 - 4 mg.

1-(pyren-1-yl)heptan-1-one (Ia): Heptanoyl chloride (7.35 g, 0.05 mol) was mixed with pyrene (10 g, 0.05 mol) and 1,2-dichloroethane (DCE, 120 ml). The mixture was cooled below 5 °C in a ice bath while adding dropwise

$TiCl_4$ (0.15 mol). After stirring overnight at RT 100 ml water was added into the dark lilac mixture. From the mixture 13 g of DCE layer was separated, water (15 ml) was added and refluxed for 30 min before DCE was distilled off. The product was extracted in 3 hours into hexane (300 ml) in a Soxhlet. The hexane was evaporated to 100 ml and left to crystallize at RT. The crystallized product was purified further by flash chromatography using a gradient of $CHCl_3$/Hexane (30:70 to 70:30) to give pale yellow solid (0.96 g, 93 % yield); mp 82-83 °C; IR (KBr): 2941, 2916, 2868, 2854, 1672, 1593, 1504, 1466, 1379, 1250, 1234, 1207, 1178, 849 and 719 cm^{-1}; ^1H NMR (500 MHz, $CDCl_3$): 0.91 (3H, t), 1.30-1.40 (4H, m), 1.47 (2H, m), 1.87 (2H, q), 3.20 (2H, t), 8.02-8.32 (8H, m) and 8.86 (1H, d, J 9.3 Hz) ppm; ^{13}C NMR (126 MHz, $CDCl_3$): 14.0, 22.5, 25.0, 29.1, 31.7, 42.7, 124.0, 124.4, 124.8, 125.0, 125.92, 125.93, 126.1, 126.3, 127.1, 129.2, 129.3, 129.4, 130.6, 131.1, 133.1, 133.6 and 205.4 ppm; LRMS: *m/z* 314 (M^+); Elemental anal. calcd for $C_{23}H_{22}O$: C, 87.86; H, 7.05. Found: C, 87.73; H, 7.03 %.

1-heptylpyrene (I): Water-DCE mixture from **Ia** synthesis was refluxed for 30 min before DCE layer was distilled off. Digol (200 ml) was added and water was distilled off before adding KOH (0.19 mol). The mixture was heated to 190 °C under nitrogen atmosphere. Hydrazine monohydrate (0.14 mol) was added slowly keeping temperature at 190-200 °C overnight. Gases were flushed with nitrogen until temperature was 225 °C. The mixture was cooled to 50 °C and the product was extracted into 5 x 200 ml hexane, filtered through silica and dried over $MgSO_4$. The extracts were left to crystallize at RT. Filtering and crystallization processes were repeated several times to obtain pure white solid (7.08 g, 51 % yield); mp 85-86 °C; IR (KBr): 2947, 2924, 2854, 1468, 837 and 710 cm^{-1}; ^1H NMR (500 MHz, $CDCl_3$): 0.90 (3H, t), 1.26-1.36 (4H, m), 1.40 (2H, q), 1.50 (2H, q), 1.86 (2H, q), 3.34 (2H, t), 7.87 (1H, d, J 7.7 Hz), 7.96-8.18 (6H, m) and 8.29 (1H, d, J 9.2 Hz) ppm; ^{13}C NMR (126 MHz, $CDCl_3$): 14.1, 22.7, 29.3, 29.8, 31.9, 32.0, 33.6, 123.5, 124.6, 124.7, 124.8, 125.11, 125.12, 125.7, 126.5, 127.1, 127.2, 127.5, 128.6, 129.7, 131.0, 131.5 and 137.4 ppm; LRMS: *m/z* 300 (M^+); Elemental anal. calcd for $C_{23}H_{24}$: C, 91.95; H, 8.05. Found: C, 91.83; H, 8.11 %.

1-(pyren-1-yl)decan-1-one (IIa): Decanoic acid (86 g, 0.5 mol) was first treated with excess of thionyl chloride (300 ml, 4.2 mol) and refluxed for 3-4 h. Excess of $SOCl_2$ was removed by distillation under reduced pressure. The decanoyl chloride (95 g, 0,5 mol) was mixed with pyrene (101 g, 0.5 mol) and DCE (1200 ml). To this mixture was added $TiCl_4$ (150 g, 0.75 mol) dropwise with stirring in ice bath below 5 °C during the addition. The brown complex formed was stirred for further 16 h at RT. The brown complex was

cleaved by the addition of water and DCE was distilled off. The product was extracted into chloroform in a Soxhlet (1500 mL) and washed with water, saturated sodium bicarbonate (2 x 100 mL) and finally with water. The chloroform layer was dried over anhydrous $MgSO_4$ and concentrated under reduced pressure. The crude material was purified by recrystallization from hexane/chloroform 99/1. The pure product (156 g, 84 %) was isolated as yellow solid; m.p. 59-61 °C; IR (KBr): 3045, 2920, 1594, 1506, 1466, 1413, 1382, 1254, 1218, 1182, 1063, 958, 842 and 714 cm^{-1}; ^{1}H NMR (500 MHz, $CDCl_3$): 0.88 (3H, t, *J* 7.0 Hz), 1.29 (10H, m), 1.46 (2H, m), 1.87 (2H, q, *J* 7.5 Hz), 3.20 (2H, t, *J* 7.5 Hz), 7.97 - 8.35 (8H, m) and 8.86 ppm (1H, d, *J* 9.5 Hz); ^{13}C NMR(126 MHz, $CDCl_3$): 14.06, 22.64, 25.03, 29.26, 29.43, 29.46, 29.49, 31.86, 42.74, 123.99, 124.40, 124.84, 124.92, 125.05, 125.91, 125.92, 126.13, 126.34, 127.08, 127.37, 129.23, 129.33, 129.41, 130.61, 131.13, 133.08, 133.54 and 205.44 ppm; HRMS (TOF-ES+): *m/z* 357.2237 (Calc. for $C_{26}H_{28}O$ + H: 357.2216); Elemental anal. calcd for $C_{26}H_{28}O$: C, 87.60; H, 7.92. Found: C, 87.96; H 7.86 %.

1-decylpyrene (II): 1-(pyren-1-yl)decan-1-one **IIa** (148 g, 0.4 mol) and KOH (90 g, 1.6 mol) were mixed with digol (800 ml) and warmed to 180 °C. The solution turned brownish in color. To this solution hydrazine monohydrate (40 ml, 0.8 mol) was added slowly keeping temperature at 190-200 °C under nitrogen atmosphere for 12 h. Finally, the temperature was slowly raised to 220 °C. All the vapours were flushed out with nitrogen flow. The mixture was cooled to 50 °C. The product was extracted into 3 x 1000 ml hexane, which were filtered through 50 g of silica and dried over anhydrous $MgSO_4$. The combined extracts were evaporated to 1000 ml volume and left to crystallize over 3 days at RT. Additional crop was obtained by evaporating the hexane down to 400 ml and crystallizing overnight with seed crystals from the first batch. The pure product (125 g, 88 %) was obtained as bright yellow solid; m.p. 69-71 °C; IR (KBr): 3039, 2954, 2917, 2850, 1463, 961, 841, 824, 760, 722, 707, 680 and 625 cm^{-1}; ^{1}H NMR (500 MHz, $CDCl_3$): 0.88 (3H, t), 1.2-1.35 (10H, m), 1.38 (2H, m), 1.50 (2H, q), 1.85 (2H, q), 3.33 (2H, q), 7.87 (1H, d, *J* 8.0 Hz), 7.97-8.20 (7H, m) and 8.29 ppm (1H, d, *J* 9.0 Hz); ^{13}C NMR (126 MHz, $CDCl_3$): 14.10, 22.68, 29.34, 29.60, 29.636, 29.644, 29.84, 31.91, 31.93, 33.60, 124.57, 124.73, 124.75, 125.107, 125.114, 125.70, 126.44, 127.04, 127.19, 127.52, 128.62, 129.70, 130.97, 131.48 and 137.35 ppm; HRMS (70 eV, EI): *m/z* 342.2355 (Calc. for $C_{26}H_{30}$: 342.2348); Elemental anal. calcd for $C_{26}H_{30}$: C, 91.17; H 8.83. Found: C, 91.09; H 8.92 %.

1-dodecylpyrene (III): Synthesis and characterization from ref. 85; mp 72-73 °C; IR (thin film): 1465 and 840 cm^{-1}; ^{1}H NMR (300 MHz, $CDCl_3$):

0.88 (3 H, t, *J* 6.8 Hz), 1.26-1.37 (16 H, m), 1.37 (2 H, q, *J* 7.5 Hz), 1.49 (2 H, m), 3.33 (2 H, t, *J* 7.7 Hz), 7.87 (1 H, d, *J* 7.8 Hz), 8.02 (2 H, m), 8.17 (5 H, m) and 8.29 (1 H, d, *J* 9.3 Hz); ^{13}C NMR (75 MHz, $CDCl_3$): 22.07, 29.36, 29.61, 29.65, 29.68, 29.85, 31.93, 31.98, 33.64, 123.55, 124.59, 124.76, 124.77, 125.08, 125.74, 126.46, 127.07, 127.25, 127.54, 129.68, 130.96, 131.47 and 137.39 ppm; LRMS: *m/z* 384 (M^+); Elemental anal. calcd for $C_{28}H_{34}$: C, 90.75; H, 9.25. Found: C, 90.95; H, 9.33 %.

1-(pyren-1-yl)tridecan-1-one (IVa): Tridecanoic acid (21.4 g, 0.1 mol) was treated with excess of thionyl chloride (60 ml, 0.84 mol) and refluxed for 3 hours. Excess of $SOCl_2$ was removed by distillation under reduced pressure. The acid chloride was mixed with pyrene (0.05 mol) and 1,2-dichloroethane (DCE, 120 ml). The mixture was cooled below 5 °C in a ice bath while adding dropwise $TiCl_4$ (0.13 mol). After stirring overnight at RT 100 ml water was added into the dark brown mixture and 10 % of DCE layer was separated for purification and analyses. Water was added and refluxed for 30 min before DCE was distilled off. The product was extracted into hexane (300 ml) in a Soxhlet overnight. The hexane was evaporated to 40 ml and left to crystallize at RT. The crystallized product was purified further on a silica column using 40/60 $CHCl_3$/Hexane as an eluent to give pure bright yellow solid (1.37 g, yield 69 %); mp 64-65 °C; IR (KBr): 2918, 2845, 1672, 1464, 1211, 1173, 850 and 719 cm^{-1}; ^{1}H NMR (500 MHz, $CDCl_3$): 0.90 (3H, t), 1.22-1.41 (16H, m), 1.46 (2H, q), 1.87 (2H, q), 3.19 (2H, t), 8.10-8.30 (8H, m) and 8.87 (1H, d, J 9.3 Hz) ppm; ^{13}C NMR (126 MHz, $CDCl_3$): 14.1, 22.7, 25.0, 29.4, 29.46, 29.52, 29.53, 29.63, 29.65, 29.7, 31.9, 42.7, 124.0, 124.4, 124.9, 125.0, 125.92, 125.95, 126.1, 126.3, 127.1, 129.25, 129.33, 129.4, 130.6, 131.1, 133.1, 133.6 and 205.4 ppm; LRMS: *m/z* 398 (M^+); Elemental anal. calcd for $C_{29}H_{34}O$: C, 87.39; H, 8.46. Found: C, 87.15; H, 8.69 %.

1-tridecylpyrene (IV): The rest of DCE layer from 1-(pyren-1-yl)tridecan-1-one **IVa** synthesis was refluxed for 30 min and water layer was removed. Digol (80 ml) was added and DCE was distilled off before adding KOH (0.18 mol). The mixture was heated to 200 °C under nitrogen atmosphere. Hydrazine monohydrate (0.093 mol) was added slowly keeping temperature at 180 °C overnight. Temperature was raised to 220 °C before mixture was cooled to 50 °C and the product was extracted into 7 x 150 ml hexane and filtered through silica and dried over $MgSO_4$. The combined extracts were evaporated to 100 ml and left to crystallize at RT. The product was obtained as a white solid (4.7 g, yield 26 %); mp 67-69 °C; IR (KBr): 2953, 2916, 2868, 2848, 1462 and 839 cm^{-1}; ^{1}H NMR (500 MHz, $CDCl_3$): 0.88 (3H, t), 1.19-1.34 (16H, m), 1.38 (2H, q), 1.49 (2H, q), 1.86 (2H, q), 3.34

(2H, t), 7.87 (1H, d, J 7.8 Hz), 7.96-8.18 (7H, m) and 8.29 (1H, d, J 9.2 Hz) ppm; ^{13}C NMR (126 MHz, $CDCl_3$): 14.1, 22.7, 29.4, 29.60, 29.64, 29.7, 29.8, 31.9, 32.0, 33.6, 123.5, 124.6, 124.75, 124.77, 125.1, 125.7, 126.5, 127.1, 127.2, 127.5, 128.6, 129.7, 131.0, 131.5 and 137.4 ppm; LRMS: *m/z* 384 (M^+); Elemental anal. calcd for $C_{29}H_{36}$: C, 90.57; H, 9.43. Found: C, 90.84; H, 9.46 %.

1-(pyren-1-yl)hexadecan-1-one (Va): Modified from Babu's procedure[85]. Palmitic acid (8.2 g, 0.032 mol) was treated with excess of thionyl chloride (60 ml, 0.84 mol) and refluxed for 3 hours. Excess of $SOCl_2$ was removed by distillation under reduced pressure. The acid chloride was mixed with pyrene (0.029 mol) and DCE (70 ml). The mixture was cooled below 5 °C in a ice bath while adding dropwise $TiCl_4$ (0.054 mol). After stirring overnight at RT 100 ml water was added into the dark brown mixture. Water was added and refluxed for 30 min before DCE was distilled off. Water was removed and the product was extracted into hexane (300 ml) in a Soxhlet overnight. 10 % of hexane solution was left to crystallize at RT. The crystallized product was purified further on a silica column using 30/70 $CHCl_3$/Hexane as an eluent to give pure pale yellow solid (0.89 g, yield 70 %); mp 70-71 °C [Babu: 60-61 °C]; IR (KBr): 2954, 2913, 2848, 1672, 1471, 845 and 715 cm^{-1}; ^{1}H NMR (500 MHz, $CDCl_3$): 0.88 (3H, t), 1.21-1.40 (22H, m), 1.46 (2H, q), 1.86 (2H, q), 3.21 (2H, t), 8.04-8.33 (8H, m) and 8.86 (1H, d, J 9.4 Hz) ppm; ^{13}C NMR (126 MHz, $CDCl_3$): 14.1, 22.7, 25.0, 29.3, 29.4, 29.49, 29.50, 29.60, 29.64, 29.7, 31.9, 42.8, 124.0, 124.4, 124.9, 125.1, 125.9, 126.2, 126.4, 127.1, 129.3, 129.36, 129.43, 130.6, 131.2, 133.1, 133.6 and 205.5 ppm; LRMS: *m/z* 440 (M^+); Elemental anal. calcd for $C_{32}H_{40}O$: C, 87.22; H, 9.15. Found: C, 86.79; H, 9.20 %.

1-hexadecylpyrene (V): Modified from Babu's procedure[85]. The hexane solution from 1-(pyren-1-yl)hexadecan-1-one **Va** synthesis was distilled down to 70 ml before digol (200 ml) was added and the rest of hexane was distilled off before adding KOH (0.10 mol). The mixture was heated to 200 °C under nitrogen atmosphere. Hydrazine monohydrate (2.7 ml, 0.05 mol) was added slowly keeping temperature at 180 °C overnight. Temperature was raised to 220 °C before mixture was cooled to 50 °C and the product was extracted into 7 x 150 ml hexane and filtered through silica and dried over $MgSO_4$. The combined extracts were evaporated to 100 ml and left to crystallize at RT. The crystallized product was purified further on a silica column using 99.95/0.05 Hexane/THF as an eluent to give pure white solid (5.9 g, yield 53 %); mp 82-83 °C [Babu: 79-80 °C]; IR (KBr): 2953, 2916, 2848, 1464, 841, 723 and 706 cm^{-1}; ^{1}H NMR (500 MHz, $CDCl_3$): 0.88 (3H, t), 1.22-1.34 (22H, m), 1.38 (2H, q), 1.49 (2H, q), 1.86 (2H, q), 3.34 (2H, t), 7.87 (1H, d,

J 7.7 Hz), 7.96-8.19 (7H, m) and 8.29 (1H, d, *J* 9.2 Hz) ppm; ^{13}C NMR (126 MHz, $CDCl_3$): 14.1, 22.7, 29.3, 29.59, 29.63, 29.65, 29.67, 29.69, 29.8, 31.92, 31.95, 33.6, 123.5, 124.6, 124.75, 124.76, 125.1, 125.7, 126.5, 127.1, 127.2, 127.5, 128.6, 129.7, 131.0, 131.5 and 137.4 ppm; LRMS: *m/z* 426 (M^+); Elemental anal. calcd for $C_{32}H_{42}$: C, 90.08; H, 9.92. Found: C, 89.53; H, 9.92 %.

1-(pyren-1-yl)octadecan-1-one (VIa): Stearic acid (4 g, 14.1 mmol) was first treated with excess of thionyl chloride (2.5 g, 21.2 mmol) and refluxed for 3-4 h. Excess of $SOCl_2$ was removed by distillation. The stearoyl chloride (3.6 g, 11.9 mmol) was mixed with pyrene (2.0 g, 9.9 mmol) and DCE (10 ml). To this mixture was added $TiCl_4$ (2.25 g, 11.9 mmol) dropwise with stirring over ice bath. The temperature was maintained below 5 °C during the addition. The brown complex formed was stirred for further 12 h. The brown complex was cleaved by the addition of water and dilute HCl. The product was extracted into DCM (20 mL) and washed with saturated sodium bicarbonate (2 x 85 mL), dil. HCl and finally with water. The DCM layer was dried over anhydrous Na_2SO_4 and concentrated under reduced pressure. The crude material was purified further by chromatography over Merck 60 silica gel using DCM-hexane (1:9) as eluent. The pure product (3.25 g, 70 %) was isolated as yellow solid; m.p. 74-76 °C; IR (KBr): 2953-2849, 1672, 1471, 843 and 716 cm^{-1}; ^{1}H NMR (250 MHz, $CDCl_3$): 0.88 (3H, t, *J* 6.8 Hz), 1.25 (30H, br s), 1.86 (2H, m), 3.21 (2H, t, *J* 7.5 Hz), 8.00-8.33 (8H, m) and 8.87 (1H, d, *J* 9.3 Hz) ppm; ^{13}C NMR (63 MHz, $CDCl_3$): 14.11, 22.69, 25.03, 29.36, 29.44, 29.50, 29.62, 29.66, 29.70, 31.93, 42.73, 123.99, 124.40, 124.84, 125.04, 125.92, 126.13, 126.34, 127.08, 129.24, 129.33, 129.42, 130.60, 131.12, 133.05, 133.54 and 205.43 ppm; HRMS (70eV, EI): *m/z* 469.3383 (Calc. for $C_{34}H_{44}O$: 469.3426); Elemental anal. calcd for $C_{34}H_{44}O$: C, 87.12; H, 9.46. Found: C, 87.09; H, 9.47 %.

1-octadecylpyrene (VI): 1-(pyren-1-yl)octadecan-1-one **VIa** (0.5 g, 1.07 mmol) was mixed with KOH (0.36 g, 6.4 mmol) and digol (2 mL) and warmed to 110 °C. The hydrazine hydrate was then added dropwise to the above stirring mixture. This was stirred at 120 °C for 2-3 h. The temperature of the reaction was raised to 200 °C. After 1 h the reaction mixture was cooled to room temperature. The mixture was acidified with dil. HCl till neutral to litmus. The product was extracted in to chloroform and washed with saturated sodium bicarbonate (2 x 85 mL), dil. HCl and finally with water. The DCM layer was dried over anhydrous Na_2SO_4 and concentrated under reduced pressure. The crude material was purified further by chromatography over Merck silica 60 using hexane as eluent. The pure product (0.34 g, 70 %) was isolated as white solid; m.p. 83-84 °C; IR (KBr): 3039, 2965-2849,

1463 and 840 cm^{-1}; ^{1}H NMR (250 MHz, $CDCl_3$): 0.89 (3H, t, *J* 6.8 Hz), 1.26 (30H, br s), 1.85 (2H, m), 3.34 (2H, t, *J* 7.5 Hz), 7.87 (1H, d, *J* 7.8 Hz), 7.95-8.18 (7H, m) and 8.29 (1H, d, *J* 9.3 Hz) ppm; ^{13}C NMR (63 MHz, $CDCl_3$): 14.11, 22.70, 29.37, 29.61, 29.71, 29.85, 31.94, 33.62, 123.54, 124.59, 124.75, 125.12, 125.73, 126.46, 127.06, 127.23, 127.54, 128.63, 129.70, 130.98, 131.49 and 137.38 ppm; HRMS (70eV, EI): *m/z* 454.3595 (Calc. for $C_{34}H_{46}$: 454.3599); Elemental anal. calcd for $C_{34}H_{46}$: C, 89.80; H, 10.19. Found: C, 89.57; H, 10.27 %.

1-(pyren-1-yl)tetracosan-1-one (VIIa): Tetracosanoic acid (3.5 g, 9.5 mmol) was treated with excess of thionyl chloride (60 ml, 0.84 mol) and refluxed for 3 hours. Excess of $SOCl_2$ was removed by distillation under reduced pressure. Tetracosanoic acid chloride and pyrene (1.7 g, 8.55 mmol) were dissolved separately in 35 ml of DCE before they were mixed. The mixture was cooled below 5 °C in a ice bath while adding dropwise $TiCl_4$ (14.3 mmol). After stirring overnight at RT 50 ml water was added and refluxed for 30 min before DCE was distilled off. Water was removed and the product was extracted into hexane (300 ml) in a Soxhlet overnight. 200 ml of hexane was removed by distillation and the product was left to crystallize at RT. The crystallized product was purified further on a silica column using 40/60 $CHCl_3$/Hexane as an eluent to give pure pale yellow solid (2.48 g, yield 52 %); mp 83-84 °C; IR (KBr): 2918, 2848, 1678, 1471, 1464, 847 and 717 cm^{-1}; ^{1}H NMR (500 MHz, $CDCl_3$): 0.88 (3H, t), 1.18-1.40 (38H, m), 1.46 (2H, q), 1.86 (2H, q), 3.21 (2H, t), 8.03-8.34 (8H, m) and 8.86 (1H, d, J 9.3 Hz) ppm; ^{13}C NMR (126 MHz, $CDCl_3$): 14.1, 22.7, 25.0, 29.35, 29.44, 29.49, 29.51, 29.61, 29.65, 29.70, 31.9, 42.8, 124.0, 124.4, 124.9, 125.1, 125.9, 126.2, 126.4, 127.1, 129.26, 129.37, 129.44, 130.6, 131.2, 133.1, 133.6 and 205.5 ppm; LRMS: *m/z* 552 (M^+); Elemental anal. calcd for $C_{40}H_{56}O + \frac{1}{2}H_2O$: C, 85.50; H, 10.23. Found: C, 85.37; H, 10.18 %.

1-tetracosylpyrene (VII): 1-(pyren-1-yl)tetracosan-1-one **VIIa** (2.2 g, 4.0 mmol) and KOH (1.0 g) were dissolved in digol (200 ml). The mixture was heated to 200 °C under nitrogen atmosphere. Hydrazine monohydrate (0.5 ml) was added slowly keeping temperature at 180 °C overnight. Temperature was raised to 220 °C before mixture was cooled to 50 °C and the product was extracted into 5 x 300 ml hexane and 45 g silica was added. Silica was filtrated before hexane was concentrated to 300 ml and left to crystallize at RT. The crystallization process was repeated with 500 ml hexane and finally the crystallized product was purified further on a silica column using 99.95/0.05 Hexane/THF as an eluent to give white solid (1.31 g, yield 61 %); mp 92-93 °C; IR (KBr): 2951, 2918, 2848, 1473, 1464, 841, 721 and 708 cm^{-1}; ^{1}H NMR

(500 MHz, $CDCl_3$): 0.88 (3H, t), 1.21-1.34 (38H, m), 1.38 (2H, q), 1.49 (2H, q), 1.86 (2H, q), 3.34 (2H, t), 7.87 (1H, d, J 7.7 Hz), 7.96-8.20 (7H, m) and 8.29 (1H, d, J 9.3 Hz) ppm; ^{13}C NMR (126 MHz, $CDCl_3$): 14.1, 22.7, 29.4, 29.59, 29.63, 29.65, 29.67, 29.69, 29.71, 29.8, 31.93, 31.95, 33.6, 123.5, 124.6, 124.75, 124.77, 125.12, 125.13, 125.73, 126.5, 127.1, 127.2, 127.5, 128.6, 129.7, 131.0, 131.5 and 137.4 ppm; LRMS: *m/z* 538 (M^+); Elemental anal. calcd for $C_{40}H_{58}$: C, 89.15; H, 10.85. Found: C, 88.49; H, 10.81 %.

4-oxo-4-(pyren-1-yl)butanoic acid (VIIIa): Succinic acid (0.4 g, 3.4 mmol) was refluxed with excess of acetic anhydride (5 mL) for 10 h. After the reaction acetic anhydride and acetic acid were removed by distillation. A mixture containing pyrene (0.5 g, 2.5 mmol) and above succinic anhydride (about 0.39 g, 3 mmol) were dissolved in DCE (3 mL) and kept for stirring on ice bath. To this stirring solution $TiCl_4$ (0.56 g, 3 mmol) was added dropwise for 5 min and the stirring was continued for 24 h. The complex was hydrolyzed by the addition of water and dil. HCl. The product formed was extracted into EtOAc (15 mL) and washed with water (2 x 5 mL). The organic layer was dried over anhydrous Na_2SO_4 and concentrated under reduced pressure. The final product was further purified by chromatography over Merck silica 60 using acetone-DCM (1:9) as eluent. The pure product (0.51 g, 68 %) was obtained as pale yellow crystalline solid; m.p. 184-185 °C; IR (KBr): 3453, 1695, 1665 and 842 cm^{-1}; ^{1}H NMR(250 MHz, DMSO-d6): 2.76 (2H, t, *J* 6.0 Hz), 3.49 (2H, t, *J* 6.0 Hz), 8.12-8.43 (7H, m), 8.57 (1H, d, *J* 8.3 Hz) and 8.77 (1H, d, *J* 9.5 Hz) ppm; ^{13}C NMR (63 MHz, DMSO-d6): 28.55, 36.92, 123.47, 123.96, 124.44, 125.97, 126.39, 126.44, 126.72, 127.15, 128.12, 129.14, 129.29, 129.94, 130.63, 132.48, 133.01, 173.89 and 203.18 ppm; HRMS (TOF-ES-): *m/z* 301.0365 (Calc. for $C_{20}H_{13}O_3$ -H: 301.0865); Elemental anal. calcd for $C_{20}H_{13}O_3$ + 1/4 H_2O: C, 78.55; H, 4.28. Found: C, 78.80; H, 4.52 %.

4-(pyren-1-yl)butanoic acid (VIII): To a reaction mixture containing 4-oxo-4-(pyren-1-yl)butanoic acid **VIIIa** (0.5 g, 1.65 mmol), digol (2.0 mL) and KOH (0.74 g, 13.2 mmol) at 110 °C was added hydrazine monohydrate (0.83 g, 16.5 mmol) slowly and stirred for 2 h at 120 °C. The temperature of the reaction was increased to 180 °C with continued stirring for at least 50 minutes. The reaction mixture was poured into ice bath and acidified till neutral to litmus and extracted with ethyl acetate (15 mL, 3 x 5 mL). Organic layer washed with water (2 x 5 mL) and dried over anhydrous Na_2SO_4. The crude product was further purified by column chromatography over Merck silica 60 using acetone-DCM (5:95) as eluent. The final product (0.31 g, 65 %) was obtained as pale yellow solid; m.p. 182-183 °C; IR (KBr): 3433,

2920, 2845, 1701 and 843 cm^{-1}; ^{1}H NMR (250 MHz, $CDCl_3$): 2.22 (2H, m), 2.52 (2H, t, *J* 7.0 Hz), 3.43 (2H, m), 7.87 (1H, d, *J* 7.8 Hz), 7.95-8.20 (7H, m) and 8.30 (1H, d, *J* 9.3 Hz) ppm; ^{13}C NMR (63 MHz, $CDCl_3$): 26.53, 32.68, 33.27, 123.25, 124.83, 124.86, 124.97, 125.03, 125.17, 125.88, 127.37, 127.50, 128.79, 130.09, 130.94, 131.46, 135.49 and 177.69 ppm; HRMS (70eV, EI): *m/z* 288.1145 (Calc. for $C_{20}H_{16}O_2$: 288.1150); Elemental anal. calcd for $C_{20}H_{16}O_2$ + 1/2 H_2O: C, 80.84; H, 5.76. Found: C, 80.41; H, 5.42 %.

12-oxo-12-(pyren-1-yl)dodecanoic acid (IXa): Dodecanedioic acid (23 g, 0.1 mol) was first treated with excess of thionyl chloride (50 ml, 0.7 mol) and refluxed for 3-4 h. Excess of $SOCl_2$ was removed by distillation under reduced pressure. The dodecanedioic chloride was used without further purification. To a reaction mixture containing pyrene (10 g, 49.5 mmol) and dodecanedioic chloride (14 g, 52.4 mmol) in DCE (20 mL) was cooled in an ice bath for 15 min. To this stirring solution $TiCl_4$ (5.7 g, 52 mmol) was added dropwise for 20 min. The dark brown complex formed was allowed to warm to room temperature. The stirring was continued until the starting material disappeared by TLC. The complex was cleaved by the addition of water and the product was extracted into $CHCl_3$. Washed with water (2 x 5 mL) and dried over anhydrous Na_2SO_4. The solvent was removed under reduced pressure. The product was further purified by chromatography over Merck silica 60 using acetone-DCM (1:9) as eluent. The pure product (5.0 g, 25 %) was obtained as pale yellow solid; m.p. 116-117 °C ; IR (KBr): 3425, 3043, 2924, 2889, 2848, 1716, 1666 and 843 cm^{-1}; ^{1}H NMR (250 MHz, DMSO-d6): 1.18 (10H, br s), 1.26-1.45 (4H, m), 1.71 (2H, m), 2.14 (2H, t, *J* 7.5 Hz), 3.22 (2H, t, *J* 7.0 Hz), 8.09-8.39 (7H, m), 8.50 (1H, d, *J* 8.0 Hz) and 8.70 (1H, d, *J* 9.3 Hz) ppm; ^{13}C NMR (63 MHz, DMSO-d6): 24.38, 24.48, 28.52, 28.61, 28.68, 28.79, 28.83, 33.67, 42.00, 123.56, 124.06, 124.36, 124.47, 125.99, 126.43, 126.45, 126.77, 127.20, 128.15, 129.22, 129.27, 129.99, 130.68, 132.88, 132.96, 174.51 and 205.09 ppm; HRMS (TOF-ES-): *m/z* 413.2171 (Calc. for $C_{28}H_{30}O_3$ -H: 413.2117); Elemental anal. calcd for $C_{28}H_{30}O_3$ + 14 H_2O: C, 50.43; H, 8.76. Found: C, 50.27; H, 8.20 %.

12-(pyren-1-yl)dodecanoic acid (IX): 12-oxo-12-(pyren-1-yl)dodecanoic acid **IXa** (0.3 g, 0.7 mmol) and KOH (0.3 g, 5.5 mmol) were mixed with digol (1 mL) and warmed to 110 °C the solution turned brownish in color. To this solution hydrazine monohydrate was added slowly and stirred at 120 °C for 2-3 h. Then the temperature was slowly raised to 200 °C. All the vapours were allowed to escape out under nitrogen flow. The mixture was cooled to room temperature and acidified with dil. HCl till neutral to litmus. The product was extracted into EtOAc, washed with water (2 x 5 mL)

and dried over anhydrous Na_2SO_4. The crude product was concentrated to dryness under reduced pressure. The product was further purified by chromatography over Merck silica 60 using acetone-DCM (5:95) as eluent. The pure product (0.19 g, 67 %) was obtained as pale yellow solid; m.p. 110-111 °C; IR (KBr): 3435, 2921, 2846, 1705 and 844 cm^{-1}; ^{1}H NMR (500 MHz, $CDCl_3$): 1.27 (10H, br s), 1.38 (2H, t, *J* 7.5 Hz), 1.49 (2H, q, *J* 7.5 Hz), 1.63 (2H, q, *J* 7.5 Hz), 1.86 (2H, q, *J* 8.0 Hz), 2.34 (2H, t, *J* 7.5 Hz), 3.34 (2H, t, *J* 8.0 Hz), 7.87 (1H, d, *J* 8.0 Hz), 7.96-8.17 (7H, m) and 8.29 (1H, d, *J* 9.5 Hz) ppm; ^{13}C NMR (126 MHz, $CDCl_3$): 24.67, 29.03, 29.19, 29.38, 29.54, 29.55, 29.56, 29.79, 31.92, 33.60, 33.88, 123.53, 124.59, 124.75, 124.76, 125.10, 125.11, 125.73, 126.45, 127.06, 127.23, 127.53, 128.62, 129.70, 130.97, 131.48, 137.35 and 179.21 ppm; HRMS (TOF-ES-): *m/z* 399.2137 (Calc. for $C_{28}H_{32}O_2$ -H: 399.2324); Elemental anal. calcd batch 1 for $C_{28}H_{32}O_2$+H_2O: C, 80.35; H, 8.18. Found: C, 80.52; H, 7.72 %; batch 2 for $C_{28}H_{32}O_2$+ 1/2 H_2O: C, 82.20; H, 8.12. Found: C, 82.58; H, 7.96 %.

Methyl-12-(pyren-1-yl)dodecanoate (X): 12-(pyren-1-yl)dodecanoic acid **IX** (0.3 g, 0.75 mmol) was added to a solution containing 2 mL MeOH and 0.2 mL H_2SO_4 and refluxed for 4-5 h. After the completion, the reaction the mixture was neutralized with saturated $NaHCO_3$ and extracted into $CHCl_3$. The chloroform layer was washed with water (2 x 5 mL) and dried over anhydrous Na_2SO_4. The solvent was removed under reduced pressure and purified further by column chromatography over Merck silica 60 using $CHCl_3$-hexane (2:8) as eluent. The pure product (0.28 g, 90 %) was obtained as pale yellow solid; m.p. 57.5-58.0 °C; IR (KBr): 3455, 3040, 2928, 2852, 1741, 1155 and 841 cm^{-1}; ^{1}H NMR (500 MHz, $CDCl_3$): 1.29 (10H, br s), 1.39 (2H, m), 1.50 (2H, q, *J* 7.5 Hz), 1.63 (2H, m), 1.87 (2H, q, *J* 7.5 Hz), 2.31 (2H, t, *J* 7.5 Hz), 3.34 (2H, t, *J* 8.0 Hz), 3.68 (3H, s), 7.87 (1H, d, *J* 7.8 Hz), 7.97-8.17 (7H, m) and 8.29 (1H, d, *J* 9.0 Hz) ppm; ^{13}C NMR (126 MHz, $CDCl_3$): 24.94, 29.12, 29.21, 29.40, 29.54, 29.55, 29.56, 29.79, 31.90, 33.57, 34.09, 51.36, 123.50, 124.56, 124.72, 124.74, 125.08, 125.09, 125.70, 126.43, 127.04, 127.19, 127.51, 128.60, 129.68, 130.95, 131.46, 137.31 and 174.26 ppm; HRMS (70eV, EI): *m/z* 414.2551 (Calc. for $C_{29}H_{34}O_2$: 414.2558); Elemental anal. calcd for $C_{29}H_{34}O_2$ + 1/2 H_2O: C, 84.01; H, 8.27. Found: C, 84.02; H, 8.31 %.

12-(pyren-1-yl)dodecanehydrazide (XI): To a solution containing methyl-12-(pyren-1-yl)dodecanoate **X** (0.25 g, 0.6 mmol) in 3 mL methanol was added hydrazine hydrate (0.21 g, 4.2 mmol) and refluxed for 4 h. After the reaction the mixture was extracted into chloroform. The chloroform layer was washed with water (2 x 5 mL x 2) and dried over anhydrous Na_2SO_4. Chloroform was removed under reduced pressure. The crude material was purified

further by column chromatography over Merck silica 60 using acetone-DCM (1:9) as the eluent. The pure product (0.21 g, 80 %) was obtained as white solid; m.p. 122-123 °C; IR (KBr): 3430, 3300, 2918, 2850, 1631, 1530 and 842 cm^{-1}; ^{1}H NMR (500 MHz, $CDCl_3$): 1.27 (10H, br s), 1.38 (2H, m), 1.48 (2H, m), 1.60 (2H, m), 1.86 (2H, q, *J* 7.5 Hz), 2.12 (2H, t, *J* 8.0 Hz), 3.34 (2H, t, *J* 8.0 Hz), 3.88 (2H, br s), 6.60 (1H, br s), 7.87 (1H, d, *J* 8.0 Hz), 7.96-8.17 (7H, m) and 8.28 (1H, d, *J* 9.5 Hz) ppm; ^{13}C NMR (126 MHz, $CDCl_3$): 25.47, 29.25, 29.41, 29.54, 29.55, 29.79, 31.93, 33.60, 34.59, 123.54, 124.60, 124.77, 125.11, 125.13, 125.75, 126.47, 127.07, 127.24, 127.54, 128.64, 129.71, 130.98, 131.49 and 137.36 ppm; HRMS (TOF-ES+): *m/z* 415.2757 (Calc. for $C_{28}H_{34}N_2O$ +H: 415.2749); Elemental anal. calcd for $C_{28}H_{34}N_2O$ + 1/2 H_2O: C, 79.50; H, 8.33; N, 6.61. Found: C, 79.97; H, 8.11; N, 6.39 %.

1-(pyren-1-yl)octadecan-1-ol (XII): 1-(pyren-1-yl)octadecan-1-one **IIIa** (0.1 g, 0.21 mmol) was dissolved in 1 mL of dry THF. This solution was added dropwise to a stirring suspension of LAH (0.08 g, 2.1 mmol) in 1 mL of dry THF. The resulting mixture was stirred for 3-4 h at RT. After the reaction, excess of LAH was neutralized by addition EtOAc and moist EtOH. The mixture was filtered and filtrate was concentrated and dried. The crude product was further purified by column chromatography over Merck silica 60 column using EtOAc-DCM (5:95) as eluent. The pure product (0.072 g, 72 %) was isolated as a pale yellow powder; m.p. 85-87 °C; IR (KBr): 3440, 2920, 2850, 1466, 1055 and 842 cm^{-1}; ^{1}H NMR (250 MHz, $CDCl_3$): 0.88 (3H, t, *J* 6.8 Hz), 1.24-1.61 (30H, m), 2.00-2.13 (2H, m), 5.79 (1H, t, *J* 6.5 Hz), 7.95-8.20 (8H, m) and 8.36 (1H, d, *J* 9.3 Hz) ppm; ^{13}C NMR (63 MHz, $CDCl_3$): 14.33, 22.91, 26.49, 29.58, 29.92, 32.15, 39.42, 71.67, 122.79, 123.55, 125.14, 125.20, 125.21, 125.27, 125.43, 126.13, 127.40, 127.72, 127.77, 127.81, 130.84, 130.93, 131.66 and 138.68 ppm; HRMS (TOF-ES+): *m/z* 493.2900 (Calc. for $C_{34}H_{46}ONa$: 493.3446); Elemental anal. calcd for $C_{34}H_{46}O$ + 1/4 H_2O: C, 85.93; H, 9.81. Found: C, 85.89; H, 9.90 %.

12-(pyren-1-yl)dodecan-1-ol (XIII): Methyl-12-(pyren-1-yl)dodecanoate **X** (0.1 g, 0.24 mmol) was dissolved in 1 mL of dry THF. This solution was added dropwise to a stirring suspension of LAH (0.092 g, 2.4 mmol) in 1 mL of dry THF. The resulting mixture was stirred for 3-4 h at RT. After the reaction, the excess of LAH was neutralized by addition EtOAc and moist EtOH. The mixture was filtered. Filtrate was concentrated and dried. The crude product was further purified by column chromatography over Merck silica 60 column using DCM-EtOAc (98:2) as the eluent. The pure product (0.061 g, 66 %) was isolated as a white powder; m.p. 72-75 °C; IR (KBr): 3411, 3038, 2920, 2849, 1465, 1057 and 843 cm^{-1}; ^{1}H NMR (250

MHz, $CDCl_3$): 1.18 (1H, br s), 1.28 (17H, br s), 1.53 (2H, m), 1.86 (2H, q, *J* 8.0 Hz), 3.34 (2H, t, *J* 7.8 Hz), 3.63 (2H, t, *J* 6.8 Hz), 7.87 (1H, d, *J* 7.8 Hz), 7.93-8.20 (7H, m) and 8.29 (1H, d, *J* 9.3 Hz) ppm; ^{13}C NMR (63 MHz, $CDCl_3$): 25.96, 29.64, 29.81, 30.05, 32.17, 33.05, 33.84, 63.33, 123.77, 124.82, 124.99, 125.33, 125.97, 126.69, 127.29, 127.47, 127.77, 128.85, 129.93, 131.20, 131.71 and 137.60 ppm; HRMS (TOF-ES+): *m/z* 409.1206 (Calc. for $C_{28}H_{34}ONa$: 409.2507); Elemental anal. calcd for $C_{28}H_{34}O$: C, 86.99; H, 8.86. Found: C, 86.54; H, 8.43 %.

1-(pyren-1-yl)dodecane-1,12-diol (XIV): 12-oxo-12-(pyren-1-yl)dodecanoic acid **IXa** (0.1 g, 0.24 mmol) was dissolved in 1 mL of dry THF. This solution was added dropwise to a stirring suspension of LAH (0.09 g, 2.4 mmol) in 1 mL of dry THF. The resulting mixture was stirred for 5-6 h at RT. After the reaction, excess of LAH was neutralized by addition EtOAc and moist EtOH. The mixture was filtered. Filtrate was concentrated and dried. The crude product was further purified by column chromatography over Merck silica 60 column using EtOAc/DCM (5:95) as eluent. The pure product (0.068 g, 70 %) was isolated as a pale yellow powder; m.p. 111-112 °C; IR (KBr): 3415, 2920, 2850, 1465, 1057 and 843 cm^{-1}; ^{1}H NMR (250 MHz, $CDCl_3$): 1.25 (14H, br s), 1.54 (2H, m), 2.05 (2H, m), 3.62 (2H, t, *J* 6.5 Hz), 5.80 (1, t, *J* 6.3 Hz), 7.97-8.21 (8H, m) and 8.37 (1H, d, *J* 9.5 Hz) ppm; ^{13}C NMR (63 MHz, $CDCl_3$): 25.94, 26.47, 29.61, 29.73, 29.76, 29.81, 33.04, 39.42, 63.33, 71.68, 122.81, 123.57, 125.16, 125.22, 125.29, 125.46, 126.16, 127.42, 127.73, 127.79, 127.83, 130.86, 130.94, 131.67 and 138.69 ppm; HRMS (TOF-ES+): *m/z* 425.2405 (Calc. for $C_{28}H_{34}O_2Na$: 425.2457); Elemental anal. calcd for $C_{28}H_{34}O_2$ + 2 H_2O: C, 76.67; H, 8.73. Found: C, 76.29; H, 8.93 %.

1,1'-(dodecane-1,12-diyl)dipyrene (XV): To a reaction mixture containing pyrene (10.1 g, 0.05 mol) and dodecanedioic chloride (7 g, 0.026 mol) in dichloroethane (150 mL) was cooled in an ice bath for 15 minutes. To this stirred solution $TiCl_4$ (40 g, 0.2 mol) was added dropwise during 4 h at 5 °C or lower temperature. The dark brown complex formed was allowed to warm to room temperature. The stirring was continued until the pyrene disappeared by TLC. The complex was cleaved by the addition of water and the product was extracted into $CHCl_3$ in Soxhlet apparatus and washed with water (2 x 50 mL) and dried over anhydrous $MgSO_4$. The solvent was removed under reduced pressure yielding a mixture of impure 1,12-di(pyren-1-yl)dodecane-1,12-dione and 12-oxo-12-(pyren-1-yl)dodecanoic acid **IXa**, which were used as such in the next reaction.

Digol (200 ml) was added with KOH (25 g, 0.45 mol) and the mixture

was heated to 180 °C under nitrogen purge. Hydrazine hydrate (10 ml, 0.2 mol) was added dropwise keeping temperature above 180 °C under 20 h. After all hydrazine was added, temperature was raised to 220 °C for 4 h under nitrogen flush and the mixture was cooled to 50 °C. Hexane (5 x 500 ml) was added and refluxed for 20 minutes under vigorous stirring for each batch. The hexane phase was separated and mixed with 10 g of silica, filtered and evaporated under reduced pressure to 20 ml and then let evaporate to dryness slowly at normal pressure in a flask in a hood. Colorless crystalline powder of 1,1'-(dodecane-1,12-diyl)dipyrene **XV** (2.2 g, 15%) was obtained.

The digol phase was neutralized with 10 % HCl and extracted with chloroform (3 x 250 ml). The chloroform was washed with 2 x 100 ml of water and dried over $MgSO_4$. 75 g of silica was added to the chloroform and the solvent was evaporated to dryness under reduced pressure. The silica was eluted with THF-hexane-methanol (19:80:1) over 1.5 kg of Merck silica 60 in a preparative MPLC. The pure product **IX** (3.5g, 18%) was recovered.

1,1'-(dodecane-1,12-diyl)dipyrene **XV** (2.2 g, 15 %); m.p. 129-132 °C; IR (KBr): 3038, 2918, 2851, 1604, 1466, 1418, 1180, 963, 844, 758, 723, 706, 681 and 620 cm^{-1}; ^1H NMR (500 MHz, $CDCl_3$): 1.28 (8H, m), 1.37 (4H, m), 1.48 (4H, q), 1.82 (4H, q), 3.33 (4H, t), 7.86 (2H, d, *J* 8.0 Hz), 7.96-8.03 (6H, m), 8.08-8.16 (8H, m) and 8.28 (2H, d, *J* 9.5 Hz) ppm; ^{13}C NMR (126 MHz, $CDCl_3$): 29.56, 29.58, 29.61, 29.80, 31.93, 33.60, 123.54, 124.58, 124.75, 124.76, 125.11, 125.12, 125.73, 126.46, 127.06, 127.23, 127.53, 128.63, 129.70, 130.97, 131.49 and 137.37 ppm; HRMS (70 eV, EI): *m/z* 570.3280 (Calc. for $C_{44}H_{42}$: 570.3287); Elemental anal. calcd for $C_{44}H_{42}$: C, 92.58; H, 7.42. Found: C, 92.57; H, 7.49 %.

Bibliography

1. P. Terech and R. G. Weiss, *Chem. Rev.*, **1997**, *97*, 3133–3159.

2. N. M. Sangeetha and U. Maitra, *Chem. Soc. Rev.*, **2005**, *34*, 821–836.

3. S. Banerjee, R. K. Das, and U. Maitra, *J. Mater. Chem.*, **2009**, *19*, 6649–6687.

4. M. George and R. G. Weiss, Low Molecular-Mass Organic Gelators, In *Molecular Gels. Materials with Self-Assembled Fibrillar Networks*, R. G. Weiss and P. Terech, eds., Springer, Dordrecht, The Netherlands, **2006**, 449–551.

5. A. R. Hirst and D. K. Smith, *Chem. Eur. J.*, **2005**, *11*, 5496–5508.

6. U. Maitra, P. VijayKumar, N. Chandra, L. J. D'Souza, M. D. Prasanna, and A. R. Raju, *Chem. Commun.*, **1999**, 595–596.

7. C. M. Hansen, *Hansen Solubility Parameters: A User's Handbook*, 2nd edition, CRC Press, Boca Raton, FL, **2007**.

8. R. G. Weiss and P. Terech, eds., *Molecular Gels. Materials with Self-Assembled Fibrillar Networks*, Springer, Dordrecht, The Netherlands, **2006**.

9. A. von Lipowitz, *Liebigs Ann. Chem. Pharm.*, **1841**, *38*, 348–355.

10. T. Graham, *Phil. Trans. Roy. Soc.*, **1861**, *151*, 183–224.

11. D. J. Lloyd, The problem of gel structure, In *Colloid Chemistry*, J. Alexander, ed., The Chemical Catalogue Company, New York, USA, **1926**, 767–782.

12. P. J. Flory, *Discuss. Faraday Soc.*, **1974**, *57*, 7–18.

13. D. J. Abdallah and R. G. Weiss, *Adv. Mater.*, **2000**, *12*, 1237–1247.

14. K. Almdal, J. Dyre, S. Hvidt, and O. Kramer, *Polym. Gels Netw.*, **1993**, *1*, 5–17.

15. L. L. Hench and J. K. West, *Chem. Rev.*, **1990**, *90*, 33–72.

16. D. J. Abdallah and R. G. Weiss, *Langmuir*, **2000**, *16*, 352–355.

17. A. Ajayaghosh, V. K. Praveen, and C. Vijayakumar, *Chem. Soc. Rev.*, **2008**, *37*, 109–122.

18. M. de Loos, *Hydrogen-Bonded Low Molecular Weight Gelators Structure-Property Relations*, Ph.D. thesis, University of Groningen, **2005**.

19. J. L. Atwood and J. W. Steed, eds., *Organic Nanostructures*, 111–154, Wiley-VCH, Weinheim, **2008**.

20. M.-O. M. Piepenbrock, G. O. Lloyd, N. Clarke, and J. W. Steed, *Chem. Rev.*, **2010**, *110*, 1960–2004.

21. J. H. van Esch and B. L. Feringa, *Angew. Chem. Int. Ed.*, **2000**, *39*, 2263–2266.

22. J. H. van Esch, *Langmuir*, **2009**, *25*, 8392–8394.

23. M. Žinić, F. Vögtle, and F. Fages, *Top. Curr. Chem.*, **2005**, *256*, 39–76.

24. F. Fages, F. Vögtle, and M. Žinić, *Top. Curr. Chem.*, **2005**, *256*, 77–131.

25. A. R. Hirst and D. K. Smith, *Top. Curr. Chem.*, **2005**, *256*, 237–273.

26. T. Ishi-i and S. Shinkai, *Top. Curr. Chem.*, **2005**, *258*, 119–160.

27. D. J. Abdallah, S. A. Sirchio, and R. G. Weiss, *Langmuir*, **2000**, *16*, 7558–7561.

28. R. J. Twieg, T. P. Russell, R. Siemens, and J. F. Rabolt, *Macromolecules*, **1985**, *18*, 1361–1362.

29. C.-Y. Ku, P. L. Nostro, and S.-H. Chen, *J. Phys. Chem. B*, **1997**, *101*, 908–914.

30. T. Tachibana, T. Mori, and K. Hori, *Bull. Chem. Soc. Jpn.*, **1980**, *53*, 1714–1719.

31. P. Terech, D. Pasquier, V. Bordas, and C. Rossat, *Langmuir*, **2000**, *16*, 4485–4494.

32. G. Mieden-Gundert, L. Klein, M. Fischer, F. Vögtle, K. Heuzé, J.-L. Pozzo, M. Vallier, and F. Fages, *Angew. Chem. Int. Ed.*, **2001**, *40*, 3164–3166.

33. D. W. Knight and I. R. Morgan, *Tetrahedron Lett.*, **2009**, *50*, 6610–6612.

34. R. J. H. Hafkamp, M. C. Feiters, and R. J. M. Nolte, *J. Org. Chem.*, **1999**, *64*, 412–426.

35. G. John, J. H. Jung, M. Masuda, and T. Shimizu, *Langmuir*, **2004**, *20*, 2060–2065.

36. O. Gronwald and S. Shinkai, *Chem. Eur. J.*, **2001**, *7*, 4329–4334.

37. A. Friggeri, O. Gronwald, K. J. C. van Bommel, S. Shinkai, and D. N. Reinhoudt, *J. Am. Chem. Soc.*, **2002**, *124*, 10754–10758.

38. R. Luboradzki and Z. Pakulski, *Tetrahedron*, **2004**, *60*, 4613–4616.

39. G. John, G. Zhu, J. Li, and J. S. Dordick, *Angew. Chem. Int. Ed.*, **2006**, *45*, 4772–4775.

40. T. Kida, K. Kishimoto, K. Hatano, M. Muraoka, Y. Nakatsuji, and M. Akashi, *Chem. Lett.*, **2010**, *39*, 1206–1208.

41. R. Luboradzki, Z. Pakulski, and B. Sartowska, *Tetrahedron*, **2005**, *61*, 10122–10128.

42. D. J. Mercurio and R. J. Spontak, *J. Phys. Chem. B*, **2001**, *105*, 2091–2098.

43. O. Martin-Borret, R. Ramasseul, and R. Rassat, *Bull. Soc. Chim. Fr.*, **1979**, *II-401*, 7–8.

44. R. Mukkamala and R. G. Weiss, *Langmuir*, **1996**, *12*, 1474–1482.

45. Y. Lin and R. G. Weiss, *Macromolecules*, **1987**, *20*, 414–417.

46. K. Murata, M. Aoki, T. Suzuki, T. Harada, H. Kawabata, T. Komori, F. Ohseto, K. Ueda, and S. Shinkai, *J. Am. Chem. Soc.*, **1994**, *116*, 6664–6676.

47. K. Murata, M. Aoki, T. Nishi, A. Ikeda, and S. Shinkai, *J. Chem. Soc., Chem. Commun.*, **1991**, 1715–1718.

48. H. J. Tian, K. Inoue, K. Yoza, T. Ishi-i, and S. Shinkai, *Chem. Lett.*, **1998**, 871–872.

49. C. Geiger, M. Stanescu, L. Chen, and D. G. Whetten, *Langmuir*, **1999**, *15*, 2241–2245.

50. E. Virtanen and E. Kolehmainen, *Eur. J. Org. Chem.*, **2004**, 3385–3399.

51. H. M. Willemen, T. Vermonden, A. T. M. Marcelis, and E. J. R. Sudhölter, *Langmuir*, **2002**, *18*, 7102–7106.

52. V. C. Edelsztein, G. Burton, and P. H. di Chenna, *Tetrahedron Lett.*, **2010**, *66*, 2162–2167.

53. M. George, S. L. Snyder, P. Terech, C. J. Glinka, and R. G. Weiss, *J. Am. Chem. Soc.*, **2003**, *125*, 10275–10283.

54. K. Hanabusa, M. Yamada, M. Kimura, and H. Shirai, *Angew. Chem. Int. Ed. Engl.*, **1996**, *35*, 1949–1951.

55. J. H. Jung, Y. Ono, K. Hanabusa, and S. Shinkai, *J. Am. Chem. Soc.*, **2000**, *122*, 5008–5009.

56. R. Schmidt, F. B. Adam, M. Michel, M. Schmutz, G. Decher, and P. J. Mésini, *Tetrahedron Lett.*, **2003**, *44*, 3171–3174.

57. S. Bhattacharya and A. Pal, *J. Phys. Chem. B*, **2008**, *112*, 4918–4927.

58. A. Pal, Y. K. Ghosh, and S. Bhattacharya, *Tetrahedron*, **2007**, *63*, 7334–7348.

59. J. Makarević, M. Jokić, B. Perić, V. Tomišić, B. Kojić-Prodić, and M. Žinić, *Chem. Eur. J.*, **2001**, *7*, 3328–3341.

60. T. Kar, S. Debnath, D. Das, A. Shome, and P. K. Das, *Langmuir*, **2009**, *25*, 8639–8648.

61. X. Luo, B. Liu, and Y. Liang, *Chem. Commun.*, **2001**, 1556–1557.

62. S. Malik, S. K. Maji, A. Banerjee, and A. K. Nandi, *J. Chem. Soc., Perkin Trans. 2*, **2002**, *1177–1186*.

63. A. Dutta, D. Chattopadhyay, and A. Pramanik, *Supramol. Chem.*, **2010**, *22*, 95–102.

64. J. Becerril, M. I. Burguete, B. Escuder, S. V. Luis, J. F. Miravet, and M. Querol, *Chem. Commun.*, **2002**, 738–739.

65. K. Hanabusa, M. Matsumoto, M. Kimura, A. Kakehi, and H. Shirai, *J. Colloid Interface Sci.*, **2000**, *224*, 231–244.

66. F. Allix, P. Curcio, Q. N. Pham, G. Pickaert, and B. Jamart-Grégoire, *Langmuir*, **2010**, *26*, 16818–16827.

67. M. George, G. Tan, V. T. John, and R. G. Weiss, *Chem. Eur. J.*, **2005**, *11*, 3243–3254.

68. P. K. Vemula and G. John, *Chem. Commun.*, **2006**, 2218–2220.

69. J. van Esch, S. de Feyter, R. M. Kellogg, F. D. Schryver, and B. L. Feringa, *Chem. Eur. J.*, **1997**, *3*, 1238–1243.

70. F. S. Schoonbeek, J. H. van Esch, R. Hulst, R. M. Kellogg, and B. L. Feringa, *Chem. Eur. J.*, **2000**, *6*, 2633–2643.

71. M. de Loos, A. G. J. Ligtenbarg, J. van Esch, H. Kooijman, A. L. Spek, R. Hage, R. M. Kellogg, and B. L. Feringa, *Eur. J. Org. Chem.*, **2000**, 3675–3678.

72. M. Yamanaka, T. Nakagawa, R. Aoyama, and T. Nakamura, *Tetrahedron*, **2008**, *64*, 11558–11567.

73. M. Yamanaka and H. Fujii, *J. Org. Chem.*, **2009**, *74*, 5390–5394.

74. G. Clavier, M. Mistry, F. Fages, and J.-L. Pozzo, *Tetrahedron Lett.*, **1999**, *40*, 9021–9024.

75. T. Brotin, R. Utermöhlen, F. Fages, H. Bouas-Laurent, and J. P. Desvergne, *J. Chem. Soc., Chem. Commun.*, **1991**, 416–418.

76. P. Terech, H. Bouas-Laurent, and J.-P. Desvergne, *J. Colloid Interface Sci.*, **1995**, *174*, 258–263.

77. J.-L. Pozzo, G. M. Clavier, M. Colomes, and H. Bouas-Laurent, *Tetrahedron*, **1997**, *53*, 6377–6390.

78. G. M. Clavier, J.-F. Brugger, H. Bouas-Laurent, and J.-L. Pozzo, *J. Chem. Soc., Perkin Trans. 2*, **1998**, 2527–2534.

79. A. Ajayaghosh and S. J. George, *J. Am. Chem. Soc.*, **2001**, *123*, 5148–5149.

80. V. K. Praveen, S. J. George, and A. Ajayaghosh, *Macromol. Symp.*, **2006**, *241*, 1–8.

81. A. Ajayaghosh, S. J. George, and V. K. Praveen, *Angew. Chem. Int. Ed.*, **2003**, *42*, 332–335.

82. T. Ishi-i, T. Hirayama, K. Murakami, H. Tashiro, T. Thiemann, K. Kubo, A. Mori, S. Yamasaki, T. Akao, A. Tsuboyama, T. Mukaide, K. Ueno, and S. Mataka, *Langmuir*, **2005**, *21*, 1261–1268.

83. X.-Q. Li, V. Stepanenko, Z. Chen, P. Prins, L. D. A. Siebbeles, and F. Würthner, *Chem. Commun.*, **2006**, 3871–3873.

84. X. Li, *Hydrogen Bond-directed Self-assembly of Perylene Bisimide Organogelators*, Ph.D. thesis, Julius-Maximilians-Universität Würzburg, **2009**.

85. P. Babu, N. M. Sangeetha, P. Vijaykumar, U. Maitra, K. Rissanen, and A. R. Raju, *Chem. Eur. J.*, **2003**, *9*, 2–12.

86. S. Tamaru, S. Uchino, M. Takeuchi, M. Ikeda, T. Hatano, and S. Shinkai, *Tetrahedron Lett.*, **2002**, *43*, 3751–3755.

87. S. Tanaka, M. Shirakawa, K. Kaneko, M. Takeuchi, and S. Shinkai, *Langmuir*, **2005**, *21*, 2163–2172.

88. C. F. van Nostrum, S. J. Picken, A. J. Schouten, and R. J. M. Nolte, *J. Am. Chem. Soc.*, **1995**, *117*, 9957–9965.

89. H. Engelkamp, S. Middelbeek, and R. J. M. Nolte, *Science*, **1999**, *284*, 785–788.

90. S. Samorí, H. Engelkamp, P. de Witte, A. E. Rowan, R. J. M. Nolte, and J. P. Rabe, *Angew. Chem. Int. Ed.*, **2001**, *40*, 2348–2350.

91. F. Fages, *Angew. Chem. Int. Ed.*, **2006**, *45*, 1680–1682.

92. P. Terech, C. Chachaty, J. Gaillard, and A. M. Giroud-Godquin, *J. Phys. France*, **1987**, *48*, 663–671.

93. P. Terech, G. Gebel, and R. Ramasseul, *Langmuir*, **1996**, *12*, 4321–4323.

94. P. Terech, C. Scherer, B. Demé, and R. Ramasseul, *Langmuir*, **2003**, *19*, 10641–10647.

95. G. P. Funkhouser, N. Tonmukayakul, and F. Liang, *Langmuir*, **2009**, *25*, 8672–8677.

96. M. Shirakawa, N. Fujita, T. Tani, K. Kaneko, and S. Shinkai, *Chem. Commun.*, **2005**, 4149–4151.

97. B. Escuder, S. Martí, and J. F. Miravet, *Langmuir*, **2005**, *21*, 6776–6787.

98. T. Ishi-i, R. Iguchi, E. Snip, M. Ikeda, and S. Shinkai, *Langmuir*, **2001**, *17*, 5825–5833.

99. B. G. Bag, G. C. Maity, and S. K. Dinda, *Org. Lett.*, **2006**, *8*, 5457–5460.

100. S. W. Jeong, K. Murata, and S. Shinkai, *Supramol. Sci.*, **1996**, *3*, 83–86.

101. S. R. Nam, H. Y. Lee, and J.-I. Hong, *Tetrahedron*, **2008**, *64*, 10531–10537.

102. O. Simalou, P. Xue, and R. Lu, *Tetrahedron Lett.*, **2010**, *51*, 3685–3690.

103. M. Suzuki, H. Saito, H. Shirai, and K. Hanabusa, *New J. Chem.*, **2007**, *31*, 1654–1660.

104. M. Suzuki, H. Saito, and K. Hanabusa, *Langmuir*, **2009**, *25*, 8579–8585.

105. Y. Zhou, M. Xu, T. Yi, S. Xiao, Z. Zhou, F. Li, and C. Huang, *Langmuir*, **2007**, *23*, 202–208.

106. A. Hahma, S. Bhat, K. Leivo, J. Linnanto, M. Lahtinen, and K. Rissanen, *New J. Chem.*, **2008**, *32*, 1438–1448.

107. M. George, G. P. Funkhouser, P. Terech, and R. G. Weiss, *Langmuir*, **2006**, *22*, 7885–7893.

108. S. Kawano, N. Fujita, and S. Shinkai, *Chem. Commun.*, **2003**, 1352–1353.

109. S. Yagai, M. Higashi, T. Karatsu, and A. Kitamura, *Chem. Mater.*, **2004**, *16*, 3582–3585.

110. S. Yagai, T. Karatsu, and A. Kitamura, *Langmuir*, **2005**, *21*, 11048–11052.

111. K. Hanabusa, T. Miki, Y. Taguchi, T. Koyama, and H. Shirai, *J. Chem. Soc., Chem. Commun.*, **1993**, 1382–1384.

112. X. Xu, M. Ayyagari, M. Tata, V. T. John, and G. L. McPherson, *J. Phys. Chem.*, **1993**, *97*, 11350–11353.

113. M. Tata, V. T. John, Y. Y. Waguespack, and G. L. McPherson, *J. Am. Chem. Soc.*, **1994**, *116*, 9464–9470.

114. M. Tata, V. T. John, Y. Y. Waguespack, and G. L. McPherson, *J. Phys. Chem.*, **1994**, *98*, 3809–3817.

115. M. Singh, G. Tan, V. Agarwal, G. Fritz, K. Maskos, A. Bose, V. John, and G. McPherson, *Langmuir*, **2004**, *20*, 7392–7398.

116. B. A. Simmons, C. E. Taylor, F. A. Landis, V. T. John, G. L. McPherson, D. K. Schwartz, and R. Moore, *J. Am. Chem. Soc.*, **2001**, *123*, 2414–2421.

117. S.-H. Tung, Y.-E. Huang, and S. R. Raghavan, *Soft Matter*, **2008**, *4*, 1086–1093.

118. K. S. Partridge, D. K. Smith, G. M. Dykes, and P. T. McGrail, *Chem. Commun.*, **2001**, 319–320.

119. A. R. Hirst, D. K. Smith, M. C. Feiters, H. P. M. Geurts, and A. C. Wright, *J. Am. Chem. Soc.*, **2003**, *125*, 9010–9011.

120. A. R. Hirst and D. K. Smith, *Langmuir*, **2004**, *20*, 10851–10857.

121. M. Ayabe, T. Kishida, N. Fujita, K. Sada, and S. Shinkai, *Org. Biomol. Chem.*, **2003**, *1*, 2744–2747.

122. K. Tao, T. Wu, D. Lu, R. Bai, H. Li, and L. An, *J. Mol. Liq.*, **2008**, *142*, 118–123.

123. T. Ishi-i, J. H. Jung, and S. Shinkai, *J. Mater. Chem.*, **2000**, *10*, 2238–2240.

124. K. Oishi, T. Ishi-i, M. Sano, and S. Shinkai, *Chem. Lett.*, **1999**, *28*, 1089–1090.

125. Y. Jeong, A. Friggeri, I. Akiba, H. Masunaga, K. Sakurai, S. Sakurai, S. Okamoto, K. Inoue, and S. Shinkai, *J. Colloid and Interface Sci.*, **2005**, *283*, 113–122.

126. D. Rizkov, J. Gun, O. Lev, R. Sicsic, and A. Melman, *Langmuir*, **2005**, *21*, 12130–12138.

127. F. M. Winnik, *Chem. Rev.*, **1993**, *93*, 587–614.

128. K. Kalyanasundaram and J. K. Thomas, *J. Am. Chem. Soc.*, **1977**, *99*, 2039–2044.

129. I. Aoki, T. Harada, T. Sakaki, Y. Kawahara, and S. Shinkai, *J. Chem. Soc., Chem. Commun.*, **1992**, 1341–1345.

130. J. R. Lakowicz, *Principles of Fluorescence Spectroscopy*, 3rd edition, Springer, New York, USA, **2006**.

131. S. Nishizawa, Y. Kato, and N. Teramae, *J. Am. Chem. Soc.*, **1999**, *121*, 9463–9464.

132. L. Li, Z. Zhang, W. Long, and A. Tong, *Spectrochim. Acta A*, **2001**, *57*, 385–393.

133. T. Hassheider, S. A. Benning, H.-S. Kitzerow, M.-F. Achard, and H. Bock, *Angew. Chem. Int. Ed.*, **2001**, *40*, 2060–2063.

134. V. Percec, M. Glodde, T. K. Bera, Y. Miura, I. Shiyanovskaya, K. D. Singer, V. S. K. Balagurusamy, P. A. Heiney, I. Schnell, A. Rapp, H.-W. Spiess, S. D. Hudson, and H. Duan, *Nature*, **2002**, *419*, 384–387.

135. Y. Kamikawa and T. Kato, *Org. Lett.*, **2006**, *8*, 2463–2466.

136. T. Otsubo, Y. Aso, and K. Takimiya, *J. Mater. Chem.*, **2002**, *12*, 2565–2575.

137. H.-Y. Oh, C. Lee, and S. Lee, *Org. Electron.*, **2009**, *10*, 163–169.

138. N. Nakashima, Y. Tomonari, and H. Murakami, *Chem. Lett.*, **2002**, *31*, 638–639.

139. H. Ihara, T. Yamada, M. Nishihara, T. Sakurai, M. Takafuji, H. Hachisako, and T. Sagawa, *J. Mol. Liq.*, **2004**, *111*, 73–76.

140. S. Mukhopadhyay, U. Maitra, Ira, G. Krishnamoorthy, J. Schmidt, and Y. Talmon, *J. Am. Chem. Soc.*, **2004**, *126*, 15905–15914.

141. C. Wang, Z. Wang, D. Zhang, and D. Zhu, *Chem. Phys. Lett.*, **2006**, *428*, 130–133.

142. M. I. Burguete, F. Galindo, R. Gavara, M. A. Izquierdo, J. C. Lima, S. V. Luis, A. J. Parola, and F. Pina, *Langmuir*, **2008**, *24*, 9795–9803.

143. I. A. Coates and D. K. Smith, *Chem. Eur. J.*, **2009**, *15*, 6340–6344.

144. L. J. D'Souza and U. Maitra, *J. Org. Chem.*, **1996**, *61*, 9494–9502.

145. U. Maitra, V. K. Potluri, N. M. Sangeetha, P. Babu, and A. R. Raju, *Tetrahedron: Asymmetry*, **2001**, *12*, 477–480.

146. R. K. Das, R. Kandanelli, J. Linnanto, K. Bose, and U. Maitra, *Langmuir*, **2010**, *26*, 16141–16149.

147. M. Soliman and M. Kröhn, *Synth. Met.*, **2000**, *111-112*, 611–614.

148. P. M. Borsenberger and D. S. Weiss, *Organic Photoreceptors for Xerography*, Marcel Dekker, New York, **1998**.

149. J. R. Moffat and D. K. Smith, *Chem. Commun.*, **2008**, 2248–2250.

150. T. Sagawa, S. Fukugawa, T. Yamada, and H. Ihara, *Langmuir*, **2002**, *18*, 7223–7228.

151. M.-N. Yang, N. Yan, G. He, T.-H. Liu, and Y. Fang, *Acta Phys. -Chim. Sin.*, **2009**, *25*, 1040–1046.

152. Y. Kamikawa and T. Kato, *Langmuir*, **2007**, *23*, 274–278.

153. S. Diring, F. Camerel, B. Donnio, T. Dintzer, S. Toffarin, R. Capelli, M. Muccini, and R. Ziessel, *J. Am. Chem. Soc.*, **2009**, *131*, 18177–18185.

154. S. Bhuniya and B. H. Kim, *Chem. Commun.*, **2006**, 1842–1844.

155. B. Xing, C.-W. Yu, K.-H. Chow, P.-L. Ho, D. Fu, and B. Xu, *J. Am. Chem. Soc.*, **2002**, *124*, 14846–14847.

156. Y. Zhang, Z. Yang, F. Yuan, H. Gu, P. Gao, and B. Xu, *J. Am. Chem. Soc.*, **2004**, *126*, 15028–15029.

157. S. Nagarajan and T. M. Das, *New J. Chem.*, **2009**, *33*, 2391–2396.

158. M. Kimura, N. Miki, D. Suzuki, N. Adachi, Y. Tatewaki, and H. Shirai, *Langmuir*, **2009**, *25*, 776–780.

159. M. Ma, Y. Kuang, Y. Gao, Y. Zhang, P. Gao, and B. Xu, *J. Am. Chem. Soc.*, **2010**, *132*, 2719–2728.

160. A. R. Hirst, I. A. Coates, T. R. Boucheteau, J. F. Miravet, B. Escuder, V. Castelletto, I. W. Hamley, and D. K. Smith, *J. Am. Chem. Soc.*, **2008**, *130*, 9113–9121.

161. H. M. Willemen, A. T. M. Marcelis, E. J. R. Sudhölter, W. G. Bouwman, B. Demé, and P. Terech, *Langmuir*, **2004**, *20*, 2075–2080.

162. A. R. Katritzky, R. Sakhuja, L. Khelashvili, and K. Shanab, *J. Org. Chem.*, **2009**, *74*, 3062–3065.

163. P. Xue, R. Lu, D. Li, M. Jin, C. Tan, C. Bao, Z. Wang, and Y. Zhao, *Langmuir*, **2004**, *20*, 11234–11239.

164. T. Patra, A. Pal, and J. Dey, *J. Colloid Interface Sci.*, **2010**, *344*, 10–20.

165. M. de Loos, J. H. van Esch, R. M. Kellogg, and B. L. Feringa, *Tetrahedron*, **2007**, *63*, 7285–7301.

166. P. Terech, C. Rossat, and F. Volino, *J. Colloid Interface Sci.*, **2000**, *227*, 363–370.

167. T. Brand, P. Nolis, S. Richter, and S. Berger, *Magn. Reson. Chem.*, **2008**, *46*, 545–549.

168. S. R. Raghavan and B. H. Cipriano, Gel Formation: Phase Diagrams Using Tabletop Rheology and Calorimetry, In *Molecular Gels. Materials with Self-Assembled Fibrillar Networks*, R. G. Weiss and P. Terech, eds., Springer, Dordrecht, The Netherlands, **2006**, 241–252.

169. M. Watase, Y. Nakatani, and H. Itagaki, *J. Phys. Chem. B*, **1999**, *103*, 2366–2373.

170. N. Zweep, *Control of Structure and Function of Organogels through Self-Assembly*, Ph.D. thesis, University of Groningen, **2006**.

171. P. W. Atkins, *Physical Chemistry*, 6th edition, Oxford University Press, Oxford, **1998**.

172. N. Amanokura, K. Yoza, H. Shinmori, S. Shinkai, and D. N. Reinhoudt, *J. Chem. Soc., Perkin Trans. 2*, **1998**, *2*, 2585–2591.

173. S. Kawano, N. Fujita, and S. Shinkai, *Chem. Eur. J.*, **2005**, *11*, 4735–4742.

174. P. Xue, R. Lu, X. Yang, L. Zhao, D. Xu, Y. Liu, H. Zhang, H. Nomoto, M. Takafuji, and H. Ihara, *Chem. Eur. J.*, **2009**, *15*, 9824–9835.

175. C. Tan, L. Su, R. Lu, P. Xue, C. Bao, X. Liu, and Y. Zhao, *J. Mol. Liq.*, **2006**, *124*, 32–36.

176. K. Sugiyasu, N. Fujita, M. Takeuchi, S. Yamada, and S. Shinkai, *Org. Biomol. Chem.*, **2003**, *1*, 895–899.

177. S. Bhattacharya and S. K. Samanta, *Langmuir*, **2009**, *25*, 8378–8381.

178. G. Gottarelli, S. Lena, S. Masiero, S. Pieraccini, and G. P. Spada, *Chirality*, **2008**, *20*, 471–485.

179. J. G. Hardy, A. R. Hirst, I. Ashworth, C. Brennan, and D. K. Smith, *Tetrahedron*, **2007**, *63*, 7397–7406.

180. M. Suzuki, Y. Nakajima, M. Yumoto, M. Kimura, H. Shirai, and K. Hanabusa, *Langmuir*, **2003**, *19*, 8622–8624.

181. Y. Jeong, K. Hanabusa, H. Masunaga, I. Akiba, K. Miyoshi, S. Sakurai, and K. Sakurai, *Langmuir*, **2005**, *21*, 586–594.

182. C. Baddeley, Z. Yan, G. King, P. M. Woodward, and J. D. Badjić, *J. Org. Chem.*, **2007**, *72*, 7270–7278.

183. G. Palui, A. Garai, J. Nanda, A. K. Nandi, and A. Banerjee, *J. Phys. Chem. B*, **2010**, *114*, 1249–1256.

184. A. R. Hirst, J. F. Miravet, B. Escuder, L. Noirez, V. Castelletto, I. W. Hamley, and D. K. Smith, *Chem. Eur. J.*, **2009**, *15*, 372–379.

185. D. C. Duncan and D. G. Whitten, *Langmuir*, **2000**, *16*, 6445–6452.

186. R. Luboradzki, O. Gronwald, M. Ikeda, S. Shinkai, and D. N. Reinhoudt, *Tetrahedron*, **2000**, *56*, 9595–9599.

187. A. G. L. Olive, G. Raffy, H. Allouchi, J.-M. Léger, A. del Guerzo, and J.-P. Desvergne, *Langmuir*, **2009**, *25*, 8606–8614.

188. J. Chen, J. W. Kampf, and A. J. McNeil, *Langmuir*, **2010**, *26*, 13076–13080.

189. J. Makarević, M. Jokić, Z. Raza, Z. Štefanić, B. Kojić-Prodić, and M. Žinić, *Chem. Eur. J.*, **2003**, *9*, 5567–5580.

190. M.-O. M. Piepenbrock, G. O. Lloyd, N. Clarke, and J. W. Steed, *Chem. Commun.*, **2008**, 2644–2646.

191. J. van Esch, F. Schoonbeek, M. de Loos, H. Kooijman, A. L. Spek, R. M. Kellogg, and B. L. Feringa, *Chem. Eur. J.*, **1999**, *5*, 937–950.

192. U. K. Das, D. R. Trivedi, N. N. Adarsh, and P. Dastidar, *J. Org. Chem.*, **2009**, *74*, 7111–7121.

193. D. J. Abdallah, L. Lu, and R. G. Weiss, *Chem. Mater.*, **1999**, *11*, 2907–2911.

194. X. Huang, S. R. Raghavan, P. Terech, and R. G. Weiss, *J. Am. Chem. Soc.*, **2006**, *128*, 15341–15352.

195. Y. Li, J. Liu, G. Du, H. Yan, H. Wang, H. Zhang, W. An, W. Zhao, T. Sun, F. Xin, L. Kong, Y. Li, A. Hao, and J. Hao, *J. Phys. Chem. B*, **2010**, *114*, 10321–10326.

196. D. Danino and Y. Talmon, Direct-Imaging and Freeze-Fracture Cryo-Transmission Electron Microscopy of Molecular Gels, In *Molecular Gels. Materials with Self-Assembled Fibrillar Networks*, R. G. Weiss and P. Terech, eds., Springer, Dordrecht, The Netherlands, **2006**, 253–274.

197. S. van der Laan, B. L. Feringa, R. M. Kellogg, and J. van Esch, *Langmuir*, **2002**, *18*, 7136–7140.

198. A. Ajayaghosh and V. K. Praveen, *Acc. Chem. Res.*, **2007**, *40*, 644–656.

199. P. Terech, I. Furman, R. G. Weiss, H. Bouas-Laurent, J. P. Desvergne, and R. Ramasseul, *Faraday Discuss.*, **1995**, *101*, 345–358.

200. P. Terech, E. Ostuni, and R. G. Weiss, *J. Phys. Chem.*, **1996**, *100*, 3759–3766.

201. P. Terech, G. Clavier, H. Bouas-Laurent, J.-P. Desvergne, B. Demé, and J.-L. Pozzo, *J. Colloid Interface Sci.*, **2006**, *302*, 633–642.

202. P. Terech, Molecular Gels and Small-Angle Scattering, In *Molecular Gels. Materials with Self-Assembled Fibrillar Networks*, R. G. Weiss and P. Terech, eds., Springer, Dordrecht, The Netherlands, **2006**, 275–324.

203. K. Sakurai, Y. Ono, J. H. Jung, S. Okamoto, S. Sakurai, and S. Shinkai, *J. Chem Soc., Perkin Trans. 2*, **2001**, 108–112.

204. N. M. Sangeetha, S. Bhat, A. R. Choudhury, U. Maitra, and P. Terech, *J. Phys. Chem. B*, **2004**, *108*, 16056–16063.

205. T. G. Mezger, *The Rheology Handbook*, 2nd edition, Vincentz Network, Hannover, **2006**.

206. G. Schramm, *A Practical Approach to Rheology and Rheometry*, 2nd edition, Thermo Electron, Karlsruhe, **2004**.

207. J. W. Goodwin and R. W. Hughes, *Rheology for Chemists: An Introduction*, 2nd edition, RSC Publishing, Cambridge, UK, **2008**.

208. E. Carretti, M. George, and R. G. Weiss, *Beilstein J. Org. Chem.*, **2010**, *6*, 984–991.

209. V. Kim, A. V. Bazhenov, and K. I. Kienskaya, *Colloid J.*, **1997**, *59*, 455–460.

210. I. S. Chronakis, M. Egermayer, and L. Piculell, *Macromolecules*, **2002**, *35*, 4113–4122.

211. A. Deshpande, J. M. Krishnan, and P. B. Kumar, eds., *Rheology of Complex Fluids*, Springer, New York, **2010**.

212. S. Bhat and U. Maitra, *Tetrahedron*, **2007**, *63*, 7309–7320.

213. P. Terech, *Ber. Bunsen-Ges. Phys. Chem.*, **1998**, *102*, 1630–1643.

214. P. Kirilov, F. Gauffre, S. Franceschi-Messant, E. Perez, and I. Rico-Lattes, *J. Phys. Chem. B*, **2009**, *113*, 11101–11108.

215. S. R. Raghavan and E. W. Kaler, *Langmuir*, **2001**, *17*, 300–306.

216. S. M. Tosh, P. J. Wood, Q. Wang, and J. Weisz, *Carb. Polym.*, **2004**, *55*, 425–436.

217. S. Commereuc, *J. Chem. Educ.*, **1999**, *76*, 1528–1532.

218. J. Brinksma, B. L. Feringa, R. M. Kellogg, R. Vreeker, and J. van Esch, *Langmuir*, **2000**, *16*, 9249–9255.

219. P. Terech and S. Friol, *Tetrahedron*, **2007**, *63*, 7366–7374.

220. A. J. Wright and A. G. Marangoni, *J. Am. Oil Chem. Soc.*, **2006**, *83*, 497–503.

221. Y. Zhao, Y. Cao, Y. Yang, and C. Wu, *Macromolecules*, **2003**, *36*, 855–859.

222. J. Cho, M.-C. Heuzey, and M. Hamdine, *Macromol. Mater. Eng.*, **2007**, *292*, 571–581.

223. S. M. Tosh and A. G. Marangoni, *Appl. Phys. Lett.*, **2004**, *84*, 4242–4244.

224. H. H. Winter and F. Chambon, *J. Rheol.*, **1986**, *30*, 367–382.

225. F. Chambon and H. H. Winter, *J. Rheol.*, **1987**, *31*, 683–687.

226. H. H. Winter, *Polym. Eng. Sci.*, **1987**, *27*, 1698–1702.

227. L. Li, P. M. Thangamathesvaran, C. Y. Yue, K. C. Tam, X. Hu, and Y. C. Lam, *Langmuir*, **2001**, *17*, 8062–8068.

228. N. Lorén and A.-M. Hermansson, *Int. J. Biol. Macromol.*, **2000**, *27*, 249–262.

229. L. Weng, L. Zhang, D. Ruan, L. Shi, and J. Xu, *Langmuir*, **2004**, *20*, 2086–2093.

230. S. Bhattacharya and Y. K. Ghosh, *Chem. Commun.*, **2001**, 185–186.

231. L. F. Fieser, G. C. Harris, E. B. Hershberg, M. Morgana, F. C. Novello, and S. T. Putnam, *Ind. Eng. Chem.*, **1946**, *38*, 768–773.

232. J.-T. Simonnet and S. Legret, *Eur. Pat. Appl.*, EP 1063007, **2000**.

233. J.-T. Simonnet and S. Legret, *Eur. Pat. Appl.*, EP 1082956, **2001**.

234. E. Carretti, L. Dei, and R. G. Weiss, *Soft Matter*, **2005**, *1*, 17–22.

235. M. de Loos, J. van Esch, R. M. Kellogg, and B. L. Feringa, *Angew. Chem. Int. Ed.*, **2001**, *40*, 613–616.

236. H. Ihara, K. Shudo, C. Hirayama, H. Hachisako, and K. Yamada, *Liq. Cryst.*, **1996**, *20*, 807–809.

237. J.-L. Pozzo, G. M. Clavier, and J.-P. Desvergne, *J. Mater. Chem.*, **1998**, *8*, 2575–2577.

238. Q. Liu, Y. Wang, W. Li, and L. Wu, *Langmuir*, **2007**, *23*, 8217–8223.

239. M. F. Choi and S. Shaung, *Analyst*, **2000**, *125*, 301–305.

240. R. J. H. Hafkamp, B. P. A. Kokke, I. M. Danke, H. P. M. Geurts, A. E. Rowan, M. C. Feiters, and R. J. M. Nolte, *Chem. Commun.*, **1997**, 545–546.

241. J. H. Jung, Y. Ono, and S. Shinkai, *Chem. Eur. J.*, **2000**, *6*, 4552–4557.

242. S. Kobayashi, K. Hanabusa, N. Hamasaki, M. Kimura, H. Shirai, and S. Shinkai, *Chem. Mater.*, **2000**, *12*, 1523–1525.

243. K. Sugiyasu, N. Fujita, and S. Shinkai, *Angew. Chem. Int. Ed.*, **2004**, *43*, 1229–1233.

244. A. Ajayaghosh, V. K. Praveen, S. Srinivasan, and R. Varghese, *Adv. Mater.*, **2007**, *19*, 411–415.

245. T. Kato, Y. Hirai, S. Nakaso, and M. Moriyama, *Chem. Soc. Rev.*, **2007**, *36*, 1857–1867.

246. K. Hanabusa, K. Hiratsuka, M. Kimura, and H. Shirai, *Chem. Mater.*, **1999**, *11*, 649–655.

247. F. Placin, J.-P. Desvergne, and J.-C. Lassègues, *Chem. Mater.*, **2001**, *13*, 117–121.

248. T. Fukushima and T. Aida, *Chem. Eur. J.*, **2007**, *13*, 5048–5058.

249. A. Dodabalapur, L. Torsi, and H. E. Katz, *Science*, **1995**, *268*, 270–271.

250. F. S. Schoonbeek, J. H. van Esch, B. Wesewijs, D. B. A. Rep, M. P. de Haas, T. M. Klapwojk, R. M. Kellogg, and B. L. Feringa, *Angew. Chem. Int. Ed.*, **1999**, *38*, 1393–1397.

251. F. Würthner, *Chem. Commun.*, **2004**, 1564–1579.

252. S. Li, V. T. John, G. C. Irvin, S. H. Rachakonda, G. L. McPherson, and C. J. O'Connor, *J. Appl. Phys.*, **1999**, *85*, 5965–5967.

253. H. Koshima, W. Matsusaka, and H. Yu, *J. Photochem. Photobiol., A*, **2003**, *156*, 83–90.

254. K. Nagayama, K. Karaiwa, T. Doi, and M. Imai, *Biochem. Eng. J.*, **1998**, *2*, 121–126.

255. F. Galindo, M. I. Burguete, R. Gavara, and S. V. Luis, *J. Photochem. Photobiol., A*, **2006**, *178*, 57–61.

256. J. F. Miravet and B. Escuder, *Org. Lett.*, **2005**, *7*, 4791–4794.

257. M. Lal, S. Pakatchi, G. S. He, K. S. Kim, and P. N. Prasad, *Chem. Mater.*, **1999**, *11*, 3012–3014.

258. A. Vintiloiu and J.-C. Leroux, *J. Controlled Release*, **2008**, *125*, 179–192.

259. A. Motulsky, M. Lafleur, A.-C. Couffin-Hoarau, D. Hoarau, F. Boury, J.-P. Benoit, and J.-C. Leroux, *Biomaterials*, **2005**, *26*, 6242–6253.

260. R. Kumar and O. P. Katare, *AAPS PharmSciTech*, **2005**, *6*, E298–E310.

261. N. E. Hughes, A. G. Marangoni, A. J. Wright, M. A. Rogers, and J. W. E. Rush, *Trends Food Sci. Tech.*, **2009**, *20*, 470–480.

262. A. F. M. Barton, *Chem. Rev.*, **1975**, *75*, 731–753.

263. C. M. Hansen, Solubility Parameters, In *Paint and Coating Testing Manual: Fourteenth Edition of the Gardner-Sward Handbook*, J. V. Koleske, ed., ASTM, Philadelphia, **1995**, 383–404.

264. M. Şen and O. Güven, *J. Polym. Sci. Pol. Phys.*, **1998**, *36*, 213–219.

265. T. Çaykara, G. Özyürek, Ö. Kantoğlu, and O. Güven, *J. Polym. Sci. Pol. Phys.*, **2002**, *40*, 1995–2003.

266. J. Thimmasetty, C. V. S. Subrahmanyam, P. R. S. Babu, M. A. Maulik, and B. A. Viswanath, *J. Solution Chem.*, **2008**, *37*, 1365–1378.

267. J. Breitkreutz, *Pharm. Res.*, **1998**, *15*, 1370–1375.

268. E. T. Zellers, D. H. Anna, R. Sulewski, and X. Wei, *J. Appl. Polym. Sci.*, **1996**, *62*, 2081–2096.

269. H. T. Ham, Y. S. Choi, and I. J. Chung, *J. Colloid Interface Sci.*, **2005**, *286*, 216–223.

270. S. D. Bergin, Z. Sun, D. Rickard, P. V. Streich, J. P. Hamilton, and J. N. Coleman, *ACS Nano*, **2009**, *3*, 2340–2350.

271. Y. Hernandez, M. Lotya, D. Rickard, S. D. Bergin, and J. N. Coleman, *Langmuir*, **2010**, *26*, 3208–3213.

272. M. Bielejewski, A. Łapiński, R. Luboradzki, and J. Tritt-Goc, *Langmuir*, **2009**, *25*, 8274–8279.

273. G. Zhu and J. S. Dordick, *Chem. Mater.*, **2006**, *18*, 5988–5995.

274. D. B. Smithrud and F. Diederich, *J. Am. Chem. Soc.*, **1990**, *112*, 339–343.

275. E. B. Bagley, T. P. Nelson, and J. M. Scigliano, *J. Paint. Technol.*, **1971**, *43*, 35–42.

276. J.-C. Huang, *J. Appl. Polym. Sci.*, **2004**, *94*, 1547–1555.

277. K. Adamska and A. Voelkel, *J. Chromatogr. A*, **2006**, *1132*, 260–267.

278. G. M. Bristow and W. F. Watson, *Trans. Faraday Soc.*, **1958**, *54*, 1731–1741.

279. F. Gharagheizi and M. T. Angaji, *J. Macromol. Sci. B*, **2006**, *45*, 285–290.

280. D. W. van Krevelen, *Properties of Polymers*, 3rd edition, Elsevier, Amsterdam, **1990**.

281. D. W. van Krevelen, *Properties of Polymers*, 4th rev. edition, Nijenhuis, K. te, Ed., Elsevier, Amsterdam, **2009**.

282. R. F. Fedors, *Polym. Eng. Sci.*, **1974**, *14*, 147–154.

283. K. L. Hoy, *The Hoy Tables of Solubility Parameters*, Union Carbide Corporation, Solvent and Coatings Materials Division, South Charleston, WV, **1985**.

284. K. L. Hoy, *J. Coated Fabrics*, **1989**, *19*, 53–67.

285. E. Stefanis, L. Constantinou, and C. Panayiotou, *Ind. Eng. Chem. Res.*, **2004**, *43*, 6253–6261.

286. E. Stefanis and C. Panayiotou, *Int. J. Thermophys.*, **2008**, *29*, 568–585.

287. C. L. Judy, N. M. Pontikos, and W. E. Acree, *J. Chem. Eng. Data*, **1987**, *32*, 60–62.

288. C. T. Chiou, S. E. McGroddy, and D. E. Kile, *Environ. Sci. Technol.*, **1998**, *32*, 264–269.

289. H. Yamamoto, *Hansen Solubility Parameter (HSP) and Graphene*, http://www.pirika.com/NewHP/PirikaE/graphene.html, **2010**. [accessed 29.12.2010].

290. D. J. Greenhalgh, A. C. Williams, P. Timmins, and P. York, *J. Pharm. Sci.*, **1999**, *88*, 1182–1190.

291. A. Beerbower and J. R. Dickey, *ASLE Trans.*, **1969**, *12*, 1–20.

292. D. R. Lide, ed., *CRC Handbook of Chemistry and Physics*, 84th edition, CRC Press, Boca Raton, FL, **2003**.

293. C. Reichardt, *Chem. Rev.*, **1994**, *94*, 2319–2358.

294. R. D. Nelson, *Handbook of Powder Technology. Dispersing Powders in Liquids*, volume 7, Elsevier, Amsterdam, **1988**.

295. C. Reichardt, *Solvents and Solvent Effects in Organic Chemistry*, 3rd edition, Wiley-VCH, Weinheim, **2003**.

296. C. A. Hunter, K. R. Lawson, J. Perkins, and C. J. Urch, *J. Chem. Soc., Perkin Trans. 2*, **2001**, 651–669.

297. A. Martin and J. Mauger, *Am. J. Pharm. Educ.*, **1988**, *52*, 68–75.

298. S. B. Ross-Murphy, *Ber. Bunsen-Ges. Phys. Chem.*, **1998**, *102*, 1534–1539.

299. M. Lescanne, P. Grondin, A. d'Aléo, F. Fages, J.-L. Pozzo, O. Mondain-Monval, P. Reinheimer, and A. Colin, *Langmuir*, **2004**, *20*, 3032–3041.

300. S. Roy, A. Dasgupta, and P. K. Das, *Langmuir*, **2007**, *23*, 11769–11776.

301. M. Moniruzzaman and P. R. Sundararajan, *Langmuir*, **2005**, *21*, 3802–3807.

302. S. Bhattacharya and S. N. G. Acharya, *Chem. Mater.*, **1999**, *11*, 3121–3132.

303. M. Ikeda, M. Takeuchi, and S. Shinkai, *Chem. Commun.*, **2003**, 1354–1355.

304. K. Hanabusa, K. Shimura, K. Hirose, M. Kimura, and H. Shirai, *Chem. Lett.*, **1996**, *25*, 885–886.

305. K. Hanabusa, A. Kawakami, M. Kimura, and H. Shirai, *Chem. Lett.*, **1997**, *26*, 191–192.

306. P. Jonkheijm, P. van der Schoot, A. P. H. J. Schenning, and E. W. Meijer, *Science*, **2006**, *313*, 80–83.

307. X. Luo, Z. Li, W. Xiao, Q. Wang, and J. Zhong, *J. Colloid Interface Sci.*, **2009**, *336*, 803–807.

308. M. Bielejewski, A. Łapiński, J. Kaszyńska, R. Luboradzki, and J. Tritt-Goc, *Tetrahedron Lett.*, **2008**, *49*, 6685–6689.

309. L. E. Nielsen and R. F. Landel, *Mechanical Properties of Polymers and Composites*, 2nd edition, Marcel Dekker, New York, **1994**.

310. M. J. Frisch, G. W. Trucks, H. B. Schlegel, G. E. Scuseria, M. A. Robb, J. R. Cheeseman, J. J. A. Montgomery, T. Vreven, K. N. Kudin, J. C. Burant, J. M. Millam, S. S. Iyengar, J. Tomasi, V. Barone, B. Mennucci, M. Cossi, G. Scalmani, N. Rega, G. A. Petersson, H. Nakatsuji, M. Hada, M. Ehara, K. Toyota, R. Fukuda, J. Hasegawa, M. Ishida, T. Nakajima, Y. Honda, O. Kitao, H. Nakai, M. Klene, X. Li, J. E. Knox, H. P. Hratchian, J. B. Cross, V. Bakken, C. Adamo, J. Jaramillo, R. Gomperts, R. E. Stratmann, O. Yazyev, A. J. Austin, R. Cammi, C. Pomelli, J. W. Ochterski, P. Y. Ayala, K. Morokuma, G. A. Voth, P. Salvador, J. J. Dannenberg, V. G. Zakrzewski, S. Dapprich, A. D. Daniels, M. C. Strain, O. Farkas, D. K. Malick, A. D. Rabuck, K. Raghavachari, J. B. Foresman, J. V. Ortiz, Q. Cui, A. G. Baboul, S. Clifford, J. Cioslowski, B. B. Stefanov, G. Liu, A. Liashenko, P. Piskorz, I. Komaromi, R. L. Martin, D. J. Fox, T. Keith, M. A. Al-Laham, C. Y. Peng, A. Nanayakkara, M. Challacombe, P. M. W. Gill, B. Johnson, W. Chen, M. W. Wong, C. Gonzalez, and J. A. Pople, *Gaussian 03, Revision C.02*, Gaussian, Inc., Wallingford, CT, **2004**.

311. U. C. Singh and P. A. Kollman, *J. Comp. Chem.*, **1984**, *5*, 129–145.

312. C. Sanchez, B. Julián, P. Belleville, and M. Popall, *J. Mater. Chem.*, **2005**, *15*, 3559–3592.

313. M. Kimura, S. Kobayashi, T. Kuroda, K. Hanabusa, and H. Shirai, *Adv. Mater.*, **2004**, *16*, 335–338.

314. C. S. Love, V. Chechik, D. K. Smith, K. Wilson, I. Ashworth, and C. Brennan, *Chem. Commun.*, **2005**, 1971–1973.

315. S. Ray, A. K. Das, and A. Banerjee, *Chem. Commun.*, **2006**, 2816–2818.

316. S. Bhat and U. Maitra, *Chem. Mater.*, **2006**, *18*, 4224–4226.

317. S. Bhattacharya, A. Srivastava, and A. Pal, *Angew. Chem. Int. Ed.*, **2006**, *45*, 2934–2937.

318. H. Basit, A. Pal, S. Sen, and S. Bhattacharya, *Chem. Eur. J.*, **2008**, *14*, 6534–6545.

Appendix A

Table A.1: Hildebrand solubility parameter calculation for **II** using the Fedors method. E_{coh} is the cohesive energy and V is the molar volume

Structural groups	N	$N \times E_{coh}$	$N \times V$
Compound **II**			
CH_3	1	4710	33.5
CH_2	9	44460	144.9
=C<	7	30170	-38.5
=CH-	9	38790	121.5
ring closure (6 atoms)	4	4200	64.0
conjug. in ring for each double bond	8	13360	-17.6
	Σ	135690	307.8
Compound **TNF**			
=C<	7	30170	-38.5
=CH-	5	21550	67.5
ring closure ($\geq$ 5 atoms)	3	3150	48.0
conjug. in ring for each double bond	6	10020	-13.2
>C=O	1	17370	10.8
Ar-NO_2	3	46080	96.0
	Σ	128340	170.6

$\delta(\mathbf{II}) = (E_{coh}/V)^{1/2} = 21.0$, $\delta(\mathbf{TNF}) = 27.4$

Table A.2: Equations used to calculate HSP's by Hoy's method*

Formulae	Solvents	Polymers
Additive molar functions	$F_t = \Sigma N_i F_{t,i}$ $F_p = \Sigma N_i F_{p,i}$ $V = \Sigma N_i V_i$ $\Delta_T = \Sigma N_i \Delta_{T,i}$	$F_t = \Sigma N_i F_{t,i}$ $F_p = \Sigma N_i F_{p,i}$ $V = \Sigma N_i V_i$ $\Delta_T^{(P)} = \Sigma N_i \Delta_{T,i}^{(P)}$
Auxiliary equations	$log\,\alpha = 3.39\,log(T_b/T_{cr}) - 0.1585 - log\,V$ $T_b/T_{cr} = 0.567 + \Delta_T - (\Delta_T)^2$	$\alpha^{(P)} = 777\Delta_T^{(P)}/V$ $n = 0.5/\Delta_T^{(P)}$
HSP calculations	B = 277 $\delta_t = (F_i + B)/V$ $\delta_p = \delta_t \left(\frac{1}{\alpha}\frac{F_p}{F_t+B}\right)^{1/2}$ $\delta_h = \delta_t \left[(\alpha-1)/\alpha\right]^{1/2}$ $\delta_d = \left(\delta_t^2 - \delta_p^2 - \delta_h^2\right)^{1/2}$	B = 277 $\delta_t = (F_i + B/n)/V$ $\delta_p = \delta_t \left(\frac{1}{\alpha^{(P)}}\frac{F_p}{F_t+B/n}\right)^{1/2}$ $\delta_h = \delta_t \left[(\alpha^{(P)}-1)/\alpha^{(P)}\right]^{1/2}$ $\delta_d = \left(\delta_t^2 - \delta_p^2 - \delta_h^2\right)^{1/2}$

* F_t is the molar attraction function, F_p is its polar component, V is the molar volume of the solvent molecule or the structural unit of the polymer, Δ_T is the Lydersen correction for non-ideality, α is the molecular aggregation number, T_b is the boiling point of the solvent, T_{cr} is the critical temperature, n is the number of repeating units per effective chain segment of the polymer and B is the base value.

Table A.3: HSP calculation for **II** using the Hoy method. See Table A.2 for significance of symbols

Structural groups	Groups N	$N \times F_{t,i}$	$N \times F_{p,i}$	$N \times \Delta_T^{(P)}$	$N \times V_i$
CH_3	1	303.5	0.0	0.022	21.55
CH_2	9	2421.0	0.0	0.180	139.95
CH_{arom}	9	2169.0	562.5	0.162	120.78
C_{arom}	7	1407.0	455.0	0.105	51.94
	Σ	6300.5	1017.5	0.469	334.22
α = 1.0903 n = 1.0661		δ_d	δ_p	δ_h	δ_t
		17.3	7.4	5.6	19.6

Table A.4: Calculation for total solubility parameter δ of **II** using the Stefanis-Panayiotou method[285]

Compound **II**	N	$N_i \times F_i$
1st Order groups		
CH_3	1	-2308.6
CH_2	8	-2216.8
ACH	9	-57.6
AC	6	4105.8
$ACCH_2$-	1	1023.4
2nd Order groups		
$AC(ACH_m)_2AC(ACH_n)_2$	1	-69.8
	Σ	476.4
Constant, C		75954.1

$$\delta = (\Sigma N_i \times F_i + C)^{0.383837} - 56.14 = 18.7$$

Table A.5: HSP calculation for **II** and **TNF** using the Stefanis-Panayiotou method[286]

	Groups	Contributions		
Compound **II**	N	δ_d	δ_p	δ_h
1st Order groups				
ACH	9	0.9945	-1.73817	1.21788
AC	6	5.0676	0.98214	-1.0443
$ACCH_2$-	1	0.6933	-0.33086	-0.88084
CH_2	8	-0.2152	-1.1224	-0.9288
CH_3	1	-0.9714	-0.72412	0.29901
2nd Order groups				
$AC(ACH_m)_2AC(ACH_n)_2$	1	-0.3751	0.013012	0.086424
Constant, C		17.3231	2.7467	1.3720
	Σ	22.5	-0.2	0.1
Compound **TNF**				
1st Order groups				
ACH	5	0.5525	-2.6515	-2.1525
AC	4	3.3784	2.4748	0.0336
$ACNO_2$	3	3.4485	13.4514	-2.1501
>C=O	1	-0.4343	0.7905	1.8147
2nd Order groups				
C(cyclic)=O	1	-0.2981	0.4497	-0.4794
Constant, C		17.3231	7.3548	7.9793
	Σ	24.8	21.9	5.0